

✓STUDIES ON HEAVY ION TRACKS IN SOLID DIELECTRICS

A Thesis Submitted
In Partial Fulfilment of the Requirements
for the Degree of
DOCTOR OF PHILOSOPHY

by
Kamal Kant Dwivedi

to the

**DEPARTMENT OF CHEMISTRY
INDIAN INSTITUTE OF TECHNOLOGY KANPUR
MARCH, 1977**

LIBRARY
CENTRAL LIBRARY
Acc. No. **52181**

Dedicated

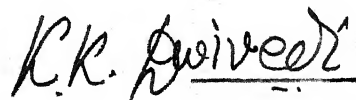
to my

PARENTS

STATEMENT

I hereby declare that the work presented in this thesis is the result of investigations carried out by me in the Department of Chemistry, Indian Institute of Technology, Kanpur, India under the supervision of Prof. Shankar Mukherji.

In keeping with the general practice of reporting scientific observations, due acknowledgement has been made wherever the work described is based on the findings of other investigators.



Kamal Kant Dwivedi

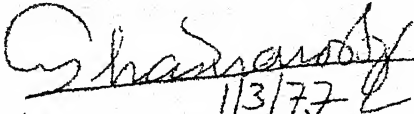
DEPARTMENT OF CHEMISTRY
INDIAN INSTITUTE OF TECHNOLOGY KANPUR

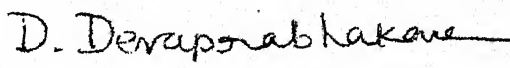
CERTIFICATE I

This is to certify that Mr. Kamal Kant Dwivedi has satisfactorily completed all the courses required for the Ph.D. degree programme. These courses include:

Chm 501 Advanced Organic Chemistry
Chm 521 Chemical Binding
Chm 523 Chemical Thermodynamics
Chm 524 Modern Physical Methods in Chemistry
Chm 541 Advanced Inorganic Chemistry I
Chm 542 Advanced Inorganic Chemistry II
Chm 543 Introduction to Nuclear Chemistry
Chm 642 Application of Nuclear Chemistry
Chm 650 Statistical Mechanics
Chm 800 General Seminar
Chm 801 Graduate Seminar
Chm 900 Post-Graduate Research

Mr. Kamal Kant Dwivedi was admitted to the candidacy of the Ph.D. degree in October 1975 after he successfully completed the written and oral qualifying examinations.


(A. Chakravorty)
Head,
Department of Chemistry


(D. Devaprabhakara)
Convener,
Departmental Post-Graduate
Committee

CERTIFICATE II

Certified that the work presented in this thesis entitled: "STUDIES ON HEAVY ION TRACKS IN SOLID DIELECTRICS" has been carried out by Mr. Kamal Kant Dwivedi under my supervision and the same has not been submitted elsewhere for a degree.

Shankar Mukherji
Shankar Mukherji
Thesis Supervisor

POST GRADUATE OFFICE This thesis has been approved for the award of the Degree of Doctor of Philosophy (Ph.D.) in accordance with the regulations of the Indian Institute of Technology, Kanpur Dated: 19/8/77 <i>B</i>
--

ACKNOWLEDGEMENTS

I feel elated in expressing my profound sense of gratitude to Professor Shankar Mukherji for his kind, able and dynamic guidance in the inception, execution and completion of this thesis.

I am very much indebted to Prof. P.S. Goel, Prof. G.K. Mehta, Prof. G.N. Rao, Prof. P.R. Singh for their generous help in providing the necessary experimental facilities and also to Dr. B.K. Kothari, University of California, San Diego, for donating the Lexan sheets. I wish to express my heartfelt appreciation and sincere thanks to Dr. Tejasvi Sharma and Dr. Brijesh K. Srivastava for their untiring help throughout the course of the present work.

My thanks are due to Sarvashree Nayak, Krish, Prabhakara, Raman, Sharma, Muddukrishna and to Drs. Sudhir Sen, K.B. Lal, S.N. Chaturvedi, Mahesh Prakash, V.R. Prakash and B.M. Bahal for many valuable discussions and suggestions.

I wish to thank my colleagues and friends Bipin, Amitabh, Harishankar, Prem Raj, Mukund, Bhushan, Prabhakar, Avadhesh, Drs. S.K. Kapoor and B.C. Mishra for their continued cooperation.

I wish to extend my heartiest appreciation to Varun, Suresh and Pradeep for their generous help in various ways.

My sincere thanks are due to Mr. B.P. Singh, Mr. P.K. Basuray, Mr. A.V. Keskar, Mr. Harish Gupta, Drs. P.N. Pandey and G.S. Pandey and their families for their kind affection.

I take this opportunity to thank Mr. R.D. Singh for excellent typing and Mr. R.K. Bajpai for neat drawings. Thanks are due to Messrs K.M.L. Jha, B.K. Jain, A.R. Korde, K.Masood, M.M. Gupta and A. Khanna for their technical assistance.

I express my deep sense of gratitude to my parents and family members especially to my 'Bhaisahab' for their sacrifice and everlasting encouragement throughout my career.

Certainly the greatest single contribution has been the patience and help of my wife, Rekha, who has been a constant source of inspiration and finally my warm appreciation is also due to my lovely daughter who had to sacrifice her playing hours gladly, although unknowingly.

Kamal Kant Dwivedi

CONTENTS

	Page
LIST OF TABLES	x
LIST OF FIGURES	xiv
PREFACE	xix
CHAPTER I INTRODUCTION	1
CHAPTER II EXPERIMENTAL MEASUREMENT OF FISSION PRODUCT TRACK LENGTHS IN MICA, LEXAN AND CELLULOSE ACETATE	5
II.1 General Procedure	5
II.2 Source of Fission Products	6
II.3 Characteristics of the Solid Dielectric Track Detectors	11
II.4 Experimental Technique	14
II.5 Microscopic Observation	22
II.6 Track length Measurement	25
CHAPTER III DETERMINATION OF ETCH RATES	31
III.1 Measurement of Bulk-Etch Rate V_G	32
III.2 Track-Diameter Kinetics	37
III.3 Determination of Activation Energy for Bulk-Etching	43
III.4 Measurement of Track-Etch Rate V_T	52

		Page
CHAPTER IV	ANALYSIS OF EXPERIMENTAL DATA ...	71
	IV.1 Track Length Distribution ...	71
	IV.2 Relation Between the Track-Etch Rate V_T and the Energy-Deposi- tion Rate dE/dX ...	87
CHAPTER V	THEORETICAL CALCULATION OF THE TRACK LENGTHS OF HEAVY IONS AND FISSION PRODUCTS IN SOLID DIELECTRICS ...	98
	V.1 Introduction ...	98
	V.2 Stopping-Power Equations for Complex Media ...	99
	V.3 Distinction Between Track Length and Range of a Heavy Ion in Solid Dielectrics ...	108
CHAPTER VI	SUMMARY AND CONTRIBUTION TO KNOWLEDGE ...	126
APPENDIX A	Determination of the Critical Angle of Incidence ϕ_c ...	128
APPENDIX B	Estimation of the Relative Errors Involved in Two Different Methods of Track Length Measurement ...	130
REFERENCES	...	133

...

LIST OF TABLES

<u>Table</u>		<u>Page</u>
II.1	^{252}Cf spontaneous fission data. ...	7
II.2	Properties of mica, Lexan and cellulose acetate detectors. ...	15
II.3	Complete etching time t_c at different temperatures for different dielectrics obtained from Figs. 14 and 15. ...	22
II.4	Calibration of the eye-piece micrometer for track length measurement at different magnifications. ...	24
III.1	The bulk-etch rate V_G for Lexan, at various etching temperatures, determined by two different techniques with 6.25 N NaOH + ethanol (1:1) as the etchant. ...	42
III.2	The bulk-etch rate V_G for cellulose acetate at various etching temperatures, determined by two different techniques with 6.25 N NaOH as the etchant. ...	42
III.3	The bulk-etch rate V_G for Lexan with 6.25 N NaOH + ethanol (1:1) at different temperatures. ...	49
III.4	The bulk-etch rate V_G for cellulose acetate with 6.25 N NaOH at different temperatures. ...	49
III.5	The bulk-etch rate V_G for mica at different etching temperatures with 40% HF as the etchant. ...	50
III.6	Values of the activation energies for bulk etching of Lexan, cellulose acetate and mica and the value of A. ...	50

<u>Table</u>		<u>Page</u>
III.7	Variation of the true etched track length with etching time for Lexan etched with 6.25 N NaOH + ethanol (1:1) at 33°C. The dip angle is 15° and the bulk-etch rate V_G is equal to 0.01404 $\mu\text{m}/\text{min}$	59
III.8	Some representative tracks, their identity (i.e., mass number of the fission product causing the track), the track-etch rate (V_T) at different etched track lengths (ETL) and the calculated energy loss rates (dE/dX). (Lexan; etchant: 6.25 N NaOH + ethanol, 1:1; temperature: 25°C). ...	61
III.9	Some representative tracks, their identity (i.e., mass number of the fission product causing the track), the track-etch rate (V_T) at different etched track lengths (ETL) and the calculated energy-loss rates (dE/dX). (Lexan; etchant: 6.25 N NaOH + ethanol, 1:1; temperature: 33°C). ...	62
III.10	Some representative tracks, their identity (i.e., mass number of the fission product causing the track), the track-etch rate (V_T) at different etched track lengths (ETL) and the calculated energy-loss rates (dE/dX). (Lexan; etchant: 6.25 N NaOH, temperature: 55°C) ...	63
III.11	Some representative tracks, their identity (i.e., mass number of the fission product causing the track), the track-etch rate (V_T) at different etched track lengths (ETL) and the calculated energy loss rates (dE/dX). (Cellulose acetate; etchant: 6.25 N NaOH, temperature: 50°C). ...	64

<u>Table</u>		<u>Page</u>
III.12	Some representative tracks, their identity (i.e., mass number of the fission product causing the track), the track-etch rate (V_T) at different-etched track lengths (ETL) and the calculated energy-loss rates (dE/dX) (Mica; etchant: 40% HF, temperature: 35°C)....	65
IV.1	^{252}Cf fission product track lengths in mica. ...	72
IV.2	Average track length of fission products in mica. ...	73
IV.3	Average track length of fission products in Lexan. ...	73
IV.4	Average track length of fission products in cellulose acetate ...	74
IV.5	Comparison between the theoretical and experimental values of track lengths in different solid dielectrics. ...	74
IV.6	^{252}Cf -fission-product mass groups, their percentage group yields, the mean masses and the corresponding calculated track lengths in mica. ...	82
IV.7	^{252}Cf -fission-product mass groups, their percentage group yields, the mean masses and the corresponding calculated track lengths in Lexan and cellulose acetate ...	83
IV.8	Values of the critical energy deposition rate $(dE/dX)_c$ for different solid dielectrics. ...	97
V.1	Ranges and track lengths of some heavy ions in mica. The calculated track lengths are based on $(dE/dX)_c = 13.0 \text{ MeV/mg/cm}^2$	113

<u>Table</u>		<u>Page</u>
V.2	Ranges and track lengths of some heavy ions in diopside. The calculated track lengths are based on $(dE/dX)_c = 19.0 \text{ MeV/mg/cm}^2$	114
V.3	Ranges and track lengths of some heavy ions in hypersthene. The calculated track lengths are based on $(dE/dX)_c = 20.0 \text{ MeV/mg/cm}^2$	115
V.4	Values of the critical energy-loss rate $(dE/dX)_c$ and the density for various solid dielectrics. . . .	116
B.1	Percentage error involved in measuring the track length from centre to tip. . . .	131
B.2	Percentage error involved in the depth measurement for a track of length = $20 \mu\text{m}$, $V_G t = 1.25 \mu\text{m}$	132

...

LIST OF FIGURES

<u>Figure</u>		<u>Page</u>
1.	Photomicrograph of ^{252}Cf fission product etched tracks in different solid dielectric track detectors:	
	(a) Uncollimated fission product tracks in Lexan.	
	(b) Collimated fission product tracks in mica entered at an angle of 30° with respect to the surface plane.	
	(c) Two parallel tracks in cellulose acetate at a magnification of 1250.	
	(d) Single track in Lexan with magnification of 1250.	... 13
2.	Diagram of the irradiation assembly showing the positions of the source, guard foil, collimator and the detector foil.	... 18
3.	Photograph of the irradiation chamber attached with the vacuum system.	... 20
4.	Schematic diagram showing track geometry:	
	(a) in mica with a negligible bulk-etch rate V_G perpendicular to the surface plane, and	
	(b) in plastics with a finite V_G 27
5.	Plot of the etching time as a function of (A) the weight of the Lexan foil and (B) the track diameter.	... 34
6.	Plot of the etching time as a function of (A) the weight of the mica foil and (B) the track diameter.	... 35
7.	Plot of the growth of the track-diameter as a function of the etching time for Lexan at various temperatures.	... 40

<u>Figure</u>	<u>Page</u>
8. Plot of the growth of the track-diameter as a function of the etching time for cellulose acetate at various temperatures. ...	41
9. Plot of the growth of the track-diameter as a function of the etching time for mica at various temperatures. ...	44
10. Plot of the logarithm of the bulk-etch rate against T^{-1} for Lexan. ...	46
11. Plot of the logarithm of the bulk-etch rate against T^{-1} for cellulose acetate. ...	47
12. Plot of the logarithm of the bulk-etch rate against T^{-1} for mica. ...	48
13. Schematic representation of the geometry of track-etching in plastics. ...	53
14. Variation of the observed and corrected track lengths with etching time in the case of Lexan. ...	56
15. Variation of the observed and corrected track lengths with etching time in the case of Lexan and cellulose acetate. ...	57
16. Variation of the observed or true track lengths with etching time in the case of mica. ...	58
17. Plots of track-etch rate V_T versus etched track length for Lexan etched with 6.25 N NaOH + ethanol (1:1) at 25°C. ...	66
18. Plots of track-etch rate V_T versus etched track length for Lexan etched with 6.25 N NaOH + ethanol (1:1) at 33°C. ...	67

<u>Figure</u>	<u>Page</u>
19. Plots of track-etch rate V_T versus etched track length for Lexan etched with 6.25 N NaOH at 55°C.	... 68
20. Plots of track-etch rate V_T versus etched track length for cellulose acetate etched with 6.25 N NaOH at 50°C.	... 69
21. Plots of track-etch rate V_T versus etched track length for mica etched with 40% HF at 35°C.	... 70
22. Distribution of the track lengths of the fission products from ^{252}Cf in mica.	... 75
23. Distribution of the track lengths of the fission products from ^{252}Cf in Lexan.	... 76
24. Distribution of the track lengths of the fission products from ^{252}Cf in cellulose acetate.	... 77
25. Constructed distribution curve for the track lengths of the fission products from ^{252}Cf in mica.	... 84
26. Constructed distribution curve for the track lengths of the fission products from ^{252}Cf in Lexan.	... 85
27. Constructed distribution curve for the track lengths of the fission products from ^{252}Cf in cellulose acetate.	... 86
28. Computed values of the energy-deposition rate (dE/dX) of a few individual fission products in Lexan plotted as a function of track length.	... 89

<u>Figure</u>	<u>Page</u>
29. Computed values of the energy-deposition rate (dE/dX) of a few individual fission products in cellulose acetate plotted as a function of track length. ...	90
30. Computed values of the energy-deposition rate (dE/dX) of a few individual fission products in mica plotted as a function of track length. ...	91
31. Dependence of track-etch rate V_T on the energy-deposition rate (dE/dX) in Lexan. ...	92
32. Dependence of track-etch rate V_T on the energy-deposition rate (dE/dX) in Lexan. ...	93
33. Dependence of track-etch rate V_T on the energy-deposition rate (dE/dX) in Lexan. ...	94
34. Dependence of track-etch rate V_T on the energy-deposition rate (dE/dX) in cellulose acetate. ...	95
35. Dependence of track-etch rate V_T on the energy-deposition rate (dE/dX) in mica. ...	96
36. Plot of the calculated stopping-power versus ion energy for mica. Energies E_1 and E_2 correspond to the lower and the higher energies of ^{28}Si ion at which the critical stopping-power is reached. ...	109
37. Plot of the calculated stopping-power versus ion energy for Lexan. ...	110
38. Plot of the calculated stopping-power versus ion energy for cellulose nitrate. ...	111

<u>Figure</u>	<u>Page</u>
39. Plot of the critical stopping-power versus the density for various solid dielectrics. ...	118
40. Track length versus energy curves for various ions in Lexan. The experimental points are from Tripier <u>et al.</u> ⁴⁶ ...	119
41. Track length versus energy curves for various ions in cellulose nitrate. The experimental points are from Tripier <u>et al.</u> ⁴⁶ ...	120
42. Plot of the computed track length versus mass number for the fission products from ²⁵² Cf in mica. ...	122
43. Plot of the computed track length versus mass number for the fission products from ²⁵² Cf in Lexan and cellulose acetate. ...	123

...

PREFACE

The thesis entitled "STUDIES ON HEAVY ION TRACKS IN SOLID DIELECTRICS" deals with the registration and measurement of the tracks of fission products from ^{252}Cf in three solid dielectric track detectors and the development of a theoretical method of computing the track length of any heavy ion in any solid dielectric of known molecular formula and density. Track-kinetics have been studied experimentally in detail to obtain information on (i) the dependence of track-etch rate on the energy-deposition rate (ii) the activation energy for bulk-etching and (iii) the different etching correction factors needed to obtain the "true" track length from the experimentally observed track length under a given set of etching conditions.

Chapter I introduces the earlier development track registration techniques and outlines the need of the present investigation.

Chapter II describes the details of the experimental methods and techniques for measuring the tracks due to fission products in mica, Lexan and cellulose acetate. The evaluation of the etching correction terms for obtaining the true track lengths from the observed ones, has also been discussed in this chapter.

In Chapter III, the experimental determination of the etch rates and the activation energies for bulk-etching have been described.

Chapter IV deals with the analysis of and a discussion on the experimental data.

Chapter V deals with the development of a theoretical method of computing the track length of a heavy ion of known energy, mass number and charge number in a solid dielectric of known molecular formula and density.

Chapter VI briefly summarizes the contribution to knowledge.

CHAPTER I

CHAPTER I

INTRODUCTION

In 1958, Young¹ reported that irradiation of lithium fluoride with fission fragments produced radiation-damaged areas around the path of the fragments. On chemical etching these areas formed pits which were visible under an optical microscope. In 1959, Silk and Barnes² found that when mica is irradiated with fission fragments, damaged regions, in the form of "tracks", could be observed by means of an electron microscope. These tracks were approximately 100 Å in diameter and practically linear. Later on, many other workers observed such tracks in thin films of different solid insulating material.³ In 1961, Price and Walker^{4,5} showed that the tracks formed initially in mica could be enlarged, breadth-wise, by immersing the irradiated mica in hydrofluoric acid.

The hydrofluoric acid dissolves the mica in the vicinity of the original charged-particle track and depending on the period of immersion, one can obtain tracks with diameters of the order of microns which can be observed under an optical microscope. Afterwards Fleischer and Price⁶⁻⁸ showed that similar optically observable tracks could be obtained by using appropriate chemical etching of irradiated samples of glasses, plastics and minerals. Since then considerable volume of work has been done by many investigators on various aspects of track formation and these have been summarized by Price and Fleischer⁹ in their review work.

A very important application of track formation in Nuclear Physics is the determination of the kinetic energy of a fast moving ion from the length of the track in a solid dielectric medium. Of all the available physical methods of kinetic energy determination, the only other method which give a permanent track of this type is the nuclear emulsion method. When a charged heavy ion passes through a uniform suspension of fine grained (diameter 0.2-0.4 μm) silver bromide in gelatin, the silver salt is affected along the path of the ion and its surroundings. By proper development procedure, which is similar to the development of an exposed photographic plate, one obtains tracks in the form of fine grains of metallic silver.¹⁰ There are some inherent drawbacks of the nuclear emulsion method which are avoidable with a solid dielectric

material. The composition of the nuclear emulsion is subject to fluctuations, the density of the material is dependent on the humidity of the surroundings, there may be local variations in the concentration of the silver bromide and there are distortions in the tracks during the humidification and the heating which is required during the development procedure. The tracks in a solid dielectric media like mica and Lexan are very stable and there is little uncertainty regarding the chemical composition of these media.

However, the usefulness of both the nuclear emulsions and the solid dielectric track detectors* is somewhat limited by the absence of a suitable theoretical equation which correlates the rate of energy loss of an ion in these media to the energy of the ion, the mass and nuclear charge of the ion, and the chemical composition of the medium. Without such relationships extensive experimental calibration procedures are required for every ion, which amount to almost an impossibility. In the case of nuclear emulsion, very empirical relationships have been proposed between the observed track length and the initial energy of a heavy ion by Heckman et al.,¹¹ while for SDTDs no reliable empirical relationship is available. The major hurdle in deducing an empirical relationship in this case is the known observation that in the high density SDTDs

*A solid dielectric track detector will be hereafter designated by SDTD.

a heavy ion ceases to produce any track much before it has lost all its kinetic energy.¹²

Very recently, Mukherji and Srivastava^{13a,b} have given semi-empirical equations based on a stopping-power equation of Bohr,¹⁴ by means of which energy-loss rate and total penetration depths or ranges of heavy ions can be calculated in any elemental medium. These equations have been extended by Mukherji and Nayak¹⁵ to the case of energy-loss and range of heavy ions in complex media like polyethylene, mylar, tissue material and nuclear emulsion and excellent agreement has been obtained between the calculated ranges and the experimental ranges reported by other workers. The present work aims at (a) experimental determination of the average track length of fission products from ^{252}Cf in mica, Lexan and cellulose acetate and (b) obtaining suitable theoretical equations for the energy-loss rates of heavy ions in SDTD and a suitable computational method for track length estimation. The main purpose of the experimental work has been to investigate the various etching corrections which have to be applied to the observed track lengths under a given set of conditions to obtain the 'true' track lengths, which have not received sufficient attention in the earlier experimental work.

CHAPTER II

CHAPTER II

EXPERIMENTAL MEASUREMENT OF FISSION PRODUCT TRACK LENGTHS IN MICA, LEXAN AND CELLULOSE ACETATE

II.1 GENERAL PROCEDURE

Fission products from ^{252}Cf were allowed to pass through collimator holes and enter the desired solid dielectric track detector (i.e., mica or Lexan or cellulose acetate) at a pre-determined angle of incidence. This was done inside a vacuum chamber. After the irradiation the SDTD was removed and treated with the appropriate chemical etchant under the proper conditions to develop the tracks. Finally the projected track lengths on the surface plane of the SDTD were measured by means of an optical microscope fitted with a calibrated eye-piece micrometer. The observed track lengths were corrected for over-etching and surface dissolution, for which detailed

experiments had to be done for obtaining the time for complete etching. Simultaneous experiments have been done on etch rate measurement at different points on the track to determine the dependence of track-etch rate at any point on the energy-deposition rate at that point. The bulk or general-etch rates have been measured at different temperatures to obtain the activation energies. The details are given in Chapter III.

II.2 SOURCE OF FISSION PRODUCTS

Experimental determination of track lengths in SDTD normally requires a heavy ion accelerator so that heavy ions of accurately known kinetic energies are available. In the absence of such a facility, ^{252}Cf which undergoes fission spontaneously, has been used as a source of heavy ions. The drawback of such a method is that the fission products have different masses, nuclear charges and kinetic energies and there would be tracks of varying lengths corresponding to them in the SDTD. One can interpret the experimental track lengths in terms of the "averaged" track length of a heavy ion of the mass and nuclear charge of the "average" fission product. ^{252}Cf has a half-life of 2.55 years. The mass yields of the fission products are well known¹⁶ and are shown in Table II.1. The kinetic energies of the fission products as determined by Schmitt et al.¹⁶ using solid state detectors are also shown in Table II.1. For theoretical calculation of the track lengths, which follows later, it is necessary to know the velocity of

TABLE II.1 ^{252}Cf spontaneous fission data.

FISSION PRODUCT MASS A	FISSION FRAGMENT MASS A'	MOST PROBABLE CHARGE Zp	KINETIC ENERGY E (MeV)	VELOCITY V (10^8 cm/sec.)	MASS YIELDS (%)
1	2	3	4	5	6
89.0	90.00	35.0	108.00	15.26	0.40
90.0	91.20	35.4	108.00	15.17	0.50
91.0	92.50	35.8	108.00	15.09	0.50
92.0	93.50	36.2	108.00	15.01	0.70
93.0	94.50	36.5	108.00	14.93	0.90
94.0	95.50	36.9	108.00	14.85	1.00
95.0	96.00	37.7	108.00	14.77	1.25
96.0	97.00	38.1	108.00	14.69	1.50
97.0	98.00	38.5	108.00	14.61	1.75
98.0	99.00	38.9	107.50	14.51	2.25
99.0	100.00	39.3	108.00	14.47	3.10
100.0	101.00	39.6	108.00	14.39	3.50
101.0	102.50	40.2	108.00	14.32	4.40
102.0	103.50	40.6	108.00	14.25	5.45
103.0	104.50	41.0	108.00	14.18	5.60
104.0	105.50	41.4	108.00	14.11	5.85
105.0	106.50	41.8	107.50	14.01	6.00 ± 0.20
106.0	107.50	42.2	107.50	13.95	5.75 ± 0.20
107.0	109.00	42.7	106.50	13.82	6.60 ± 0.20
108.0	110.00	43.1	106.00	13.72	6.30 ± 0.20
109.0	111.00	43.5	105.50	13.63	5.40
110.0	112.00	43.9	105.00	13.53	5.00
111.0	113.00	44.3	104.75	13.45	4.95
112.0	114.00	44.7	104.50	13.38	4.40
113.0	115.00	45.0	104.00	13.29	3.80
114.0	116.00	45.4	103.50	13.20	3.30

(Contd.)

TABLE II.1 (Contd.)

1	2	3	4	5	6
115.0	118.50	45.8	102.50	13.08	2.80
116.0	119.75	46.3	102.00	12.99	2.20±0.10
117.0	121.00	46.8	101.00	12.87	1.40
118.0	121.50	47.0	100.50	12.78	1.10
119.0	122.50	47.3	99.50	12.66	0.70
120.0	122.75	47.5	99.00	12.58	0.45
121.0	123.50	47.7	98.00	12.46	0.25
122.0	124.75	48.2	95.00	12.22	0.25
123.0	125.50	48.5	94.50	12.14	0.05
124.0	126.00	48.7	93.75	12.04	0.02
127.0	128.25	49.6	92.50	11.82	0.20
128.0	129.25	50.0	93.25	11.82	0.40
129.0	130.00	50.3	94.00	11.82	0.50
130.0	131.00	50.6	94.00	11.78	1.05
131.0	132.00	51.0	93.00	11.67	1.75
132.0	132.80	51.3	92.25	11.58	2.30±0.10
133.0	133.75	51.7	91.25	11.47	2.80
134.0	135.10	52.2	89.85	11.34	3.50
135.0	136.25	52.7	88.50	11.21	4.00
136.0	137.25	53.1	87.00	11.08	5.00
137.0	138.30	53.5	86.25	10.99	5.50
138.0	139.50	54.0	84.50	10.84	5.30±0.15
139.0	140.60	54.4	83.25	10.72	5.55
140.0	141.50	54.7	82.50	10.63	5.75
141.0	142.60	55.1	81.25	10.51	5.90±0.20
142.0	143.75	55.6	80.10	10.40	5.70
143.0	144.75	56.0	79.25	10.31	5.75
144.0	145.75	56.3	78.00	10.19	5.70
145.0	146.90	56.8	77.00	10.09	5.20
146.0	148.00	57.2	75.70	9.97	4.60

(Contd.)

TABLE II.1 (Contd.)

1	2	3	4	5	6
147.0	149.00	57.6	75.75	9.94	4.50
148.0	150.10	58.0	73.50	9.76	3.75
149.0	151.25	58.5	71.75	9.61	2.75
150.0	152.25	58.9	70.60	9.50	2.40
151.0	153.25	59.3	69.50	9.40	2.10±0.10
152.0	154.50	59.7	68.50	9.30	2.00
153.0	155.60	60.2	67.25	9.18	1.50
154.0	156.75	60.6	66.00	9.07	1.00
155.0	157.80	61.0	64.50	8.93	0.85
157.0	160.00	61.9	62.00	8.70	0.50
163.0	166.65	63.8	55.00	8.05	0.15

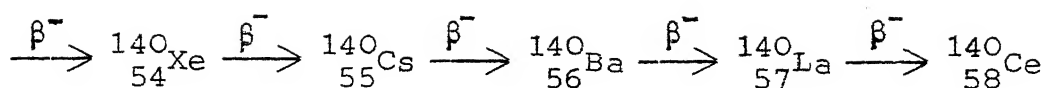
each fission product as well the nuclear charge associated with it. The velocity V of a fission product of mass number A is obtained from its kinetic energy $E(\text{MeV})$:

$$\frac{1}{2} A m_0 V^2 = E \times 1.6 \times 10^{-6} \text{ erg} \quad (2.1)$$

or
$$V = 13.85 \times 10^8 \sqrt{E/A} \text{ cm/sec} \quad (2.2)$$

where $m_0 = 1.67 \times 10^{-24} \text{ g}$ is the mass of a nucleon. The value of V , in units of 10^8 cm/sec , are also shown in Table II.1.

During fission, a fission product of mass number A is formed with nuclear charges of different values. For example, the products of mass number 140 may consist of the following chain:



If the independent yield or the yield of a product of mass number A and nuclear charge Z , as formed directly from the fission events, is designated by $Y_A(Z)$, then the probability of formation of a product of mass number A and nuclear charge Z within a mass chain is given by

$$P_A(Z) = \frac{Y_A(Z)}{\sum_Z Y_A(Z)}, \quad (2.3)$$

$P_A(Z)$ is known as the independent fractional chain yield of a product of nuclear charge Z in a chain of mass A . The nuclear charge associated with a fission product of mass number A may be taken as the weighted average of the nuclear charges of the various isobars of mass number A :

$$\bar{Z}(A) = \sum_Z P_A(Z) Z \quad (2.4)$$

If the curve of $P_A(Z)$ versus Z is a symmetrical, Gaussian-type, curve, then there is a most probable nuclear charge $Z_p(A)$ at which the peak of the curve occurs. In this case $Z_p(A)$ is identical with $\bar{Z}(A)$ and one can associate this nuclear charge with a fission product of mass number A . For a heavy fragment of mass number A_H ($A_H > 126$ in the case of californium), the most probable charge $Z_p(A)$ is given by Mukherji's prescription:¹⁷

$$Z_p(A_H) = \frac{A_H}{2.587} \quad \dots(2.5)$$

while for the complementary light fragment A_L , it would be

$$Z_p(A_L) = 98 - \frac{A_H}{2.587} , \quad (2.6)$$

since the sum of the two nuclear charges should be equal to the nuclear charge of $^{252}_{98}\text{Cf}$. As Eqs. (2.5) and (2.6) give the most probable charges for the fission fragments, to obtain the corresponding values for the fission products, it is necessary to determine first the mass number of the precursor fragment which had, by prompt neutron emission, yielded the particular fission product under consideration. This has been done with the help of the data of Schmitt et al.¹⁸ In Table II.1 are listed the precursor fragment mass number A' corresponding to a given product of mass number A . The most probable charge $Z_p(A)$ for a fission product of mass number A was then obtained, if the product is a heavy one, with $A_H = A'$ in Eq. (2.5); for a light product of mass number A , $Z_p(A)$ was obtained from Eq. (2.6) with $A_H = (252 - A')$. These values of Z_p are also listed in Table II.1.

II.3 CHARACTERISTICS OF THE SOLID DIELECTRIC TRACK DETECTORS

II.3.1 General

When a heavy ion passes through a solid insulator, considerable energy is deposited on the atoms on and around the trail. The local disordered structure is thus associated with large amount of free energy, and hence, thermodynamically, should be

much more reactive than the undamaged portions. Thus, when such an irradiated sample is placed inside a chemical etchant, the damaged trail is etched at a faster rate than the undamaged portions.

In the case of mica, appropriate period of etching of the damaged trails with hydrofluoric acid of the proper concentration yields dark cylindrical tracks easily visible under an optical microscope using bright field illumination. However, etching does not always lead to a faithful magnification of the original damaged track. Glasses usually give conical pits.⁶ By proper choice of etching condition it is possible to modify the shape of the final etch-figures. For example, zircon gives shallow surface pits⁸ when etched with a strong hydroxide solution while boiling phosphoric acid at 500°C produces long and narrow tracks.¹⁹ Figure 1 shows photomicrographs of the tracks in different SDTD obtained from the present experiments.

II.3.2 Track Geometry

An etchant usually attacks both the radiation-damaged area as well as the undamaged area, though the two rates may be appreciably different. If V_T is the etch rate along the heavy ion track and V_G is the bulk-etch rate or the rate of etching along the undamaged portion, then there would be a critical angle of incidence ϕ_c for the heavy ion. If the ion enters at an angle less than ϕ_c then the track becomes

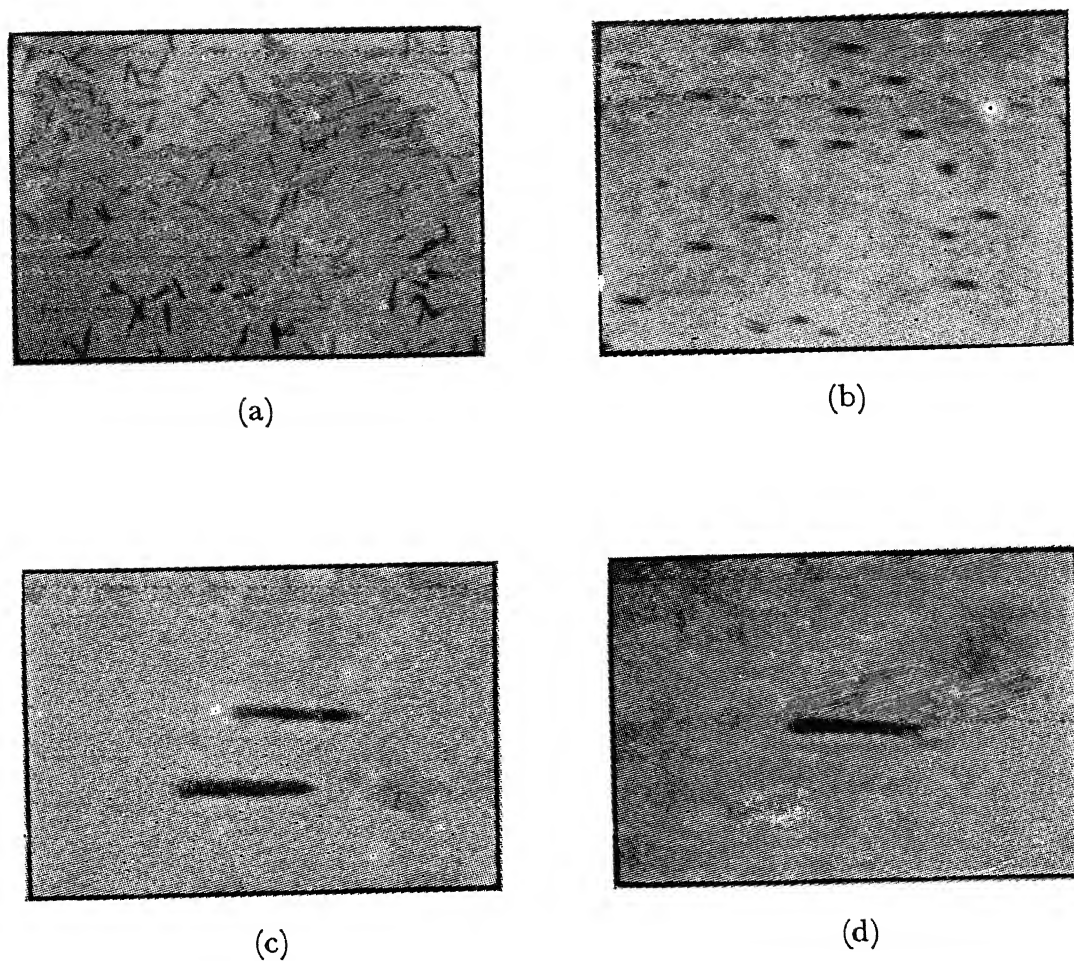


Fig. 1: Photomicrograph of ^{252}Cf fission product etched tracks in different solid dielectric track detectors.

- (a) Uncollimated fission product tracks in Lexan.
- (b) Collimated fission product tracks in mica entered at an angle of 30° with respect to the surface plane.
- (c) Two parallel tracks in cellulose acetate at a magnification of 1250.
- (d) Single track in Lexan with magnification of 1250.

completely erased due to bulk-etching. It has been shown by Fleischer and Price²⁰ that all tracks making an angle less than $\theta_c = \sin^{-1} (V_G/V_T)$ would fail to register. The shape of the track largely depends upon the magnitudes of V_T and V_G and the final shape may not be simply an enlarged version of the initial submicroscopic trail. If $V_T \gg V_G$ then the tracks look cylindrical, as in the case of mica while if V_T is not exceptionally large compared to V_G then conical tracks are formed as in the case of Lexan and cellulose acetate.

Some physical and chemical properties of the three SDTDs are listed in Table II.2.

II.4 EXPERIMENTAL TECHNIQUE

II.4.1 Target Preparation

(a) Mica: Muscovite mica was cleft into thin transparent sheets of thickness approximately 200 μm . These sheets were cut into rectangular pieces of three different sizes: 4 x 1.5 cm^2 , 5 x 1.5 cm^2 and 6 x 1.5 cm^2 . These foils were washed thoroughly with de-ionized water and then etched with 40% HF at 35°C for 100 minutes. This pre-etching enlarges the primordial tracks to a diameter of about 10 μm , which can easily be distinguished from the fission product tracks registered during irradiation. These foils were washed in running tap water for 5 minutes and then 5 times with de-ionized water, once with acetone and, finally, were allowed to dry. These

TABLE II.2

Properties of mica, Lexan, and cellulose acetate detectors

Properties	Mica (Muscovite mica)	Lexan (Bisphenol-A polycarbonate)	Cellulose acetate (Photo-film base)
1. Composition	$\text{KAl}_3\text{Si}_3\text{O}_{10}(\text{OH})_2$	$\text{C}_{16}\text{H}_{14}\text{O}_3$	$\text{C}_{10}\text{H}_{14}\text{O}_7$
2. Specific gravity	2.93	1.20	1.32
3. Foil thickness	200 μm	500 μm	125 μm
4. Uniformity	fair	good	good
5. Clarity	clear	clear	clear with light blue tinge
6. Surface view	some pits and scratches	smooth, no background pits	smooth, no background pits
7. Chemical etchant	Hydrofluoric acid	Aqueous and alcoholic NaOH	Aqueous NaOH
8. Pre-etching	40% HF 35°C/100 min.	nil	nil
9. Critical angle* of incidence(θ_c)	4°16'	3°43'	3°05'
10. Critical rate of energy loss (dE/dX) _c (MeV/mg/cm ²)	13.0	5.0	8.0 "

*Determination of the critical angle of incidence (θ_c) has been described in Appendix A.

foils were kept between layers of soft-papers in covered plastic boxes.

(b) Lexan: Lexan (Bisphenol-A polycarbonate) sheets were obtained from the U.S.A. through the courtesy of Dr. B.K. Kothari, University of California, San Diego, La Jolla, California. Lexan sheets of thickness $500\text{ }\mu\text{m}$, free from tracks and pits, were used for irradiation. These sheets were cut into rectangular pieces of the same size as that of the mica foils.

(c) Cellulose acetate: Cellulose acetate (Photo-film base) strips were obtained most conveniently by removing the photographic emulsion from photographic films (16 mm, ORWO, NP-7, Panchromatic). About one metre of photographic film was cut from a film-roll and was fixed in sodium thiosulphate solution. This makes the film transparent with a sky-blue tinge. This was treated with hot sodium hydroxide solution to remove the gelatin coating. This film-base was washed thoroughly in running tap water to remove all NaOH. Finally, it was washed with de-ionized water and was dried at room temperature.

Microanalysis of this substance shows that its chemical composition is the same as that of cellulose acetate ($\text{C}_{10}\text{H}_{14}\text{O}_7$). Its density was found to be 1.32 g/cm^3 and the thickness roughly $125\text{ }\mu\text{m}$.

II.4.2 Mounting and Bombardment

As shown in Fig. 2, the detector foil (SDTD) was fixed on the largest face of a triangular perspex block. Three perspex blocks were in use with angles between the base and the hypotenuse equal to 15° , 30° and 45° , and the appropriate one was used depending on the angle at which the fission product, after collimation, was desired to penetrate the SDTD. The mounted perspex block was attached to the collimator platform. The collimator consists of an aluminium block, containing parallel holes of $1/16$ inch diameter and 1 inch length in an area of 4 square centimeters. A circular ^{252}Cf -source on platinum backing yielding 4.6×10^4 fissions per minute was placed at a distance of about 4 to 6 cm from one face of the collimator, while the SDTD placed on the perspex block, was in front of the other face. The source, collimator and SDTD were properly aligned. The whole set-up was then placed inside a vacuum chamber. The top cover of the vacuum chamber had a Wilson seal through which a steel rod with a rotating cap was inserted. To the lower end of this rod was attached a thick aluminium guard foil which was positioned between the ^{252}Cf source and the collimator. The chamber was evacuated to a pressure of $\sim 10^{-6}$ cm of mercury and then the aluminium guard foil was turned away by rotation of the rod from outside. This ensures that the fission product energy was not degraded by the air inside the chamber before reaching the SDTD during the

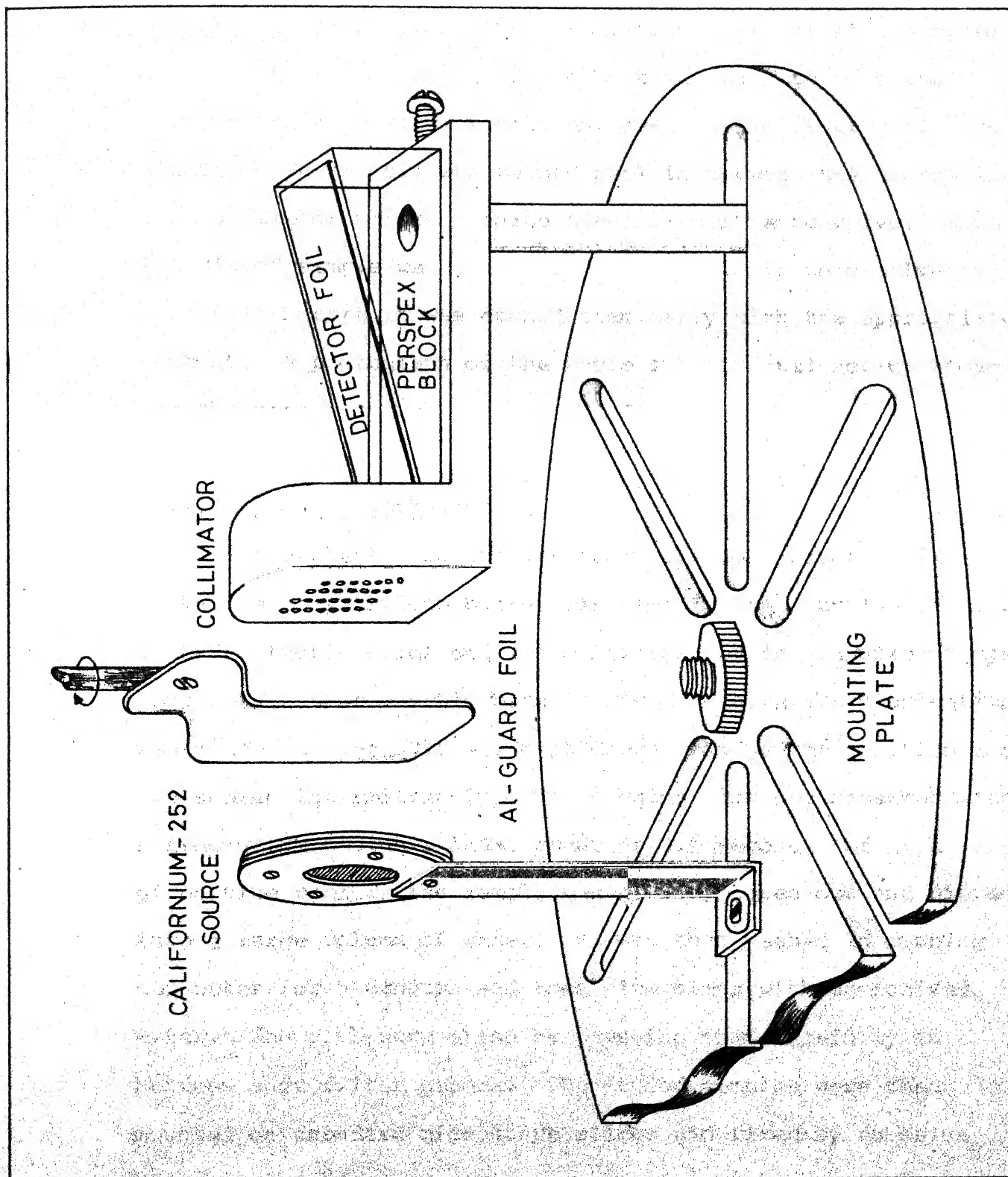


Fig. 2. Diagram of the irradiation assembly showing the positions of the source, guard foil, collimator and the detector foil.

process of evacuation. The irradiation time was of the order of 24-36 hours, which was found by trial runs to give the optimum track density without any overlapping of tracks. The aluminium guard foil was turned back in between the source and the collimator before opening the air-admittance valve. Each irradiated sample was taken out and wrapped in thin polyethylene film before it was etched chemically with the appropriate etchant. A photograph of the whole experimental set-up showing the vacuum system is given by Fig. 3.

II.4.3 Etching Technique

The etchant solution was taken inside a covered glass beaker (a polyethylene beaker was used for the etching of mica in hydrofluoric acid) and was maintained at the required temperature in a thermostatic bath (maximum temperature fluctuation was $\pm 0.5^{\circ}\text{C}$). The SDTD was kept dipped inside the solution and was shaken intermittently. The etching time was measured with a stop-watch having a least count of 0.1 second. After a given time period, the sample was quickly taken out and dipped into a large volume of water. It was then washed in running tap water for 5 minutes and then five times with de-ionized water. The foils were dried by pressing them carefully in between soft filter papers. The etched samples were then mounted on standard microscope slides and fixed by adhesive tapes at the edges.

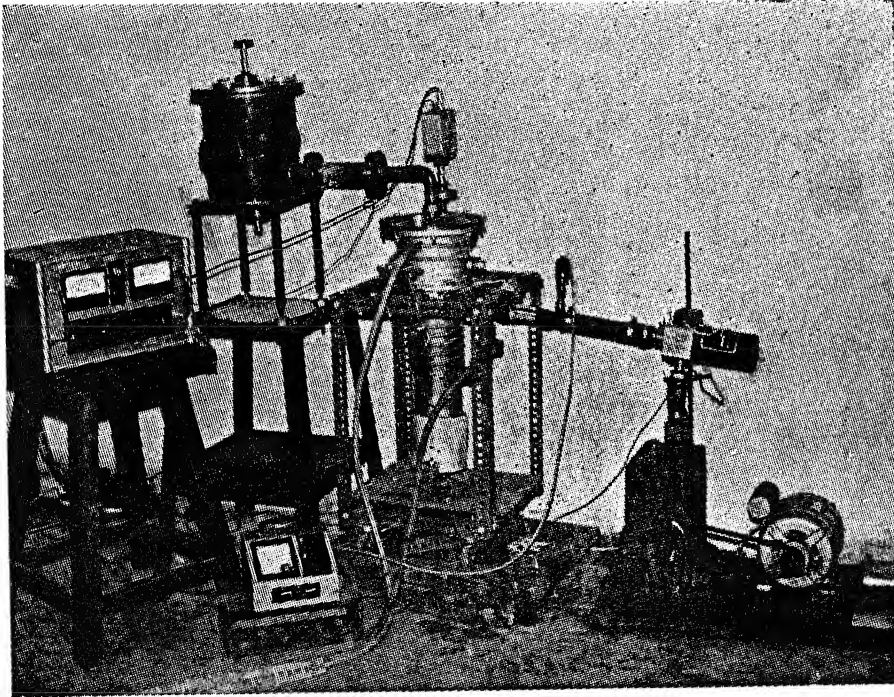


Fig. 3: Photograph of the irradiation chamber attached with the vacuum system.

For mica, Lexan, and cellulose acetate the etchants used were 40% HF, 6.25 N NaOH + ethanol (1:1) and 6.25 N NaOH respectively. To find out the time ' t_c ' required for complete etching of tracks, the following procedure was adopted:

The irradiated surface of the foil was demarcated into a few squares by scratching with a pin. The foil was then etched for a small period of time, then washed, dried, and the tracks within these squares were scanned with a microscope. At least 5 to 10 tracks were present in each of those marked squares, and their observed track lengths were measured. The process of etching, washing and microscopic observation was repeated, with accurate noting of the etching time (~ 5 minutes each time), till past the maximum track length. In the case of mica, the track lengths remained sensibly constant much beyond the complete etching time. In this case, the time t_c was noted for the first attainment of the maximum observed track length. But for Lexan and cellulose acetate the observed track length reached a maximum at time t_c and then started decreasing.

For all the three solid dielectrics the time t_c has been determined at different temperatures in the appropriate etchants. The results are listed in Table II.3. The etching conditions given in Table II.3, were used to develop fission product tracks in various dielectric materials for track length measurement. A list of solid dielectrics and etchants with the suitable etching conditions has been given by Fleischer and Hart.²¹

TABLE II.3

Complete etching time t_c at different temperatures for different dielectrics obtained from Figs. 14 and 15

SDTD	ETCHANT	TEMP. (°C)	TIME t_c (min.)
1. Mica	40% HF	35	15
2. Lexan	(i) 6.25 N NaOH + Ethanol(1:1)	33	100
	(ii) 6.25 N NaOH + Ethanol(1:1)	25	180
	(iii) 6.25 N NaOH	55	50
3. Cellulose acetate	(i) 6.25 N NaOH	70	5-7
	(ii) 6.25 N NaOH	50	60

II.5 MICROSCOPIC OBSERVATION

All the samples were viewed through a transmitted-light microscope "ERGAVAL" (VEB Carl Zeiss JENA, G.D.R.) at a magnification of 1056. For precise measurement of track-etch rate and track diameter a still higher magnification of 2560 was used. An Erma* eye-piece micrometer disc (1.0 cm divided into 100 divisions) was used for all the measurements. The eye-piece micrometer scale was calibrated against a standard Erma stage micrometer (0.1 cm divided into 100 divisions) for all objectives. The calibration procedure is as follows:

*Manufactured by Erma Optical Co., Japan.

II.5.1 Calibration of Eye-Piece Micrometer

The eye-piece micrometer divisions were calibrated in terms of microns (10^{-4} cm) using a standard Erma stage micrometer. The stage micrometer was placed on the platform of the microscope and was focused with objectives of different magnifications. The microscope has a built-in magnification of 1.6. The minimum number of divisions on the eye-piece micrometer which coincided with an integral number of divisions on the stage micrometer, was noted in each case. All observations were done with an eye-piece of stated magnification of 16. If N_1 is the number of eye-piece scale divisions which coincided with N_2 divisions on the stage micrometer scale then the "true" objective magnification M is given by Eq. (2.7):

$$M = 6.25 \left(\frac{N_1}{N_2} \right) \quad \dots(2.7)$$

At a particular objective magnification 'M' the length 'f' (in μ m) which corresponds to one division of eye-piece micrometer can be calculated from Eq. (2.8):

$$f = 62.5 \left(\frac{1}{M} \right) \quad (2.8)$$

The results of the calibration of the eye-piece micrometer are listed in Table II.4.

II.5.2 Scanning Traversal

For track length measurements, the samples were scanned at a magnification of 1056, since at the highest magnification,

TABLE II.4

Calibration of the eye-piece micrometer for track length measurement at different magnifications.

Stated objective magnification	Number of				True objective magnification M	True over-all magnification	f*
	Stated over-all magnification	eye-piece divisions N ₁	micrometer divisions	stage divisions N ₂			
I	II	III	IV	V	VI	VII	
3.2	81.92	11	20	3.4375	88	18.1	
10.0	256	16	10	10.0	256	6.25	
40.0	1024	33	5	41.25	1056	1.515	
100.0	2560	16	1	100.0	2560	0.625	

*f denotes the length in μ m of an object which corresponds to one division of eye-piece micrometer at the stated overall magnification shown in column II of the table above.

i.e., 2560, the edges of the track become fuzzy and eyes get strained during observation of thousands of tracks.

A microscope stage of the type K4E (Carl Zeiss) was used with coaxial pinion heads for displacing the sample in the cross direction (x-axis) and in the longitudinal direction (y-axis). Millimetre scales with verniers in both x- and y-axes permit the location of any point object accurately.

The area scanning was done in strips equal in width to the diameter of the field of view. The procedure involved continuous focusing and de-focusing of the sample surface by means of the fine focus knob while scanning the sample. All the samples were scanned by first focusing their left edges and traversing them along the y-axis, keeping the x-axis fixed till the back edge was reached. After moving to a field of view towards the right hand side along the x-axis, the samples were traversed in opposite direction along the y-axis upto the front edge. Again shifting a field of view in the x-direction and traversing in the y-direction and so on till the right edge comes into view.

II.6 TRACK LENGTH MEASUREMENT

The collimated fission products formed parallel tracks in solid dielectrics. The eye-piece micrometer scale was aligned with these tracks by simply rotating the eye-piece and making one track lie along the micrometer scale. Since all

the tracks are parallel every track could be aligned along the horizontal scale of the eye-piece by moving the platform along the x- and y-directions.

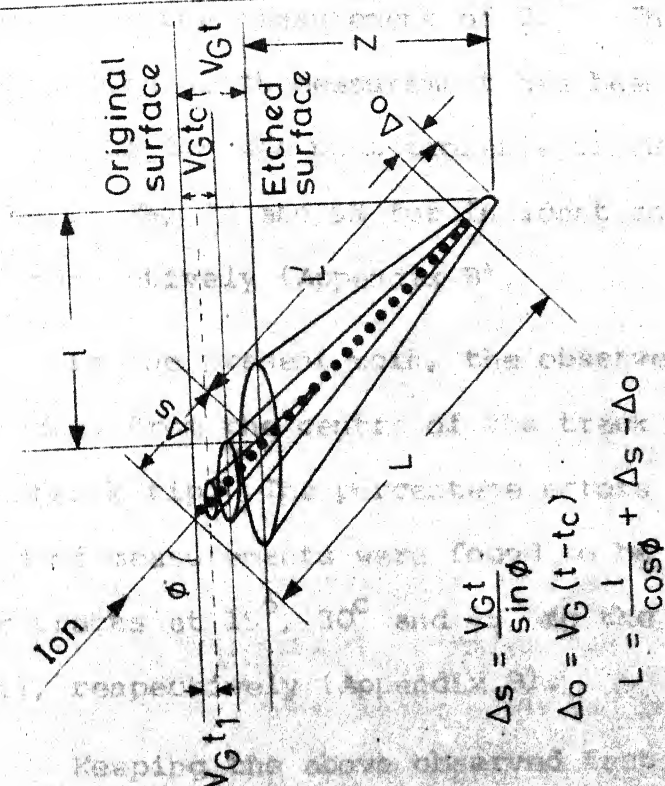
II.6.1 Measurement of Observed Track Lengths

In the case of mica, the etched tracks were found to be cylindrical with rounded tips at both ends. The observed track length was measured from the centre of one tip to the centre of the other tip. Conical tracks were observed in Lexan and cellulose acetate. The intersection between a conical track at an angle to the surface and the etched surface is an ellipse with the track position shifted away from the centre towards the track tip, as shown in Fig. 4. The amount of shift can not be measured directly but can be calculated from the equations given by Price and Fleischer.⁹ They have correlated the 'true' track length L with the directly measurable quantities Z , $V_G t$ and ϕ :

$$L = (Z + V_G t) / \sin \phi \quad (2.9)$$

where Z is the depth of the track tip below the etched surface, ϕ is the dip angle and $V_G t$ is the thickness of the material dissolved out in time t as shown in Fig. 4.

In the present experiment the dip angle ϕ is known and V_G was determined accurately as described in Chapter III. For the determination of the true track length using Eq. (2.9), the value of Z has to be measured directly. Unfortunately,



(b) PLASTICS

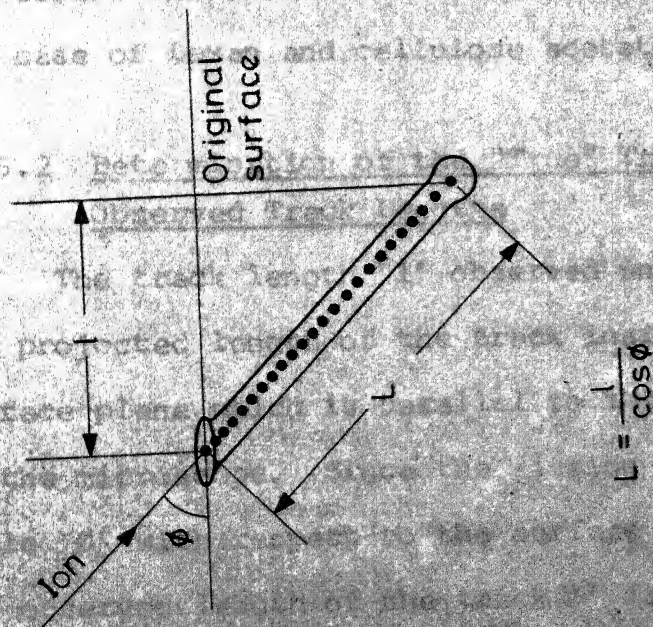


Fig. 4. Schematic diagram showing track geometry:

- (a) in mica with a negligible bulk-etch rate V_G perpendicular to the surface plane, and
- (b) in plastics with a finite V_G .

in track length measurement, the largest part of the error comes from the measurement of z .²² The error which is associated with depth measurement has been estimated with our microscope for the most probable track in Lexan and is found to be 13.6%, 7% and 5% for incident angles of 15° , 30° and 45° respectively (Appendix B).

In the present work, the observed track length was measured from the centre of the track ellipse to the end of the track tip. The percentage errors associated with this kind of measurements were found to be 4.60%, 1.40% and 0.70% for tracks at 15° , 30° and 45° to the surface plane of the foil, respectively (Appendix B).

Keeping the above observed fact in mind, it was decided to measure the observed track length from "centre to tip" in the case of Lexan and cellulose acetate.

II.6.2 Determination of the "True" Track Lengths from the Observed Track Lengths

The track length ' l ' observed under the microscope is the projected length of the track inside the dielectric on its surface plane which is parallel to the plane of the platform of the microscope. Since the fission products enter at a known angle ' ϕ ' with respect to the surface plane of the dielectric, the observed length of the track L' is given by

$$L' = \frac{l}{\cos \phi} \quad (2.10)$$

In Fig. 4 are shown the geometry of the track. The true track length L in plastics is different from L' owing to two reasons: (a) bulk-etching and (b) over-etching.

(a) Bulk-etching correction (Δ_s): As has been mentioned earlier, the etchant attacks both the radiation-affected as well as the radiation-unaffected areas. At a particular temperature and concentration of the etchant, the general or bulk-etch rate V_G is constant while the track-etch rate V_T is always greater than V_G , but varies at different points on the track owing to the variation in the energy-deposition rate at these points. Since a finite etching time t_1 is required for enlarging the track diameter to the lower limit of visibility, the etchant has time to dissolve out some amount of the dielectric from the surface.^{23,24} As shown in Fig. 4(b), $V_G t_1$ is the thickness of the surface layer removed in time ' t_1 ' of etching, the length of the track which is consequently removed is equal to $V_G t_1 / \sin \phi$. Assuming that a time ' t_c ' is just the time necessary to reveal upto the end of the track, the "true" track length would be given by

$$L = \frac{l}{\cos \phi} + \frac{V_G t_c}{\sin \phi} \quad (2.11)$$

where l is the observed projected track length on the surface plane.

However, since in order to determine the time for complete etching t_c , it is necessary to etch for some more time, some

correction has to be made for over-etching.

(b) Over-etching correction (Δ_0): If the total time of etching is t and the time for complete etching is t_c then during the period $(t-t_c)$ the track would get extended inside the dielectric along the track direction by an amount $V_G(t-t_c)$. Thus, the projected track length would be related to the true track length by

$$L = \frac{l}{\cos \phi} + \frac{V_G t}{\sin \phi} - V_G(t-t_c) \quad (2.12)$$

From Eq. (2.12) it is clear that for the determination of the true track length, it is necessary to determine experimentally both l , V_G and t_c . If $t > t_c$ then, since L is constant, a plot of L versus time would give t_c . In the next chapter, experimental details for the determination of V_G , V_T etc are described.

CHAPTER III

CHAPTER III

DETERMINATION OF ETCH RATES

As explained earlier in Chap. II, Sec. II.6.2, value of the bulk-etch rate V_G is necessary for obtaining the 'true' track length from the observed ones. Further, the temperature dependence of the bulk-etch rate provides a simple method for determining the activation energies for bulk-etching. The methods of measuring the bulk-etch rate and the results are dealt with in this chapter.

To obtain the exact dependence of the track-etch rate on the energy-deposition rate (dE/dX), the track-etch rate V_T has been measured as a function of the etched track length. The theoretical values of the energy-deposition rate at any point on the track has been calculated as explained in Chapter V. From these, the dependence of V_T on (dE/dX) has been explored.

III.1 MEASUREMENT OF BULK-ETCH RATE V_G

The bulk-etch rate V_G is defined as the speed with which the undamaged regular material of the detector foil is dissolved away by an etchant. The bulk-etch rate is isotropic in most of the plastics.⁹

In the present work the bulk-etch rates have been measured by two techniques:

- (a) Gravimetric technique
- and (b) Track-diameter technique.

III.1.1 Gravimetric Technique

This method is based on the measurement of the weight lost by a sample foil of known area after it is etched by the etchant solution of known concentration for a given period of time at a given temperature.

The detector foil was cut into rectangular pieces and the surface area 'S' was accurately measured. Each foil was then weighed on a semi-micro balance. It was then dipped inside the desired chemical etchant kept at a constant temperature in a thermostatic bath. The detector foil was attacked by the etchant uniformly normal to the two faces. After every 30 minute period of etching, the foil was washed, dried and weighed. The loss of weight ' Δm ' in grams was noted against the etching time 't' in minutes. Then the bulk-etch rate is given as:

$$V_G = \frac{\Delta m}{2S \rho t} \times 10^4 \text{ } (\mu\text{m}/\text{min}) \quad (3.1)$$

where, ρ is the density of the detector foil in g/cm^3 , and S is the surface area of the foil in cm^2 .

Here, the contribution of the material etched out from the side faces of the foil has been neglected, because of the thinness of the foil. In the present investigation, the weight-loss due to the etching of side faces is only about 1-3% of the total weight-loss.

The results obtained for Lexan and mica foils are shown in Fig. 5 and Fig. 6 respectively.

III.1.2 Track-Diameter Technique

The increase of track-diameter with etching time gives a measure of the bulk-etch rate along the surface plane. Actually the bulk-etch rate is equal to one-half of rate of increase of the diameter of a track.

If 'd' in μm , is the diameter of a track after etching for a time t in minutes, then

$$d = 2 V_G t \quad (3.2)$$

$$\text{or } V_G = \frac{1}{2} \left(\frac{d}{t} \right) \quad (3.3)$$

The gravimetric method is more convenient for higher bulk-etch rates, while the track-diameter method is reliable only upto

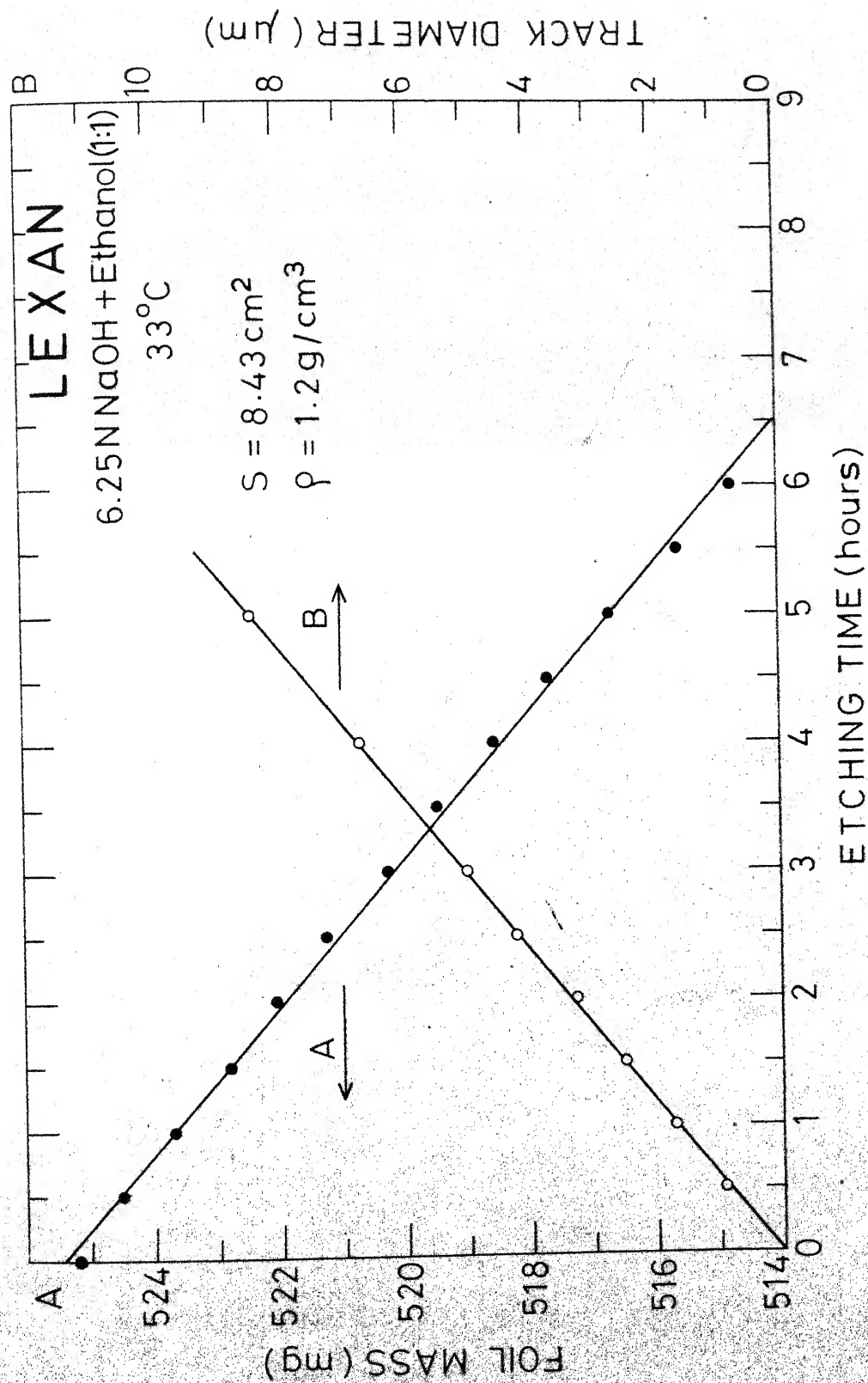


Fig. 5. Plot of the etching time as a function of (A) the weight of the Lexan foil and (B) the track diameter.

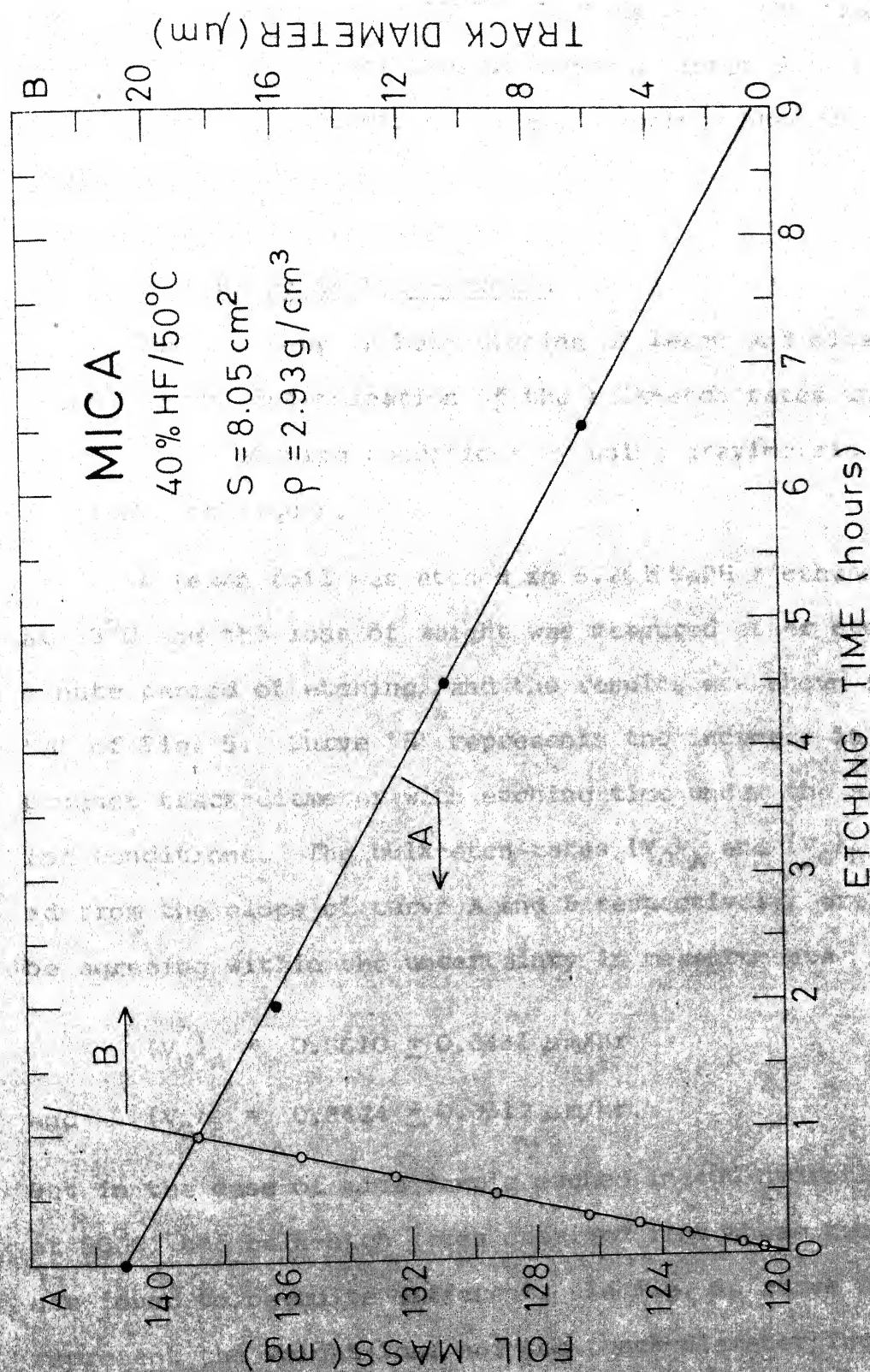


Fig. 6. Plot of the etching time as a function of (A) the weight of the mica foil and (B) the track diameter.

diameters of about $10\text{ }\mu\text{m}$.²⁶⁻²⁸ In this range the track-diameter versus etching time curve remains linear and not affected by saturation effects which are sometimes observed at larger diameters.²⁶

III.1.3 Isotropy in Bulk-Etching

The isotropy in bulk-etching of Lexan and mica has been tested by the determination of the bulk-etch rates under a given set of etching conditions by using gravimetric and track-diameter techniques.

A Lexan foil was etched in 6.25 N NaOH + ethanol (1:1) at 33°C and the loss of weight was measured after every 30-minute period of etching, and the results are shown in curve 'A' of Fig. 5. Curve 'B' represents the increase in fission product track-diameter with etching time under the same etching conditions. The bulk-etch rates $(V_G)_A$ and $(V_G)_B$, obtained from the slope of curve A and B respectively, are found to be agreeing within the uncertainty in measurements

$$(V_G)_A = 0.8610 \pm 0.0431\text{ }\mu\text{m/hr}$$

$$\text{and } (V_G)_B = 0.8424 \pm 0.0312\text{ }\mu\text{m/hr}.$$

But in the case of mica sample etched in 40% hydrofluoric acid at 50°C , the bulk-etch rates obtained from these two methods are found to be quite different. In Fig. 6, curve A and B represent the weight-loss and the track-diameter increase with

etching time respectively. It was found that the bulk-etch rate normal to the surface $(V_G)_A$ is about twenty times slower than the rate of etching along the surface $(V_G)_B$. For mica the results are as follows:

$$(V_G)_A = 0.4800 \pm 0.0431 \mu\text{m/hr}$$

and $(V_G)_B = 9.3600 \pm 0.0312 \mu\text{m/hr}.$

The above observations indicate that the bulk-etch rate is isotropic in the case of Lexan, whereas it is anisotropic in the case of mica.

III.2 TRACK-DIAMETER KINETICS

The information inherent in the diameters of etch-pits was first utilized by Fleischer and Price,²⁰ in 1964, for the determination of etchable track lengths of fission fragments entering a glass detector normal to its surface. Again in 1966, Somogyi²⁹ observed that the track-diameter evolution during the etching process depends largely on the energies and types of the track-producing particles. The phenomenon was illustrated for alpha particle tracks in cellulose nitrate, and for fission product tracks in soda glass, and was suggested as a method for the identification of nuclear reaction products. Other applications of the track diameter kinetics have been reported by many workers.³⁰⁻³⁵ Detailed investigation of the theoretical aspects of track-diameter kinetics

have been made available by Somogyi and Szalay.³⁶

The effect of temperature on the rate of increase of diameter has been studied in the case of Lexan, cellulose acetate and mica and would be discussed in the following sections.

III.2.1 Temperature Dependence of the Rate of Increase of Track-Diameter in Isotropic Solid Dielectrics

Most non-crystalline materials such as plastics show an isotropic behaviour when etched in some chemical etchants.⁹ In such solids, the bulk-etch rate V_G , normal to the surface and along the surface, are equal (Chap. III, Sec. III.1.3). The diameter of the initial damage-trails formed by undegraded fission fragments in plastics was found to be less than 100 \AA .³⁷ Chemical etching results in a preferential attack along the trail of the particle. The degree of damage and the etch rate both decrease with the depth of penetration inside the solid dielectric track detectors. The etch rate along the track beyond the damage-trail is equal to the bulk-etch rate V_G of the undamaged material.

The tracks in Lexan and cellulose acetate used in these studies were those of fission products incident at 15° to the SDTD surface as has been mentioned in Chap. II, Sec. II.4.2.

The growth of the track-diameter (minor axis of the ellipse formed by the intersection of a tilted conical track

with surface plane) with etching time has been measured for Lexan and cellulose acetate at several temperatures. Figs. 7 and 8 show these curves at different temperatures. The values of V_G has been obtained as a function of temperature from these curves. At these temperatures the bulk-etch rates were also determined for Lexan and cellulose acetate using the gravimetric technique. The results are listed in Tables III.1 and III.2.

These results indicate that in cellulose acetate also the bulk-etching is isotropic in nature.

III.2.2 Temperature Dependence of the Rate of Increase of Track-Diameter in Anisotropic Solid Dielectrics

Crystalline solids usually show anisotropic etching behaviour due to the compositional gradients within single crystals of natural minerals.⁹ This is also true in the case of mica. In mica, the acid very rapidly permeates the continuously damaged portion of a particle trajectory and then begins to dissolve the surrounding material, attacking only in a direction parallel to the cleavage planes.³⁸ As shown in Sec.III.1.3 the bulk-etch rate normal to the cleavage plane is negligibly small. For mica, therefore, the rate of increase of track-diameter is the only method for determining the bulk-etch rate along the cleavage plane.

The temperature dependence of the rate of increase of track-diameter in muscovite mica has been studied. Irradiated

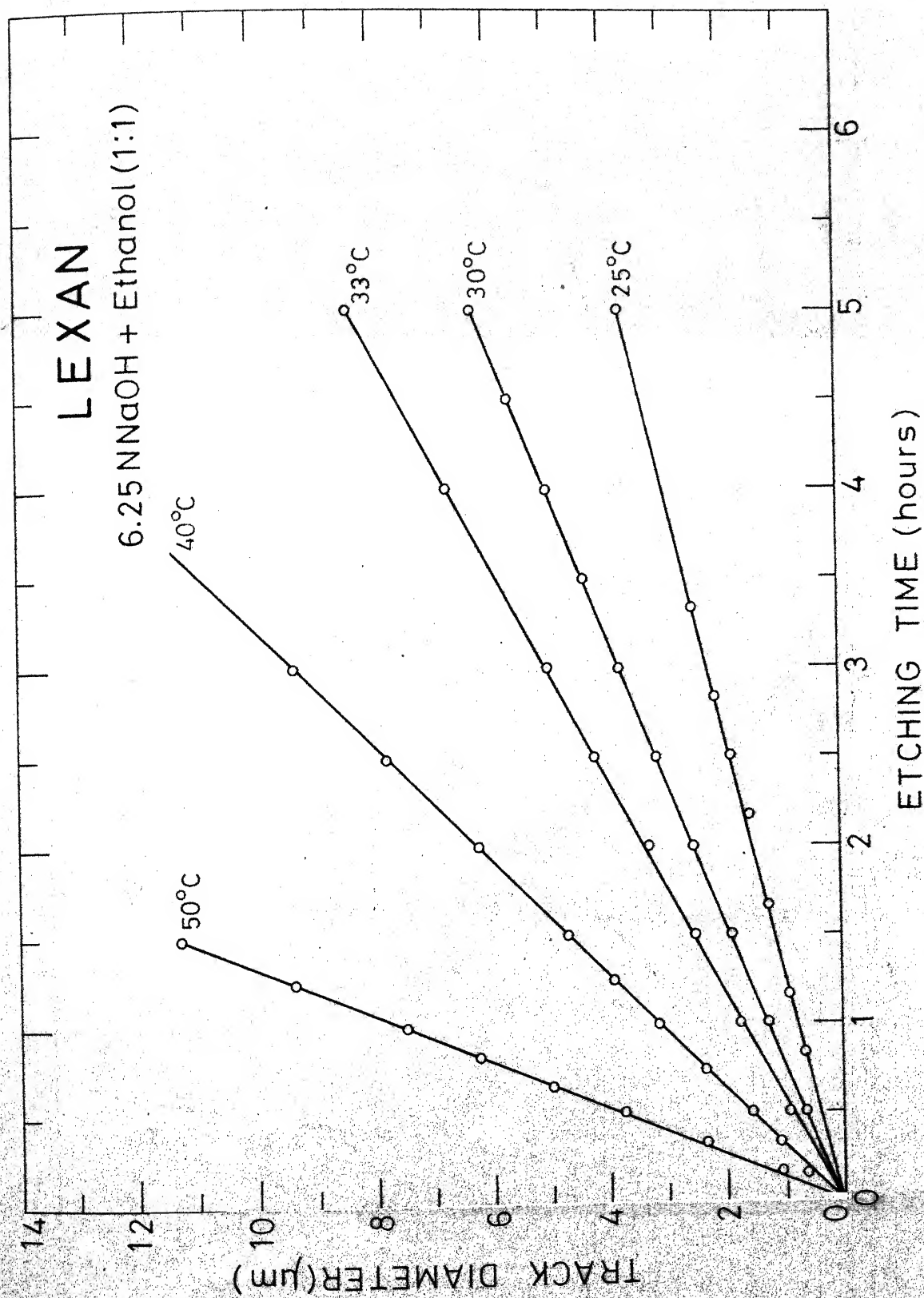


Fig. 7. Plot of the growth of the track-diameter as a function of the etching time for Lexan at various temperatures.

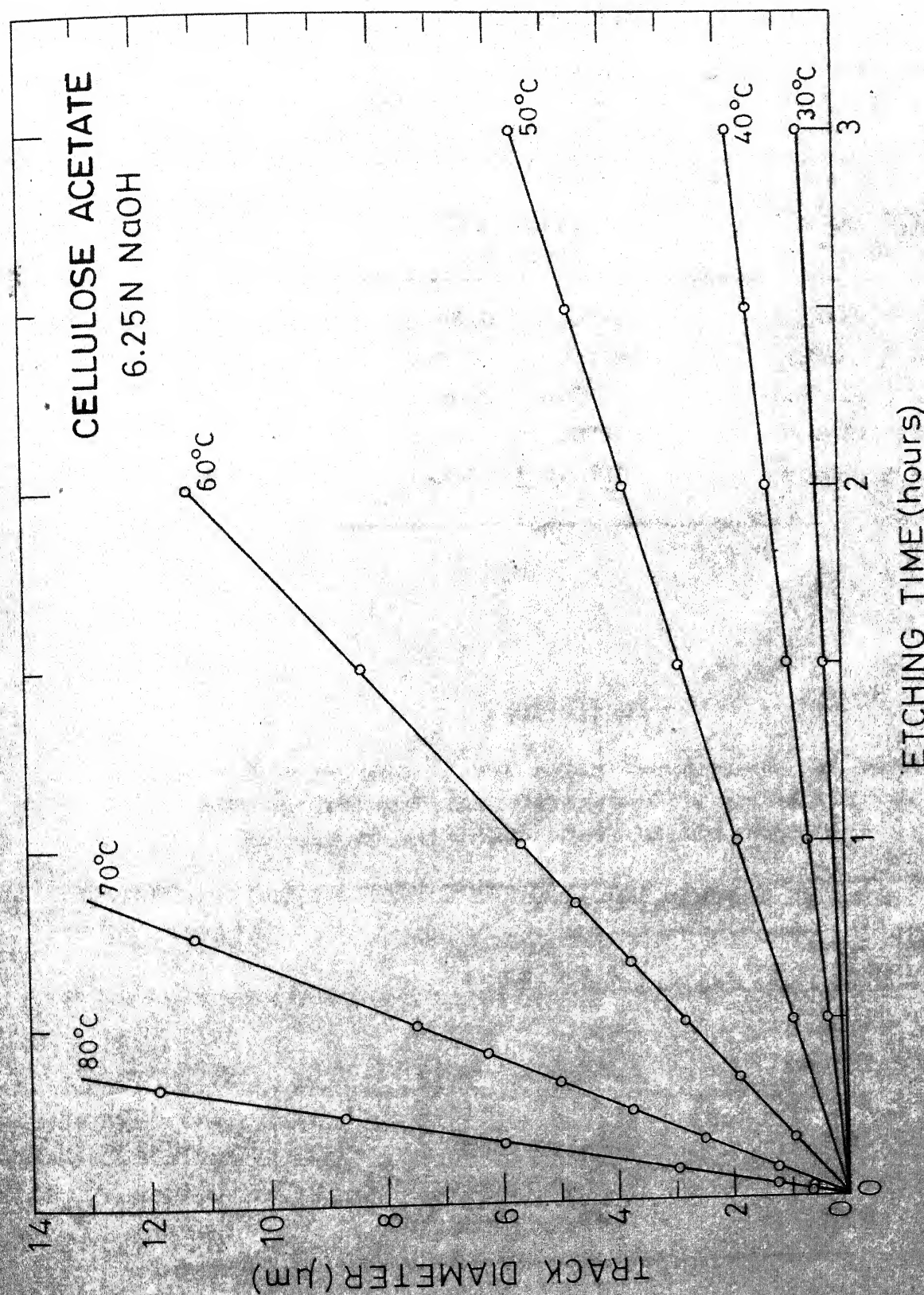


Fig. 8. Plot of the growth of the track-diameter as a function of the etching time for cellulose acetate at various temperatures.

TABLE III.1

The bulk-etch rate V_G for Lexan, at various etching temperatures, determined by two different techniques with 6.25 N NaOH + ethanol (1:1) as the etchant

Temperature (°C)	BULK-ETCH RATE V_G ($\mu\text{m/hr}$)	
	Gravimetric technique	Track-diameter technique
25 \pm 0.5	0.3510 \pm 0.0176	0.3744 \pm 0.0312
30 \pm 0.5	0.6750 \pm 0.0338	0.6250 \pm 0.0312
33 \pm 0.5	0.8610 \pm 0.0431	0.8424 \pm 0.0312
40 \pm 0.5	1.5400 \pm 0.0770	1.5625 \pm 0.0520
50 \pm 0.5	3.9500 \pm 0.1975	3.7440 \pm 0.1563

TABLE III.2

The bulk-etch rate V_G for cellulose acetate, at various etching temperatures, determined by two different techniques with 6.25 N NaOH as the etchant

Temperature (°C)	BULK-ETCH RATE V_G ($\mu\text{m/hr}$)	
	Gravimetric technique	Track-diameter technique
30 \pm 0.5	0.1020 \pm 0.0051	0.1041 \pm 0.0260
40 \pm 0.5	0.3060 \pm 0.0153	0.3125 \pm 0.0312
50 \pm 0.5	0.9150 \pm 0.0458	0.9375 \pm 0.0312
60 \pm 0.5	2.7500 \pm 0.1375	2.8125 \pm 0.0520
70 \pm 0.5	7.4230 \pm 0.3712	7.5000 \pm 0.1041
80 \pm 0.5	17.3900 \pm 0.8695	17.5000 \pm 0.1563

samples of mica were etched with 40% hydrofluoric acid and the diameters of a few fission product tracks were measured as a function of etching time at several temperatures. The tracks in mica were found to be cylindrical in shape with a track-diameter of $1.5 \mu\text{m}$ after 40 minutes of etching in 40% HF at room temperature, whereas, diamond shaped tracks with diameter of about $25 \mu\text{m}$ were observed after 12 hours of etching under same conditions. Fig. 9 shows a plot of the track diameter versus etching time at different temperatures.

The measurements of the track-diameters were done at a magnification of 2560. The uncertainty in measurement is $\pm 0.3 \mu\text{m}$.

III.3 DETERMINATION OF ACTIVATION ENERGY FOR BULK-ETCHING

Several workers²⁶⁻²⁸ have tried to correlate the variation of bulk-etch rate with temperature in analogy with a chemical reaction. If V_G is the bulk-etch rate at a temperature $T^\circ\text{K}$ for a particular solid dielectric with a particular etchant of a given concentration, then the dependence of V_G on T is given as

$$V_G = A e^{-E_a/kT} \quad (3.4)$$

where A is a constant, E_a is the activation energy for bulk-etching and k is the Boltzmann constant respectively.

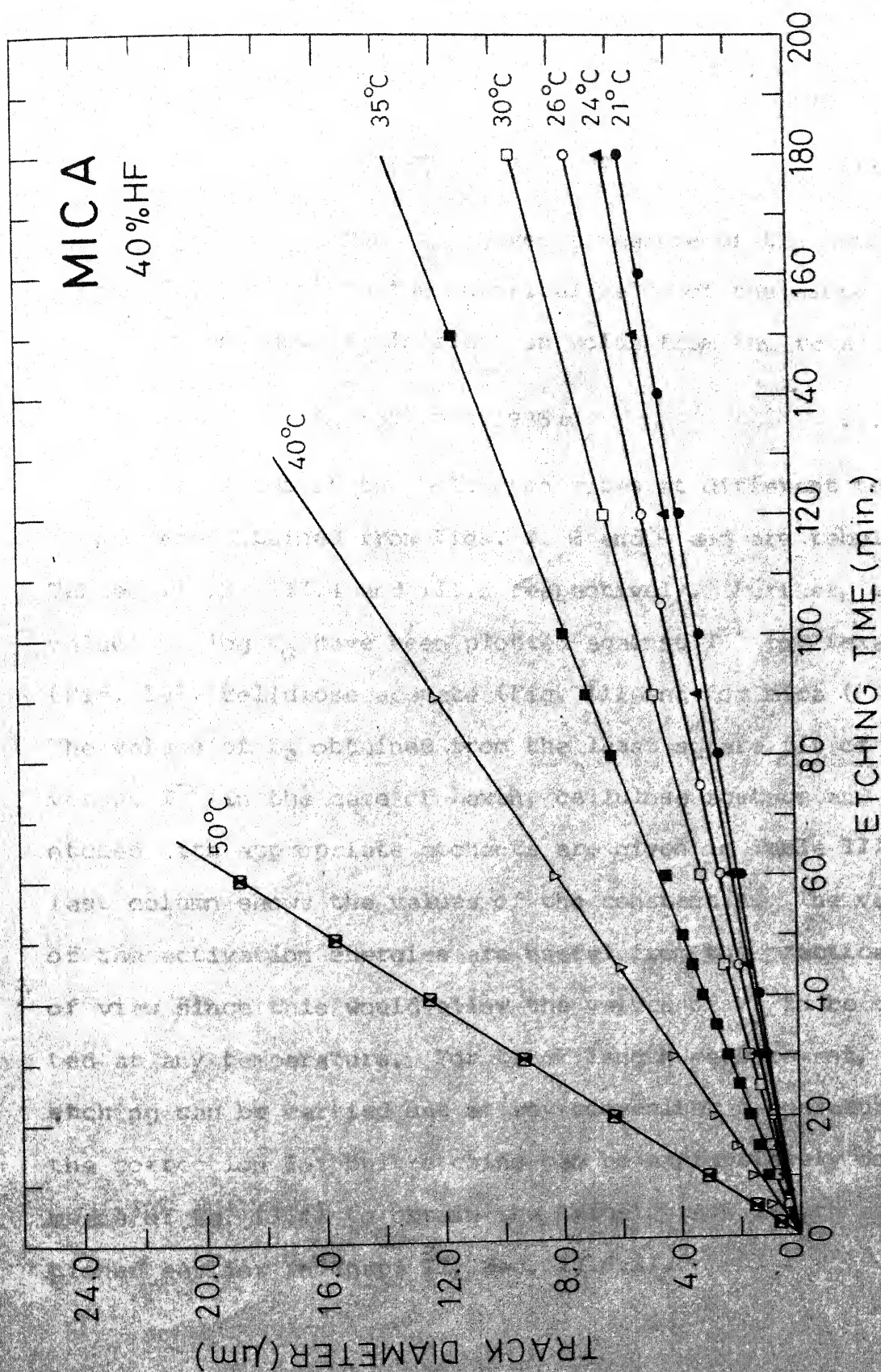


Fig. 9. Plot of the growth of the track-diameter as a function of the etching time for mica at various temperatures.

Thus,

$$\log V_G = \left(- \frac{E_a}{2.303 k} \right) \frac{1}{T} + \log A \quad \dots(3.5)$$

A plot of $\log V_G$ versus T^{-1} gives a measure of the activation energy E_a . If 'm' is the numerical value of the slope of such plot then one gets E_a in electron volts from the relation

$$E_a \text{ (eV)} = 0.1986 m \quad \dots(3.6)$$

The values of the bulk-etch rates at different temperatures were obtained from Figs. 7, 8 and 9 and are tabulated in Tables III.3, III.4 and III.5 respectively. Further, the values of $\log V_G$ have been plotted against T^{-1} for Lexan (Fig. 10), cellulose acetate (Fig. 11) and for mica (Fig. 12). The values of E_a obtained from the least square fit of $\log V_G$ versus T^{-1} in the case of Lexan, cellulose acetate and mica etched with appropriate etchants are given in Table III.6. The last column shows the values of the constant A. The values of the activation energies are useful from the practical point of view since this would allow the values of V_G to be calculated at any temperature. For track length measurement, the etching can be carried out at any convenient temperature and the correction for bulk-etching can be appropriately done by means of Eq. (3.4) to obtain the 'true' track length as mentioned earlier in Chap. II, Sec. II.6.2).

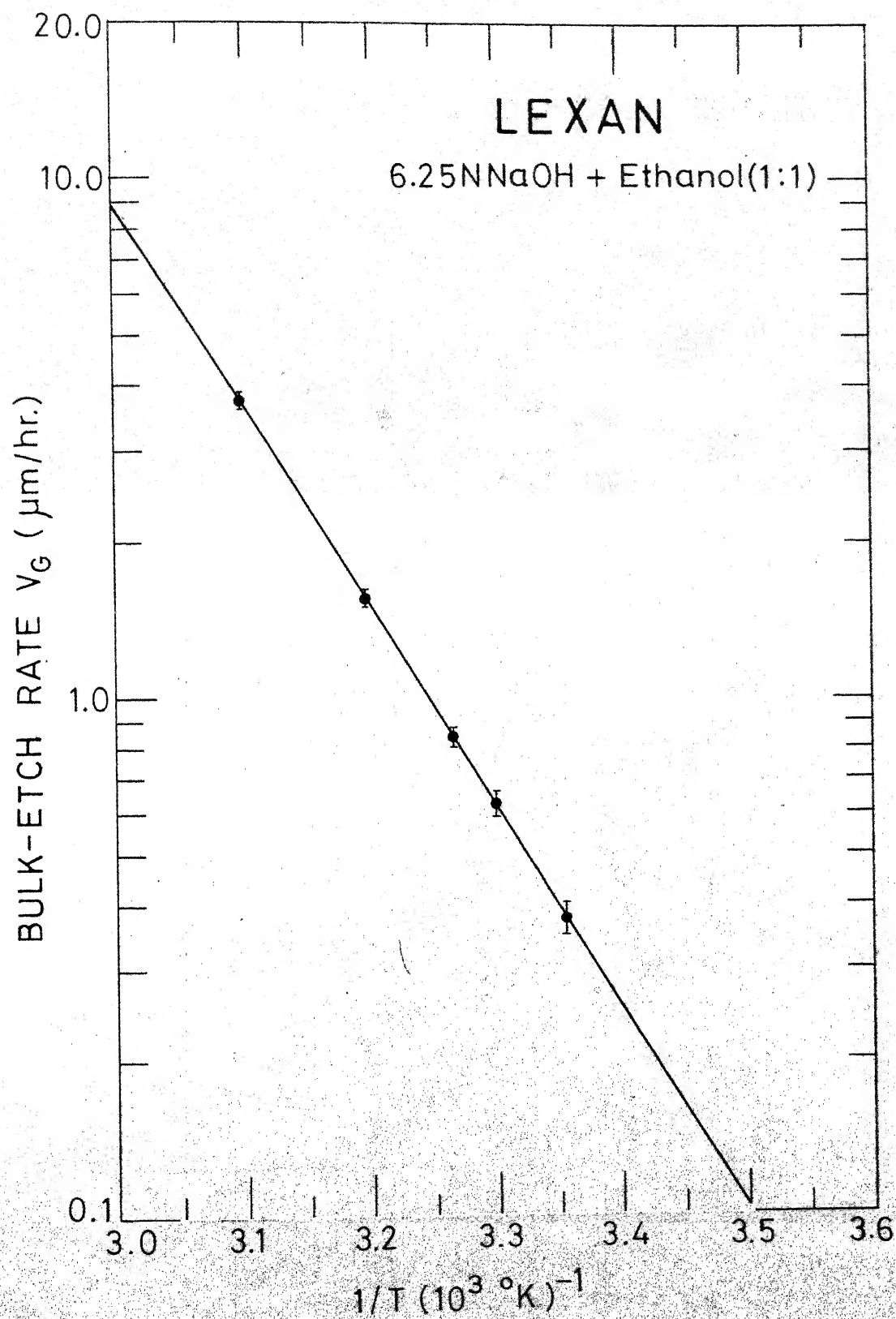


Fig. 10. Plot of the logarithm of the bulk-etch rate against T^{-1} for Lexan.

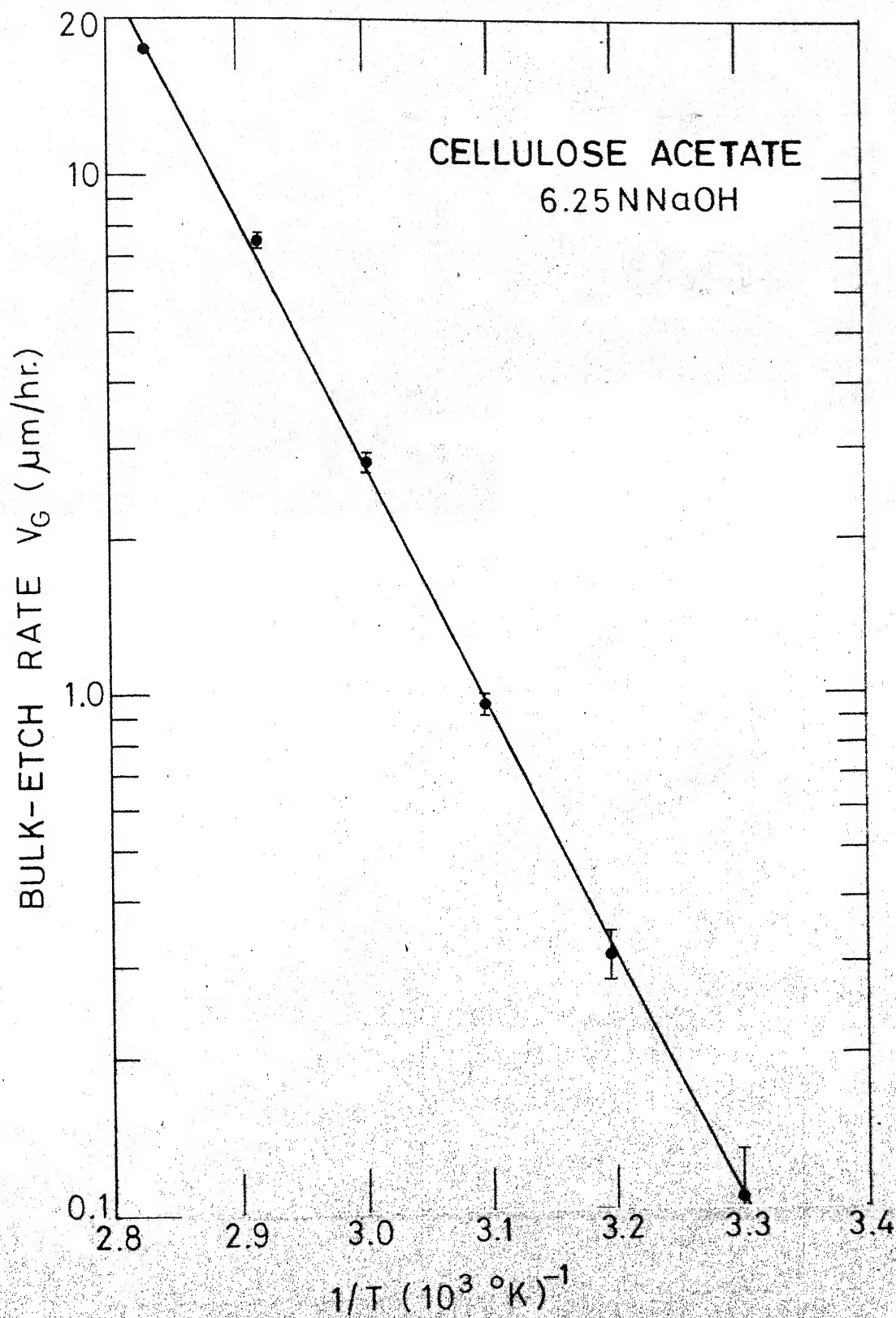


Fig. 11. Plot of the logarithm of the bulk-etch rate against T^{-1} for cellulose acetate.

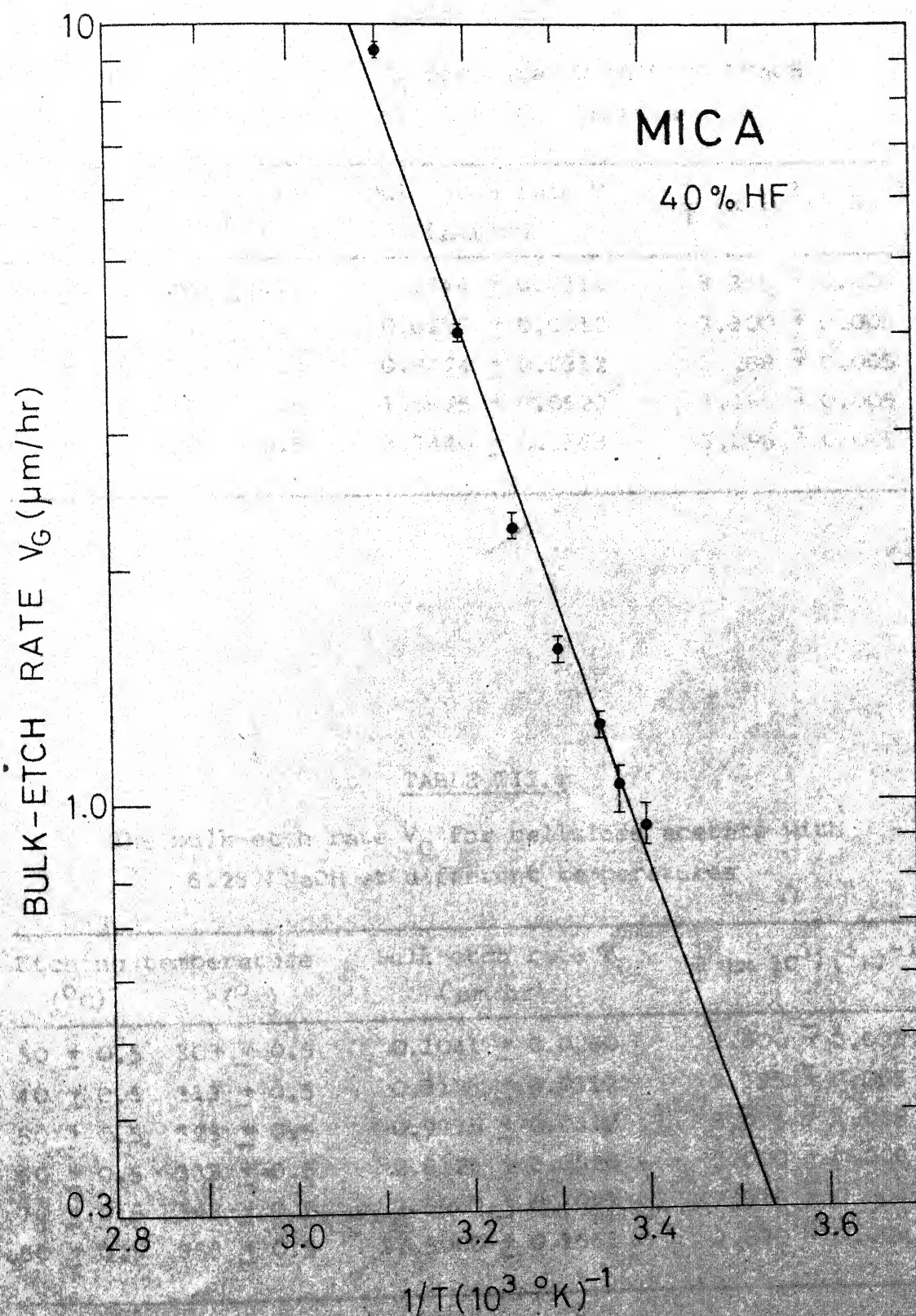


Fig. 12. Plot of the logarithm of the bulk-etch rate against T^{-1} for mica.

TABLE III.5

50

The bulk-etch rate V_G for mica at different etching temperatures with 40% HF as the etchant

Etching temperature (°C)	Etching temperature (°K)	Bulk-etch rate V_G ($\mu\text{m/hr}$)	$\frac{1}{T} (x 10^3) (^\circ\text{K})^{-1}$
21 \pm 0.5	294 \pm 0.5	0.9375 \pm 0.0520	3.401 \pm 0.006
24 \pm 0.5	297 \pm 0.5	1.0410 \pm 0.0520	3.367 \pm 0.006
26 \pm 0.5	299 \pm 0.5	1.2500 \pm 0.0520	3.345 \pm 0.006
30 \pm 0.5	303 \pm 0.5	1.5625 \pm 0.0520	3.300 \pm 0.005
35 \pm 0.5	308 \pm 0.5	2.2782 \pm 0.0625	3.247 \pm 0.005
40 \pm 0.5	313 \pm 0.5	4.0625 \pm 0.1041	3.195 \pm 0.005
50 \pm 0.5	323 \pm 0.5	9.3750 \pm 0.1563	3.096 \pm 0.005

TABLE III.6

Values of the activation energies for bulk etching of Lexan, cellulose acetate and mica with their suitable chemical etchants and calculated values of constant A

SDTD	Chemical etchants	Activation energy E_a (eV)	Constant A ($\mu\text{m/hr}$)
1. Lexan	6.25 N NaOH+Ethanol(1:1)	0.763 \pm 0.008	2.94x10 ¹²
2. Cellulose acetate	6.25 N NaOH	0.952 \pm 0.010	6.80x10 ¹⁴
3. Mica	40% HF	0.666 \pm 0.038	2.20x10 ¹¹

III.3.1 Empirical Calculation of the Complete Etching Time t_c at any Temperature

The complete etching time t_c has to be known for the determination of the true track length from the experimentally observed track length. Since it requires a laborious experiment at each temperature for obtaining t_c , an empirical method for calculating t_c would be very useful. During the present experiments it was observed that the complete etching time always corresponds to a fixed value of the track-diameter d_c which is independent of temperature for a given etchant and dielectric. These values for d_c are $1.5 \pm 0.3 \mu\text{m}$, $2.0 \pm 0.3 \mu\text{m}$ and $2.5 \pm 0.3 \mu\text{m}$ for mica (40% HF), cellulose acetate (6.25 N NaOH) and Lexan (6.25 N NaOH + ethanol, 1:1) respectively. Since the bulk-etch rates V_G (along the cleavage plane for mica) are functions of temperature, the complete etching time t_c can be calculated from the relation

$$t_c = \frac{d_c}{2 V_G} = \frac{d_c}{2 A e^{-E_a/kT}} \quad (3.7)$$

where A is a constant and E_a is the activation energy, k is Boltzmann's constant and T is the temperature at which etching is carried out. Thus, with the values of A and E_a listed in Table III.6 one can calculate the value of t_c at any temperature T .

I. I. T. KANPUR
CENTRAL LIBRARY
Acc. No. A 52181

III.4 MEASUREMENT OF TRACK-ETCH RATE V_T

When a swiftly moving 'light' heavy charged particle like ^4He or ^{16}O at ~ 10 MeV/nucleon penetrates into a solid dielectric, it causes very little damage to the surface, but as the depth of penetration increases the rate of energy-deposition also becomes high and reaches a maximum value somewhere near the end of its trajectory (Bragg curve).³⁹ However, for fission products, which are very heavy ions at initially rather low energy, the rate of energy-deposition falls continuously along the path right from the surface of the SDTD. Thus fission products cause maximum radiation-damage at the surface of the detector foil and the extent of damage decreases with the depth of penetration. Consequently, rate of chemical etching V_T along the trail of a fission product also decreases and becomes equal to the bulk-etch rate V_G at the end of the track.

Assuming that over a small portion of the track the track-etch rate V_T remains almost constant, V_T can be obtained by measuring the track length-increase at different etching times. If, over a small etching time period, Δt , the increase in track length is Δl , then

$$V_T \approx \frac{\Delta l}{\Delta t} \quad (3.8)$$

The geometry of track etching in plastics have been shown in Fig. 13. An incident fission product enters the detector



surface at a point P and at a dip angle ϕ . The point C is the end of the particle track. The actual length of the track is PC. But since during the etching process the surface of the detector foil is etched out at a rate V_G , therefore, in time t_2 , the length $V_G t_2 / \sin \phi$ (i.e., Δ_s) of the track is erased due to bulk-etching and the track length is increased by an amount $\Delta_o = V_G (t_2 - t_c)$ due to over-etching, where t_c is the complete etching time. The observed track length increases with etching time due to a faster rate V_T along the track till the point C is reached. Beyond the point C the material is undamaged and is etched at the bulk-etch rate V_G . Further etching will cause a decrease in the observed track length for all incident angles less than 90° . After applying the bulk etching (Δ_s) and over etching (Δ_o) corrections, as described in Chap. II, Sec. II.6.2, one can get the true track length for any etching time and obtain from these the track-etch

For the purpose of determining V_T , samples of Lexan cellulose acetate were exposed to fission products at an angle of 15° to the surface and that of mica at an angle of 45° . Lexan sheets were etched in 6.25 N NaOH + ethanol (1:1) at temperatures 25°C and 33°C , and in 6.25 N NaOH at 55°C . Cellulose acetate foil was etched in 6.25 N NaOH at 55°C and mica with 40% HF at 35°C . The etching procedure has been discussed in Chap. II, Sec. II.4.3. All these samples were over-etched much beyond the complete etching

After every etching, the diameters and the lengths of a few selected tracks were measured in each foil. All the measurements were done at a magnification of 2560. The uncertainty in the measurements was $\pm 0.3 \mu\text{m}$.

Figures 14, 15 and 16 show the variation of the observed and true track length with etching time. It can be seen that the observed track lengths start decreasing after time t_c , whereas, the corrected or true track lengths remain constant much beyond the etching time t_c for complete etching. In the case of mica, where the rate of dissolution normal to the surface is negligible²⁵ (see also Sec. III.1.3 of this chapter) no correction terms are required to get the true track length. This is confirmed by the fact that the observed track lengths were found to be practically constant even after the complete etching time t_c , as shown in Fig. 16.

The values of the actual or true track lengths obtained from the observed ones corresponding to different etching times for a single track in Lexan etched with 6.25 N NaOH + ethanol (1:1) at 33°C are listed in Table III.7. In a similar manner, the true track lengths have been determined at different etching time for a group of tracks in each SDTD.

The values of the track-etch rate V_T at different points on the tracks for each track studied were obtained from the values of the true track lengths at different etching time. In each case the values of the track-etch rate V_T are tabulated

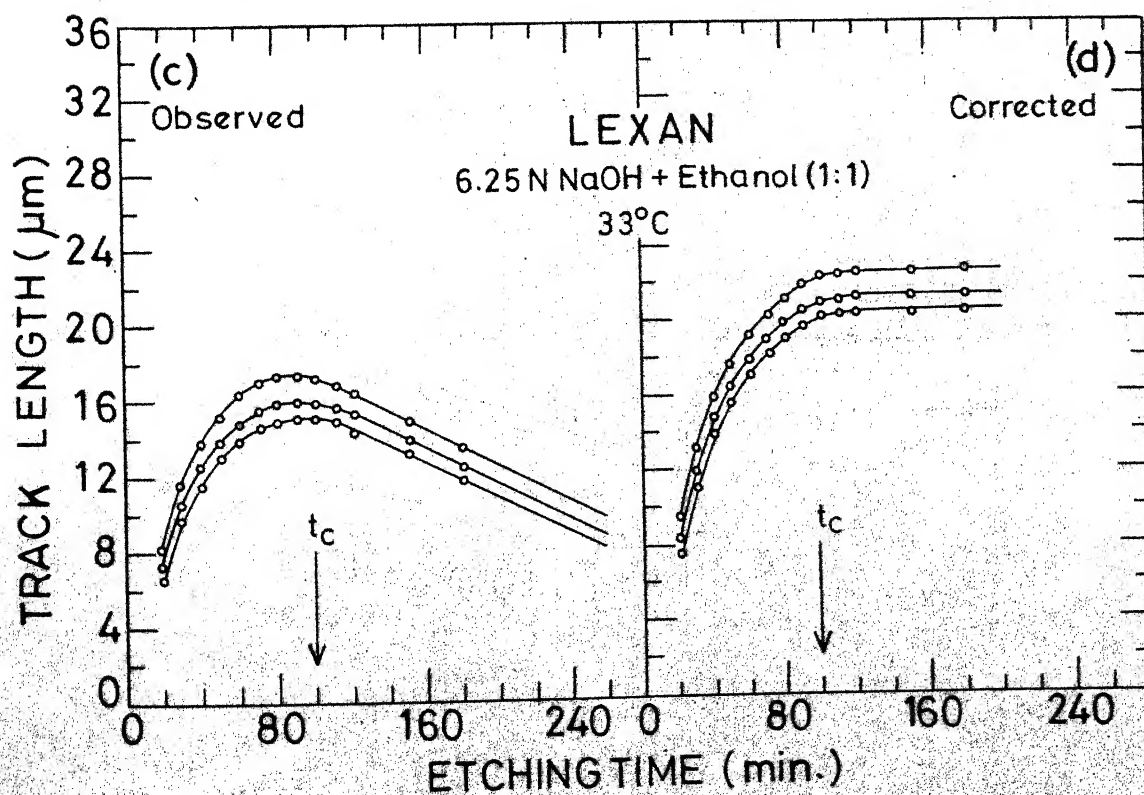
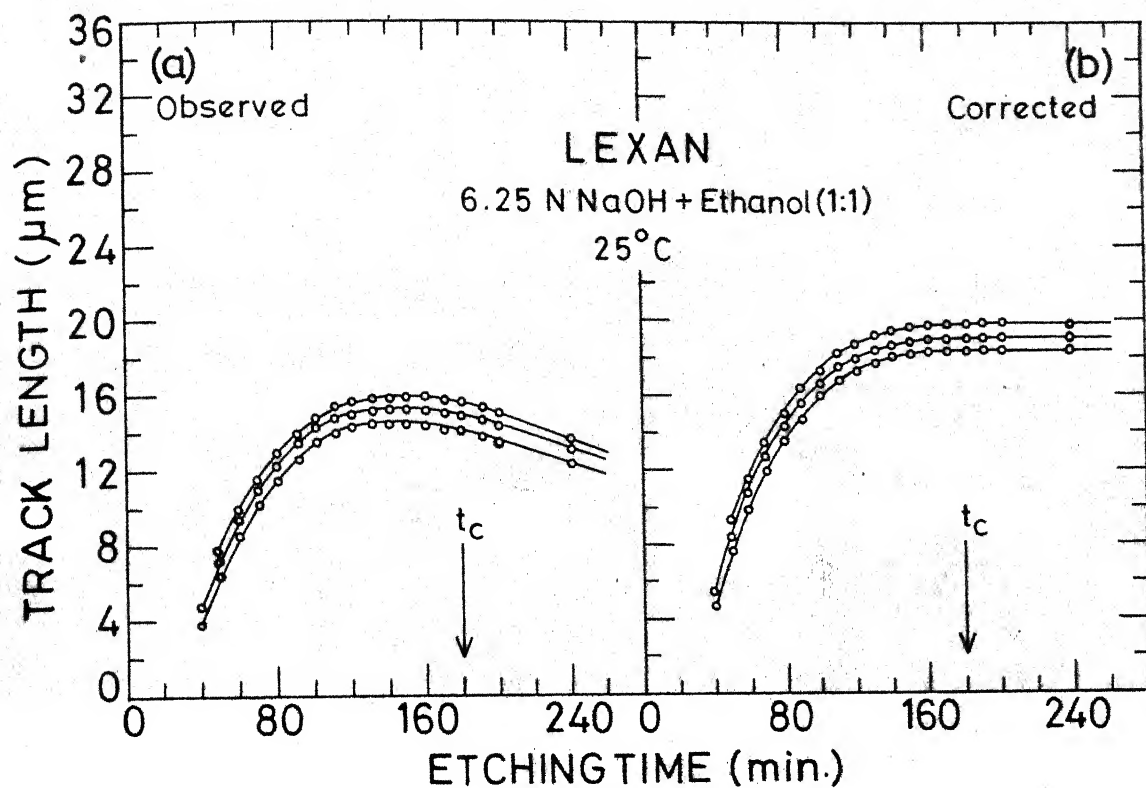


Fig. 14. Variation of the observed and corrected track lengths with etching time in the case of Lexan.

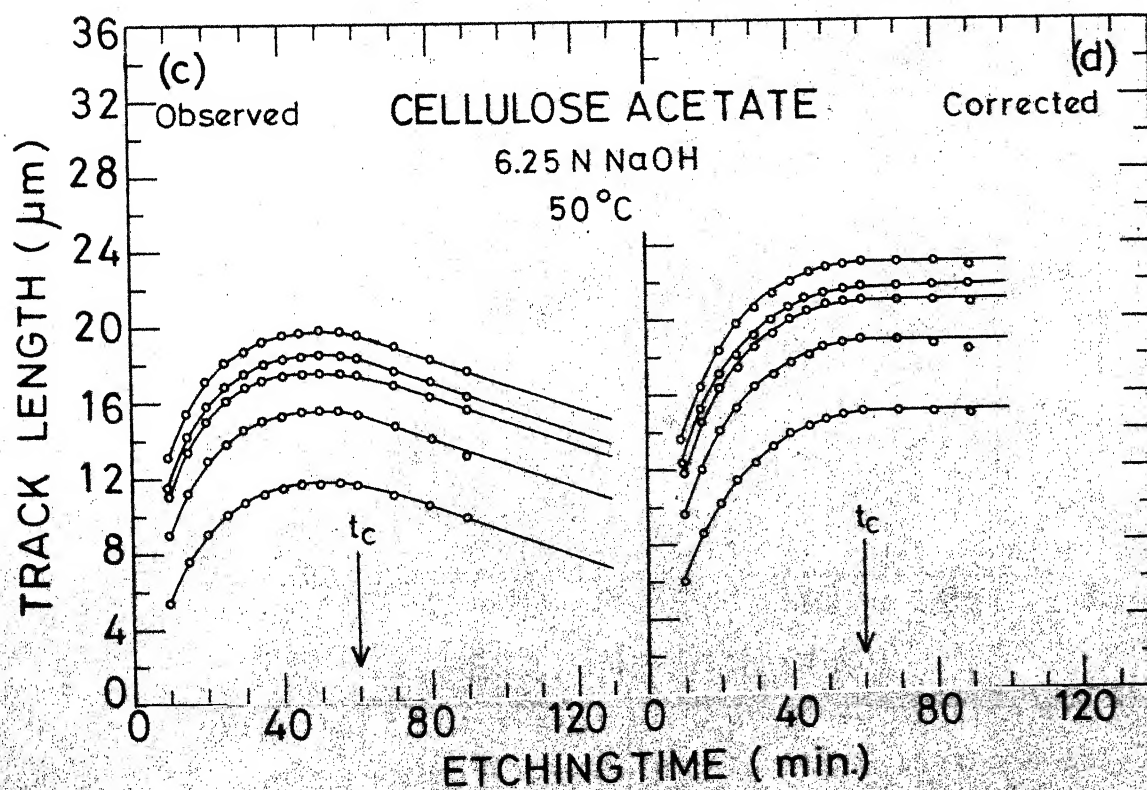
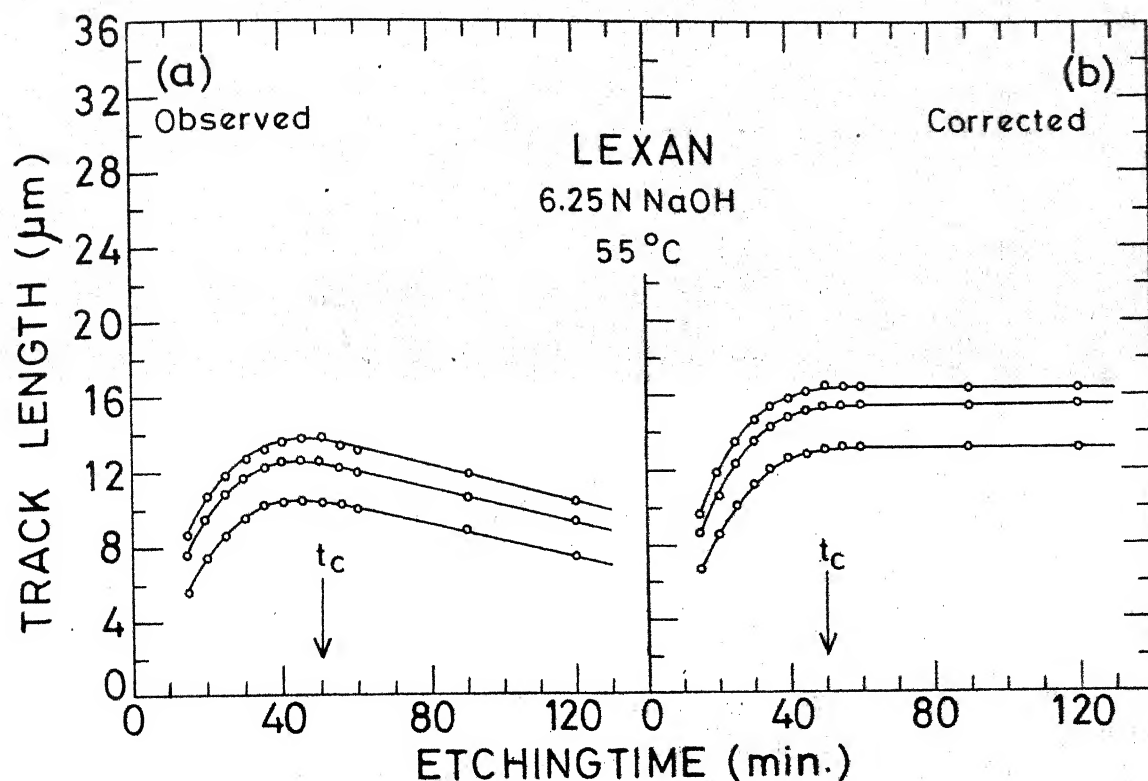


Fig. 15. Variation of the observed and corrected track lengths with etching time in the case of Lexan and cellulose acetate.

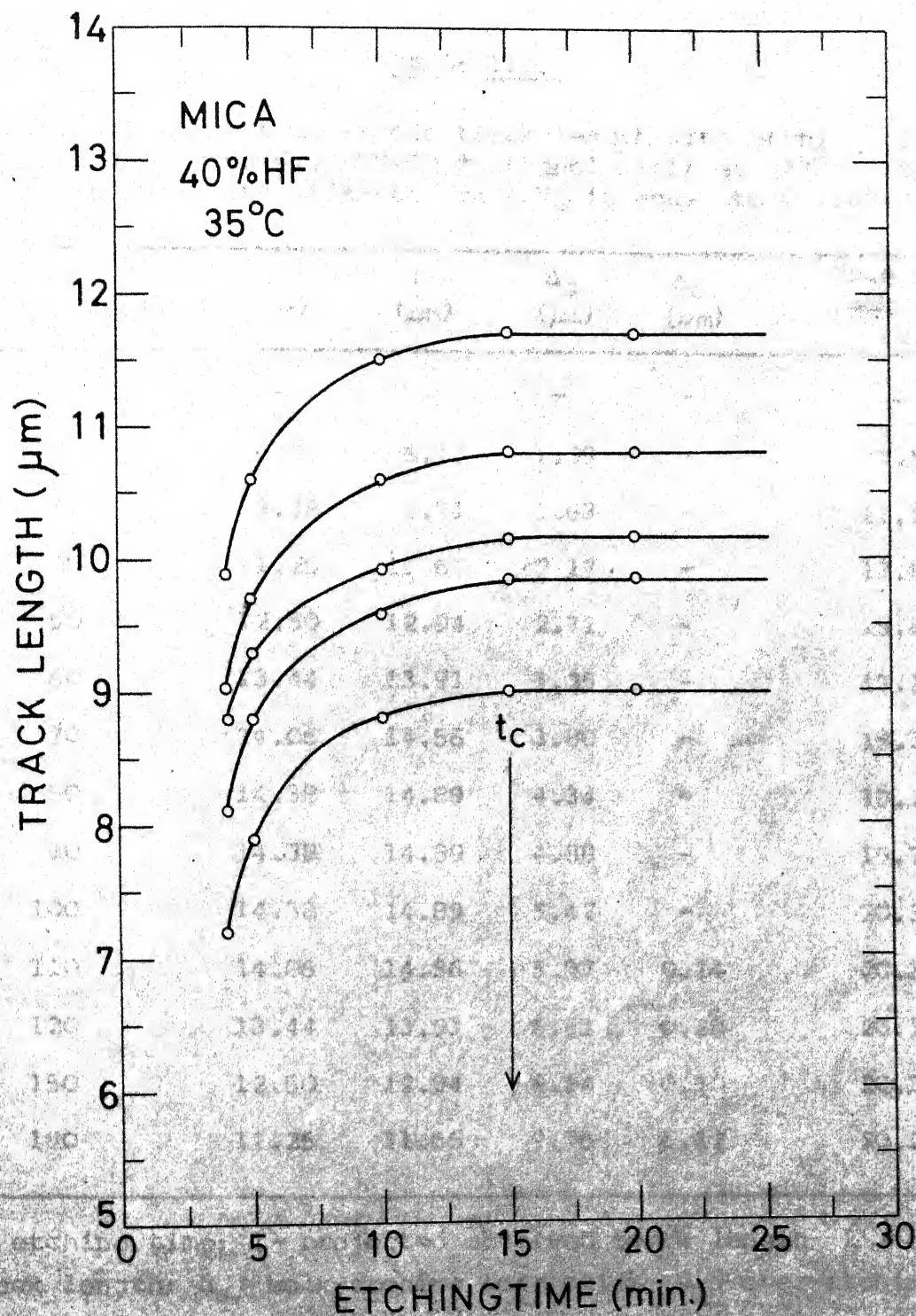


Fig. 16. Variation of the observed or true track lengths with etching time in the case of mica.

TABLE III.7

Variation of the true etched track length with etching time for Lexan etched with 6.25 N NaOH + ethanol (1:1) at 33°C. The dip angle is 15° & the bulk-etch rate V_G is equal to 0.01404 $\mu\text{m}/\text{min}$.

t (minutes)	l (μm)	L' (μm)	Δ_S (μm)	Δ_O (μm)	True etched track length (μm)
10	-	-	-	-	-
20	6.25	6.47	1.09	-	7.56
30	9.38	9.71	1.63	-	11.34
40	11.25	11.65	2.17	-	13.82
50	12.50	12.94	2.71	-	15.65
60	13.44	13.91	3.25	-	17.16
70	14.06	14.56	3.80	-	18.36
80	14.38	14.89	4.34	-	19.23
90	14.38	14.89	4.88	-	19.77
100	14.38	14.89	5.42	-	20.31
110	14.06	14.56	5.97	0.14	20.39
120	13.44	13.91	6.51	0.28	20.14
150	12.50	12.94	8.14	0.70	20.38
180	11.25	11.65	9.76	1.12	20.29

t = etching time; l = projected observed track length; L' = observed track length; Δ_S = bulk-etching correction; Δ_O = over-etching correction.

along with the penetrated depths and the theoretically calculated energy-loss rates at these penetration depths and are given in Tables III.8 to III.12.

From these tables the values of track-etch rate V_T have been plotted against etched track length L for each track studied under specified etching conditions in Lexan, cellulose acetate and mica. Figs. 17, 18, 19, 20 and 21 show the plots of V_T versus L and these seem to imply a linear relationship. The uncertainty in the track lengths is $\pm 0.3 \mu\text{m}$ and in V_T $\pm 0.044 \mu\text{m}/\text{min}$.

The procedure for obtaining the theoretical values of dE/dX , as a function of penetration depth would be explained in Chap. IV, Sec. IV.2.

TABLE III.8

Some representative tracks, their identity (i.e., mass number of the fission product causing the track), the track-etch rate (V_T) at different etched track lengths (ETL) and the calculated energy-loss rates (dE/dX).
(Lexan; etchant: 6.25 N NaOH+ethanol 1:1, temperature: 25°C)

TRACK 1			TRACK 2			TRACK 3		
L = 18.5 μm , A = 139			L = 19.1 μm , A = 136			L = 19.6 μm , A = 134		
ETL	V_T	dE/dX	ETL	V_T	dE/dX	ETL	V_T	dE/dX
6.34	0.300	44.0	6.98	0.300	43.5	-	-	-
9.00	0.234	36.5	9.65	0.234	36.5	10.13	0.234	36.0
11.10	0.186	31.0	11.75	0.185	31.0	12.23	0.186	31.0
12.80	0.153	26.5	13.44	0.153	27.0	13.93	0.153	26.5
14.25	0.137	22.5	14.89	0.137	22.5	15.38	0.137	23.0
15.46	0.105	19.0	16.10	0.105	19.0	16.59	0.105	19.5
16.34	0.072	16.0	16.99	0.073	16.5	17.47	0.072	17.0
16.99	0.057	14.0	17.64	0.057	14.5	18.12	0.057	15.0
17.47	0.040	12.5	18.12	0.039	13.0	18.60	0.040	13.5
17.80	0.025	11.5	18.44	0.025	12.0	18.93	0.025	12.0
18.04	0.024	10.5	18.68	0.024	10.5	19.17	0.025	11.0
18.20	0.007	9.0	18.84	0.008	9.0	19.33	0.007	10.0
18.29	0.011	8.5	18.92	0.008	8.5	19.40	0.008	9.5
18.37	0.005	7.0	19.00	0.008	8.0	19.48	0.008	9.0
18.43	0.008	6.0	19.08	0.008	7.5	19.56	0.008	8.0

L = maximum etchable track length; ETL = etched track length in units of μm ; V_T = track-etch rate in units of $\mu\text{m}/\text{min.}$; and dE/dX = calculated energy-loss rate in units of $\text{MeV}/\text{mg}/\text{cm}^2$.

TABLE III.9

Some representative tracks, their identity (i.e., mass number of the fission product causing the track), the track-etch rate (V_T) at different etched track lengths (ETL) and the calculated energy-loss rates (dE/dX). (Lexan; etchant: 6.25 N NaOH + ethanol 1:1, temperature: 33°C)

TRACK 1			TRACK 2			TRACK 3		
L = 20.3 μm , A = 123			L = 21.0 μm , A = 119			L = 22.2 μm , A = 111		
ETL	V_T	dE/dX	ETL	V_T	dE/dX	ETL	V_T	dE/dX
9.44	0.377	39.50	10.17	0.393	39.00	11.22	0.409	39.00
12.56	0.248	31.50	13.45	0.264	30.75	14.58	0.264	30.50
14.72	0.183	26.00	15.69	0.183	25.00	16.90	0.199	24.50
16.39	0.151	21.50	17.36	0.151	20.00	18.65	0.151	20.00
17.74	0.120	17.00	18.71	0.119	16.00	20.00	0.120	16.50
18.77	0.086	14.00	19.74	0.087	13.00	21.03	0.086	13.50
19.47	0.054	11.50	20.44	0.054	10.00	21.73	0.054	11.00
20.01	0.054	9.00	20.82	0.021	7.00	22.11	0.022	8.50

L = maximum etchable track length; ETL = etched track length in units of μm ; V_T = track-etch rate in units of $\mu\text{m}/\text{min.}$; and dE/dX = calculated energy-loss rate in units of $\text{MeV}/\text{mg}/\text{cm}^2$.

TABLE III.10

Some representative tracks, their identity (i.e., mass number of the fission product causing the track), the track-etch rate (V_T) at different etched track lengths (ETL) and the calculated energy-loss rates (dE/dX).
(Lexan; etchant: 6.25 N NaOH, temperature: 55°C)

TRACK 1			TRACK 2			TRACK 3		
L = 13.6 μm , A = 163			L = 15.6 μm , A = 154			L = 16.4 μm , A = 150		
ETL	V_T	dE/dX	ETL	V_T	dE/dX	ETL	V_T	dE/dX
7.51	0.380	28.5	9.62	0.450	28.0	10.61	0.460	27.5
9.26	0.320	23.0	11.54	0.320	22.5	12.53	0.310	22.0
10.62	0.222	18.5	12.89	0.220	17.5	13.85	0.220	18.0
11.56	0.156	15.5	13.83	0.156	14.5	14.79	0.160	15.0
12.27	0.126	13.5	14.53	0.126	12.5	15.50	0.126	13.0
12.74	0.062	11.5	14.99	0.060	10.0	15.97	0.060	10.5
13.04	0.060	10.0	15.29	0.060	8.5	16.27	0.060	8.0

L = maximum etchable track length; ETL = etched track length in units of μm ; V_T = track-etch rate in units of $\mu\text{m}/\text{min.}$; and dE/dX = calculated energy-loss rate in units of $\text{MeV}/\text{mg}/\text{cm}^2$.

TABLE III.11

Some representative tracks, their identity (i.e., mass number of the fission product causing the track), the track-etch rate (V_T) at different etched track lengths (ETL) and the calculated energy-loss rates (dE/dX).
(Cellulose acetate; etchant: 6.25 N NaOH, temperature: 50°C)

TRACK 1			TRACK 2			TRACK 3		
L = 18.94 μm , A = 122			L = 21.20 μm , A = 107			L = 21.85 μm , A = 104		
ETL	V_T	dE/dX	ETL	V_T	dE/dX	ETL	V_T	dE/dX
10.93	0.510	33.00	13.19	0.510	30.50	13.67	0.576	30.50
13.34	0.380	26.00	15.42	0.384	25.00	16.07	0.384	24.00
14.76	0.254	21.00	17.02	0.254	20.50	17.66	0.254	20.00
15.86	0.186	18.50	18.12	0.188	17.50	18.77	1.190	17.00
16.73	0.156	16.00	18.99	0.158	15.00	19.64	0.158	14.50
17.43	0.124	14.00	19.69	0.124	13.00	20.34	0.124	12.50
17.97	0.090	12.00	20.24	0.094	11.50	20.88	0.092	10.50
18.35	0.060	10.75	20.62	0.060	10.00	21.26	0.060	9.50
18.65	0.060	9.50	20.92	0.060	9.00	21.56	0.060	8.50
18.87	0.030	8.00	21.14	0.030	8.50	21.78	0.030	8.00

L = maximum etchable track length; ETL = etched track length in units of μm ; V_T = track-etch rate in units of $\mu\text{m}/\text{min.}$; and dE/dX = calculated energy-loss rate in units of $\text{MeV}/\text{mg}/\text{cm}^2$.

TABLE III.12

Some representative tracks, their identity (i.e., mass number of the fission product causing the track), the track-etch rate (V_T) at different etched track lengths (ETL) and the calculated energy-loss rates (dE/dX).

(Mica; etchant: 40% HF, temperature: 35°C)

Identification	ETL	V_T	dE/dX
TRACK 1	7.57	0.720 ± 0.220	17.50
L = 9.01 μm	8.38	0.180 ± 0.044	14.50
A = 140	8.92	0.036 ± 0.044	13.00
TRACK 2	8.47	0.720 ± 0.220	17.75
L = 9.91 μm	9.19	0.144 ± 0.044	14.50
A = 131	9.73	0.036 ± 0.044	13.50
TRACK 3	9.05	0.450 ± 0.220	16.50
L = 10.15 μm	9.60	0.132 ± 0.044	14.00
A = 122	10.04	0.044 ± 0.044	13.50
TRACK 4	9.37	0.720 ± 0.220	18.00
L = 10.81 μm	10.18	0.180 ± 0.044	15.00
A = 111	10.72	0.036 ± 0.044	13.25
TRACK 5	10.27	0.720 ± 0.220	17.00
L = 11.71 μm	11.04	0.162 ± 0.044	15.00
A = 94	11.58	0.054 ± 0.044	13.50

L = maximum etchable track length; ETL = etched track length in units of μm ; V_T = track-etch rate in units of $\mu\text{m}/\text{min.}$; and dE/dX = calculated energy loss rate in units of $\text{MeV}/\text{mg}/\text{cm}^2$.

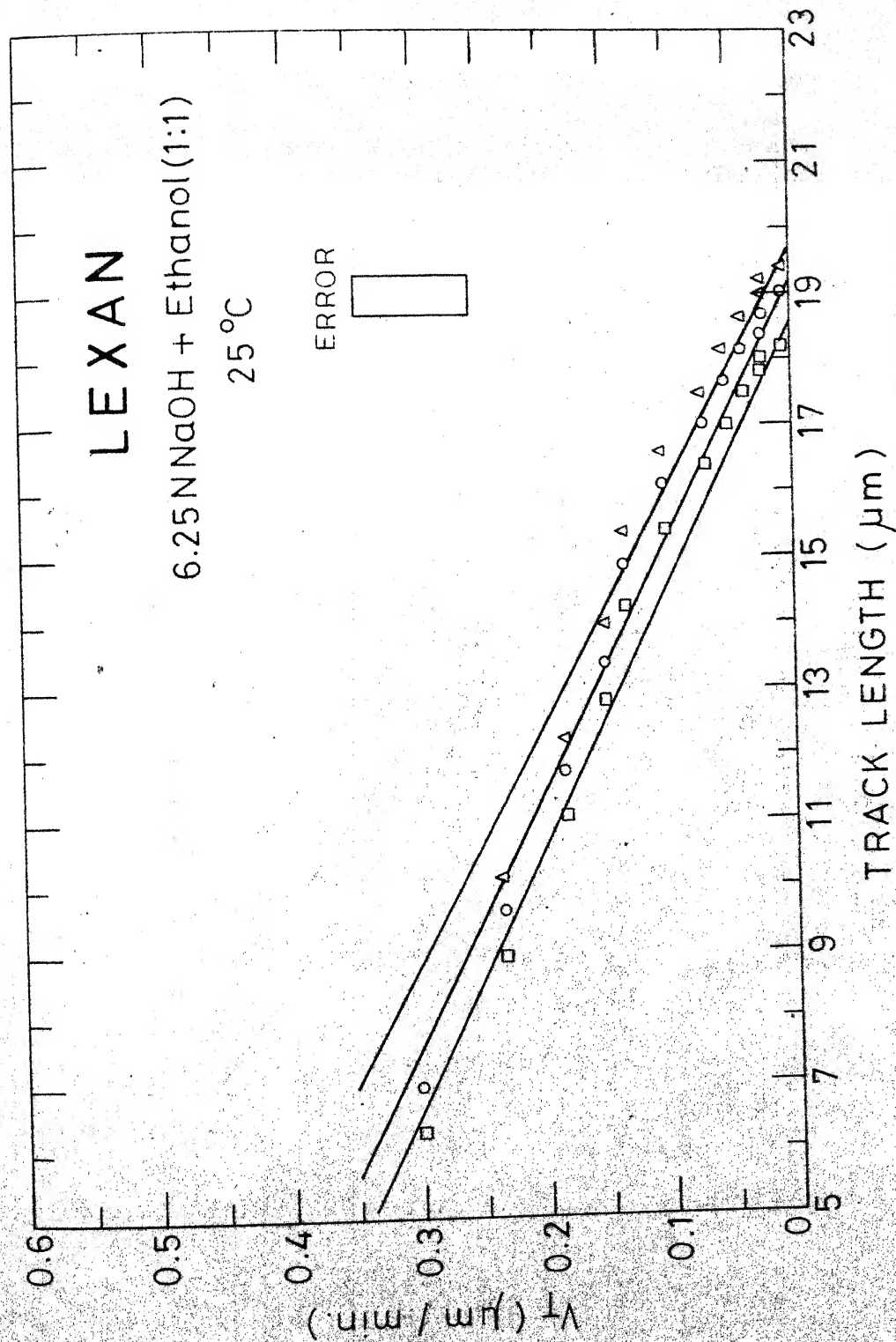


Fig. 17. Plots of track-etch rate V_T versus etched track length for Lexan etched with 6.25 N NaOH + ethanol (1:1) at 25°C.

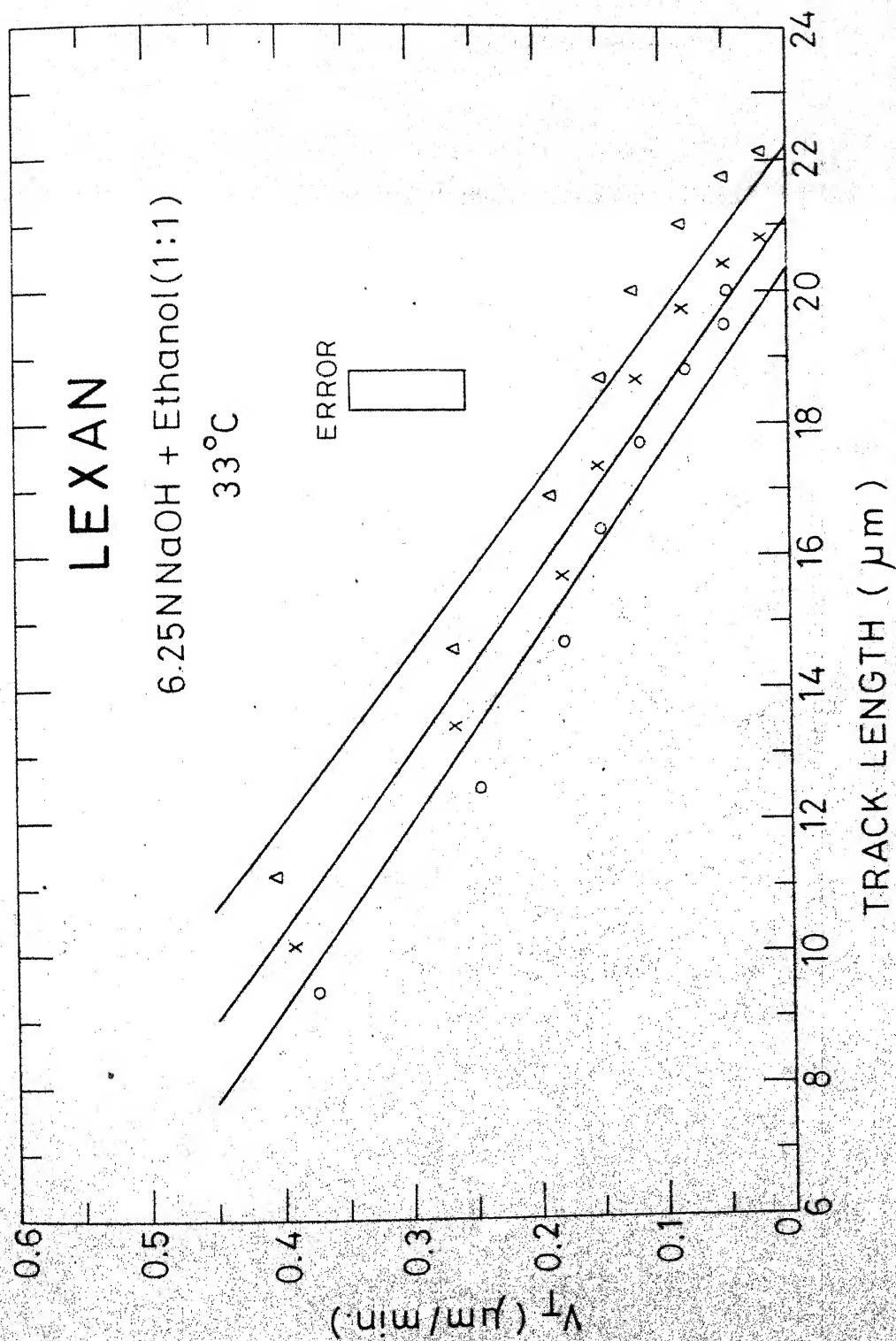


Fig. 18. Plots of track-etch rate V_T versus etched track length for Lexan etched with 6.25 N NaOH + ethanol (1:1) at 33°C.

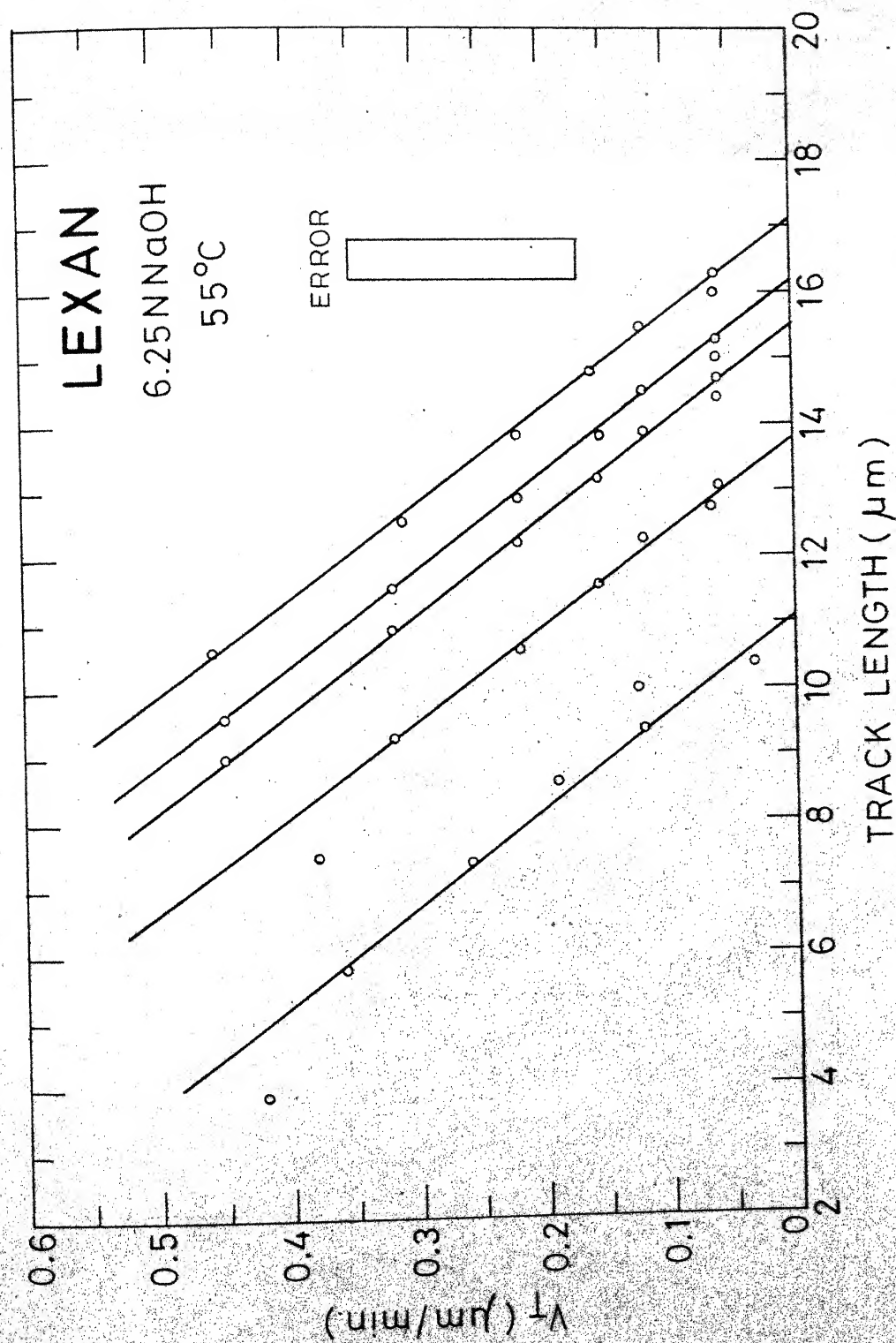


Fig.19. Plots of track-etch rate V_T versus etched track length for Lexan etched with 6.25 N NaOH at 55°C.

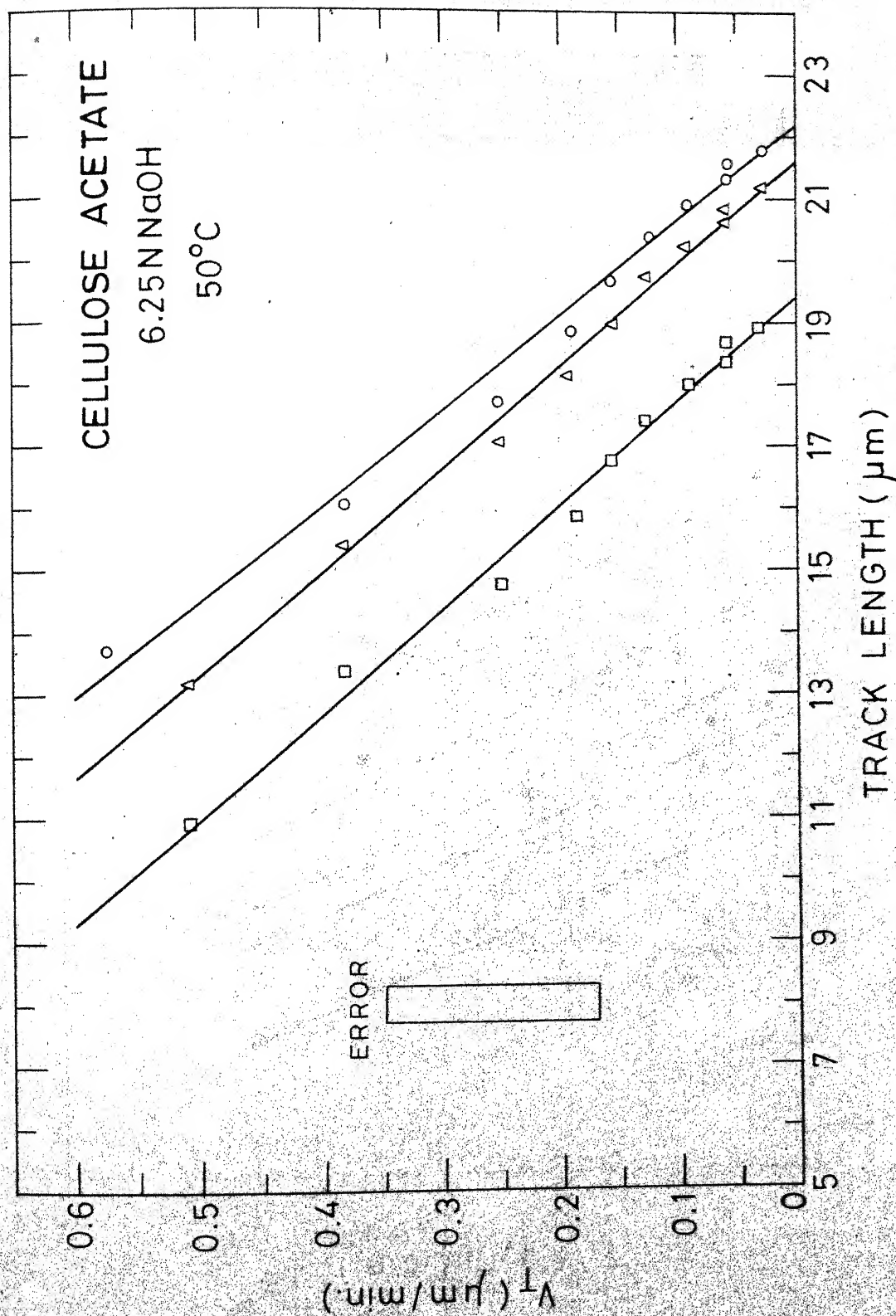


Fig. 20. Plots of track-etch rate V_T versus etched track length for cellulose acetate etched with 6.25N NaOH at 50°C.

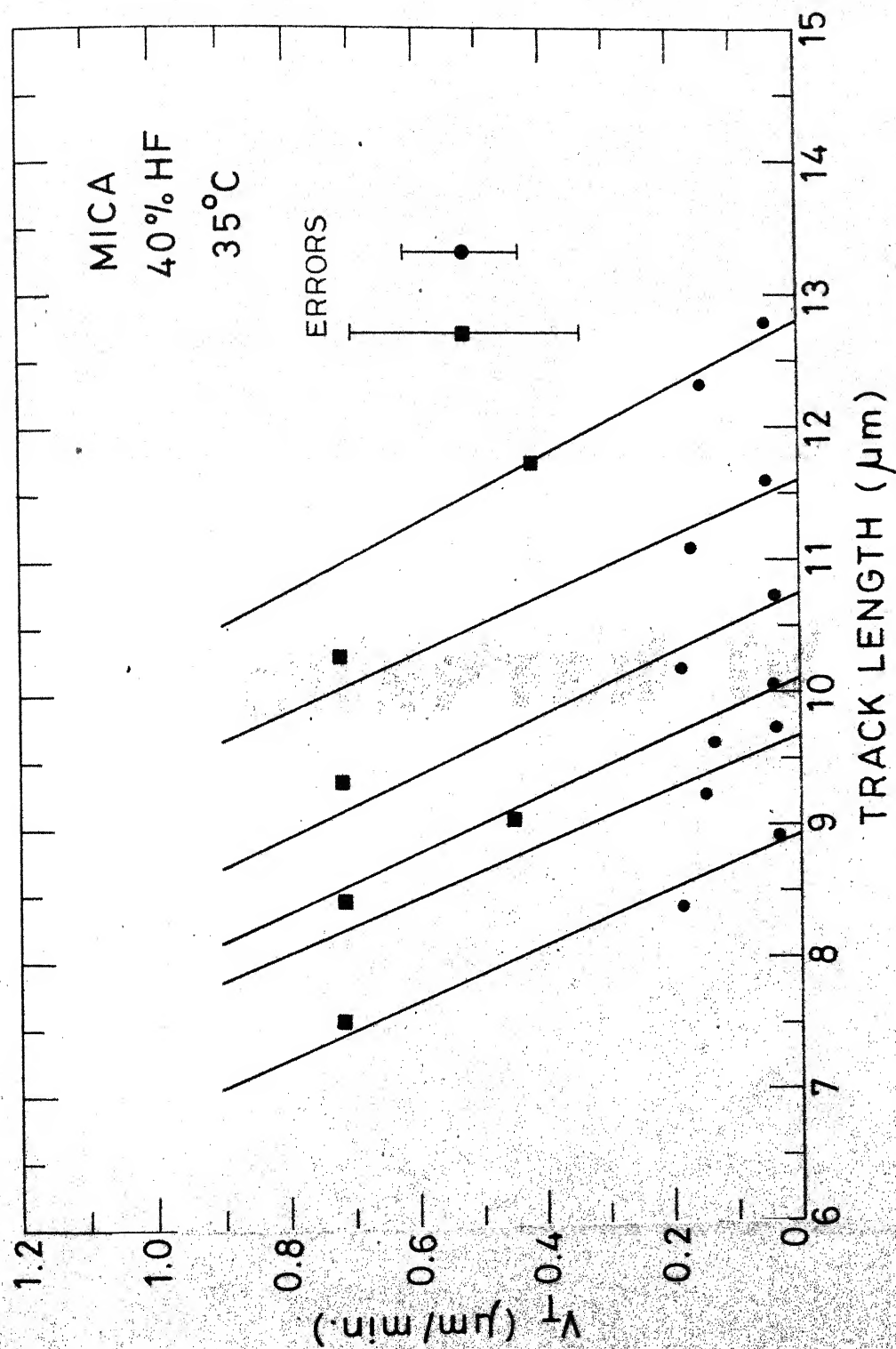


Fig. 21. Plots of track-etch rate V_T versus etched track length for mica etched with 40% HF at 35°C.

CHAPTER IV

CHAPTER IV

ANALYSIS OF EXPERIMENTAL DATA

IV.1 TRACK LENGTH DISTRIBUTION

Samples of mica, Lexan and cellulose acetate were exposed to collimated fission products at various incident angles for sufficiently long time to get a large number of tracks in each sample. The true track lengths were obtained from the observed ones by using Eq. (2.12) and in the case of mica these values are tabulated in Table IV.1 alongwith the number of tracks and the per cent of tracks having a certain track length. θ represents the angle of incidence of the collimated fission products. The experimental data are summarised in Tables IV.2- IV.4.

The track length distribution was obtained by plotting the per cent of tracks against the track length. Figures 22-24

TABLE IV.1

^{252}Cf fission product track lengths in mica

Angle of incidence 15°			Angle of incidence 30°			Angle of incidence 45°		
Track length (μm)	Number of tracks	Percent of tracks	Track length (μm)	Number of tracks	Percent of tracks	Track length (μm)	Number of tracks	Percent of tracks
14.13	18	0.37	14.00	38	1.40	13.94	36	1.53
13.35	108	2.22	13.13	171	6.26	12.86	271	11.55
12.56	379	7.80	12.25	333	12.19	11.80	450	19.17
11.78	634	13.06	11.38	491	17.97	10.72	578	24.63
10.99	942	19.40	10.50	589	21.56	9.64	376	16.02
10.21	963	19.83	9.63	410	15.00	8.58	315	13.42
9.42	639	13.16	8.75	299	10.94	7.50	120	5.11
8.64	404	8.32	7.88	145	5.31	6.43	62	2.64
7.85	261	5.37	7.00	81	2.96	5.36	53	2.26
7.07	160	3.30	6.13	43	1.57	4.30	48	2.05
6.28	93	1.92	5.25	34	1.24	3.22	38	1.62
5.50	64	1.32	4.38	34	1.24			
4.71	62	1.28	3.50	64	2.34			
3.93	79	1.63						
3.14	50	1.03						
Total number of tracks = 4856			Total number of tracks = 2732			Total number of tracks = 2347		
Av. track length = $9.99 \pm 1.00 \mu\text{m}$			Av. track length = $10.14 \pm 1.00 \mu\text{m}$			Av. track length = $10.11 \pm 1.00 \mu\text{m}$		

Av. = average.

TABLE IV.2

Average track length of fission products in mica

Incident angle ϕ	Number of samples	Number of tracks measured	Average track length (μm)
15°	2	4856	9.99 ± 1.00
30°	1	2732	10.14 ± 1.00
45°	2	2347	10.11 ± 1.00

Total number of tracks = 9935

Grand average track length in mica = $10.06 \pm 1.00 \mu\text{m}$.TABLE IV.3

Average track length of fission products in Lexan

Incident angle ϕ	Number of samples	Number of tracks measured	Average track length (μm)
15°	2	3640	19.04 ± 1.00
30°	1	1702	19.39 ± 1.00
45°	1	2196	19.48 ± 1.00

Total number of tracks = 7538

Grand average track length in Lexan = $19.25 \pm 1.00 \mu\text{m}$.

TABLE IV.4

74

Average track length of fission products in cellulose acetate

Incident angle ϕ	Number of samples	Number of tracks measured	Average track length (μm)
15°	1	1402	19.23 \pm 1.00
30°	3	3248	18.44 \pm 1.00

Total number of tracks = 4650

Grand average track length in cellulose acetate = 18.67 \pm 1.00 μm

TABLE IV.5

Comparison between the theoretical and experimental values of track lengths in different solid dielectrics

SDTD	Density (g/cm ³)	TRACK LENGTH (μm)		
		Theoretical	Expt. (a)	Expt. (b)
<u>Mica</u> ($\text{KAl}_3\text{Si}_3\text{H}_2\text{O}_{12}$)	2.93	10.00	10.7 \pm 1.0	11.25*
<u>Lexan</u> ($\text{C}_{16}\text{H}_{14}\text{O}_3$)	1.20	20.60	20.4 \pm 1.0	22.00*
<u>Cellulose acetate</u> ($\text{C}_{10}\text{H}_{14}\text{O}_7$)	1.32	19.00	19.3 \pm 1.0	-

(a) present work; (b) Reference 38.

* Experimental errors not quoted.

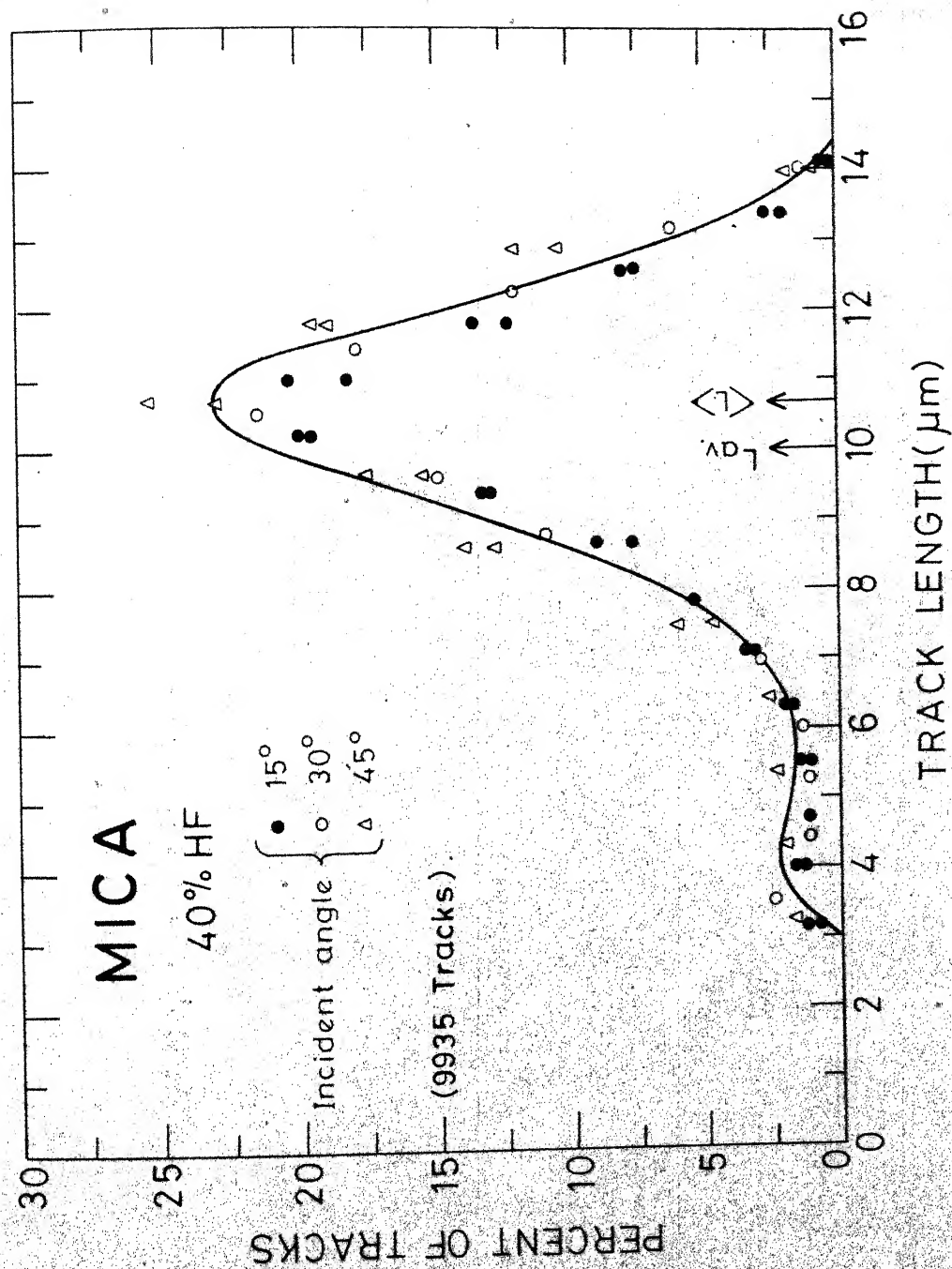


Fig. 22. Distribution of the track lengths of the fission products from ^{252}Cf in mica.

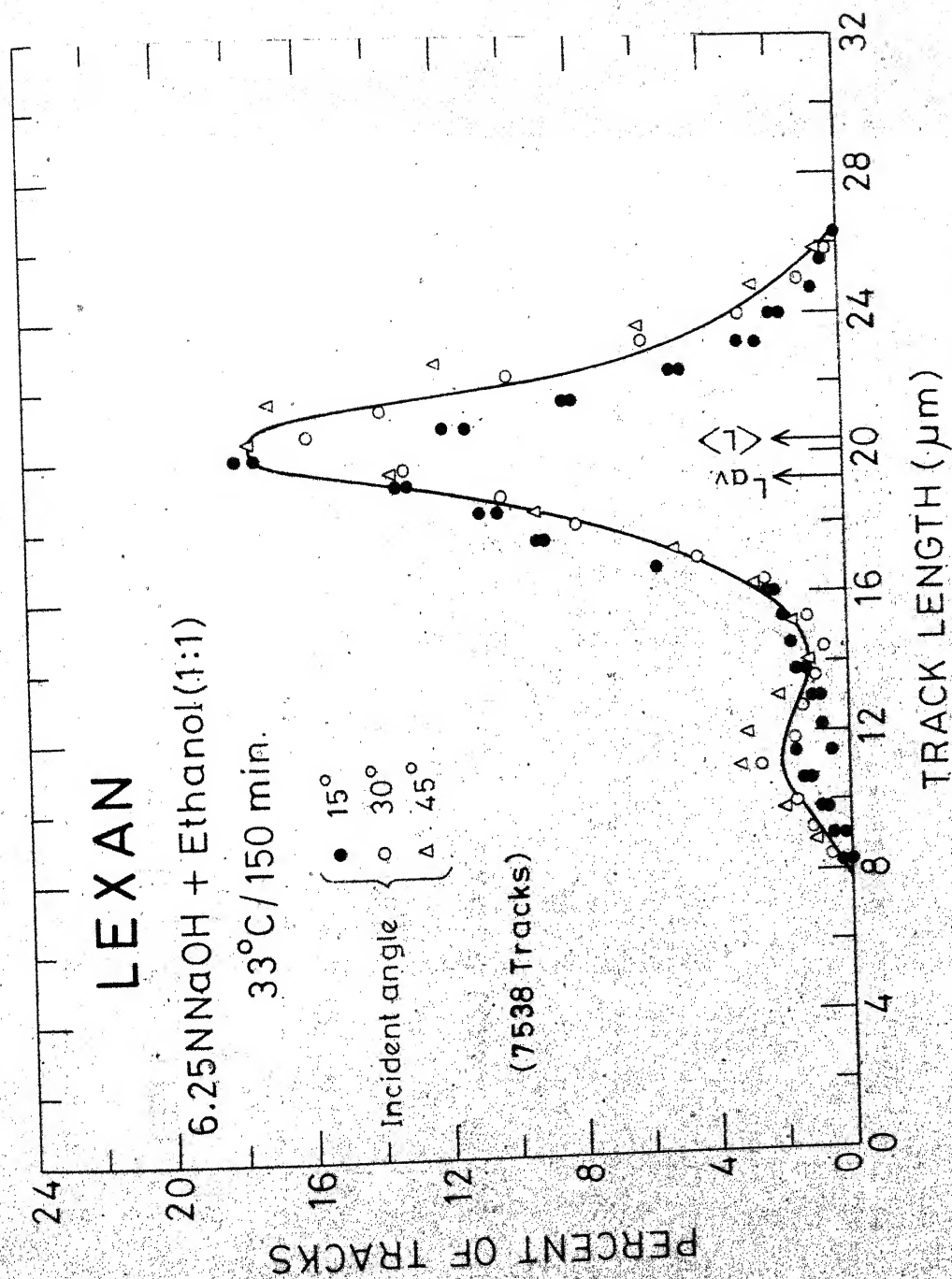


Fig. 23. Distribution of the track lengths of the ^{252}Cf fission products from Lexan.

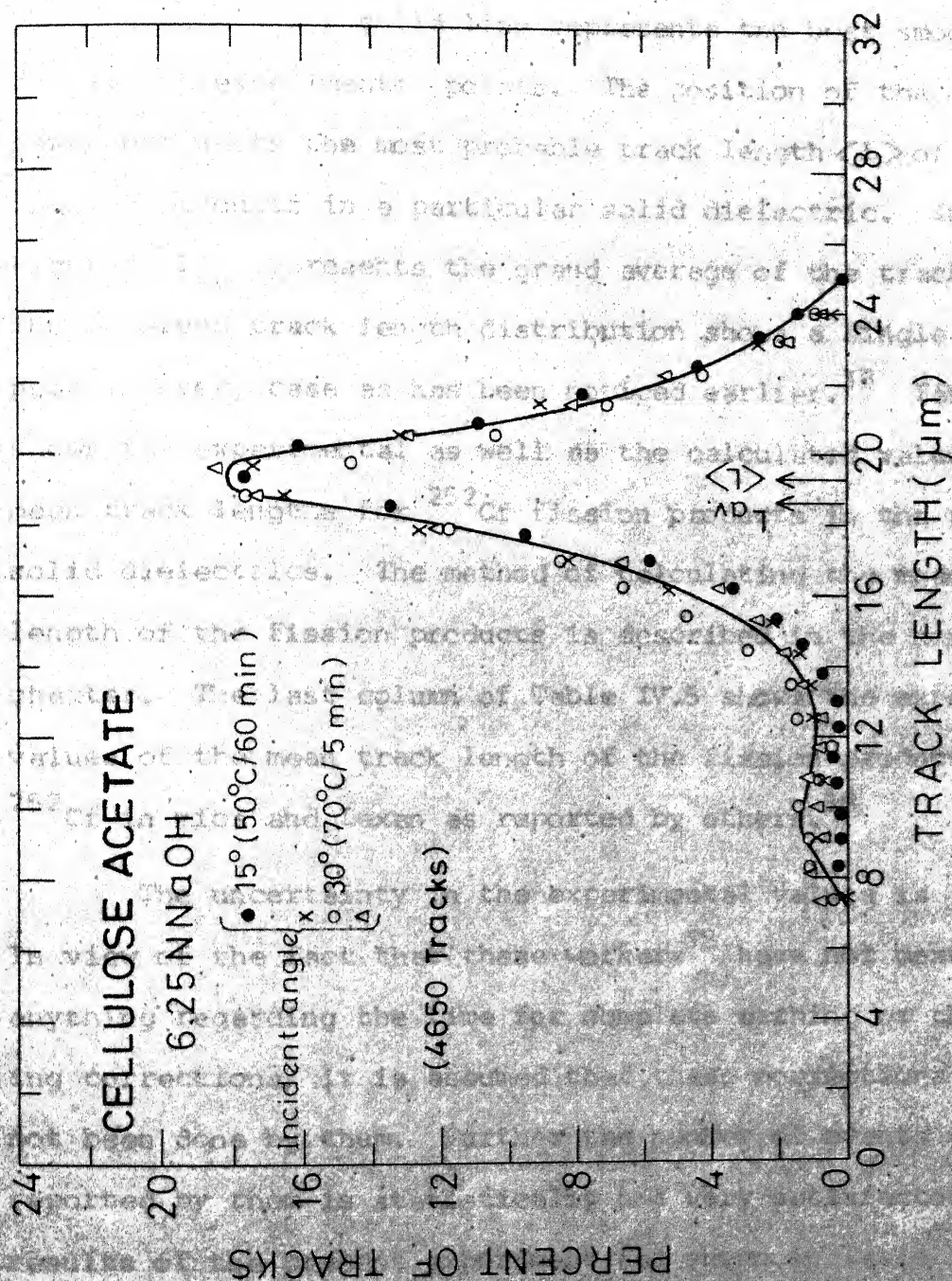


Fig. 24. Distribution of the track lengths of the fission products from ^{252}Cf in cellulose acetate.

show the track length distribution in mica, Lexan and cellulose acetate. The solid line represents the best smooth fit to all the experimental points. The position of the major peak represents the most probable track length $\langle L \rangle$ of ^{252}Cf fission products in a particular solid dielectric. In these figures, L_{av} represents the grand average of the track lengths. The observed track length distribution shows a single major peak in every case as has been noticed earlier.³⁸ Table IV.5 shows the experimental as well as the calculated values of the mean track lengths for ^{252}Cf fission products in the three solid dielectrics. The method of calculating the mean track length of the fission products is described in the next chapter. The last column of Table IV.5 shows the experimental values of the mean track length of the fission products from ^{252}Cf in mica and Lexan as reported by others.³⁸

The uncertainty in the experimental values is $\pm 1.0 \mu\text{m}$. In view of the fact that these workers³⁸ have not mentioned anything regarding the time for complete etching or the etching corrections, it is assumed that these corrections have not been done by them. Further the number of events (~ 200) reported by them is statistically not very satisfactory. The results of the present experiment (as shown in Table IV.5) may possibly be considered as more accurate than the earlier ones.³⁸

IV.1.1 Explanation for the Smaller Peaks in the Track Length Distribution Curves

A broad and rather smaller peak appears at the shorter track region in each case. This is possibly due to the fission products which have undergone grazing collision with the collimator walls during their passage through the collimator holes. To test these assumptions a few experiments were performed with a collimator with 1/32 inch holes in the case of mica at an incidence angle of 30° . It was found that the percentage of tracks of lengths less than $5.5 \mu\text{m}$ increased by a factor of two, i.e., from 5% in the case of 1/16 inch collimator holes to $\sim 10\%$ in the case of 1/32 inch collimator holes.

Further, an experiment was performed with a carbon foil of thickness $\sim 10 \mu\text{g}/\text{cm}^2$ covering the collimator holes to prevent any physical carry-over of californium by the fission products. It was found that this led to no change in the track distribution or on the abundance of the smaller tracks. Hence, grazing collisions are possibly responsible for the shorter tracks.

IV.1.2 Reproduction of the Observed Track-Distribution Curves by Calculation

Experiments with solid state detectors show a two-peaked energy versus mass yield curve, the peaks corresponding to the "most probable" light and heavy products. The observed track-distribution curves, however, always show only a single peak.³⁸ The explanation lies in the fact that the track length is not simply a linear function of the energy, but depends in a complicated way on the mass, nuclear charge, and velocity of the fission product and on the nature of the solid dielectric. Further, the energy-resolution on the basis of track length is rather poor, so that it is not possible, because of experimental uncertainties, to distinguish between the tracks of a group of fission products of closely spaced mass numbers. The mean track length, therefore, remains the only significant experimental quantity for comparison with the theoretically calculated value. An attempt is made here to "construct" the observed track-distribution curve by bunching together a group of closely occurring fission products of practically the same calculated track length. One may then plot the sum of the yields of a bunch, which may be called the "group yield", against the theoretical track length corresponding to the mean mass of each group. The only condition that has to be fulfilled is that the track length of the two fission products at the two ends of a group do not differ

from the mean track length of the group by more than the experimental uncertainty in the track length measurement. Thus the maximum number of fission products which can be included in a group depends upon the relative track length and the uncertainties in the track length measurement in a particular dielectric. Tables IV.6 and IV.7 show the constitution of the various groups, their mean masses and the calculated track length corresponding to each mean mass and the group yield. The values of the individual fission product mass yield have been taken from Schmitt et al.¹⁶ and are listed in Table II.1. The velocities corresponding to the fission products of given masses have been calculated from the kinetic energy data of Schmitt et al.¹⁶ with the help of Eq. (2.2) and the corresponding most probable charges $Z_p(A)$ have been obtained by means of Eqs. (2.5) and (2.6) as given by Mukherji's prescription.¹⁷ These data have been used to calculate the theoretical track lengths as outlined in the next chapter. The plots of the group yields versus track lengths are shown in Figs. 25-27 for comparison with the experimental track length distribution curves as shown in Figs. 22-24 for mica, Lexan and cellulose acetate. The constructed curves have good correspondence with the experimental ones in the case of Lexan and cellulose acetate but not in the case of mica. The possible reason is that in mica, the track lengths being much smaller than in the other two dielectrics, the number of possible groups is considerably

TABLE IV.6

^{252}Cf -fission-product mass groups, their percentage group yields, the mean masses and the corresponding calculated track lengths in mica

Fission product mass groups	Mean mass	Calculated track length (μm)	Group yield (%)
80-96	92.16	11.80	4.04
97-105	101.91	11.36	18.95
106-114	109.50	10.90	22.75
115-138	130.80	9.92	20.84
139-143	140.96	8.93	14.33
144-147	146.86	8.50	9.90
148-152	149.68	8.10	6.50
153-165	157.86	7.20	3.13

$$\text{Mean mass} = \frac{\sum_i Y_i A_i}{\sum_i Y_i},$$

where A_i and Y_i are the mass number and the yield of ith fission product in a group.

TABLE IV.7

^{252}Cf -fission-product mass groups, their percentage group yields, the mean masses and the corresponding calculated track lengths in Lexan and cellulose acetate

Fission product mass groups	Mean mass	Calculated track length (μm)		Group yield (%)
		Lexan	Cellulose acetate	
90-91	90.50	26.13	24.03	0.50
92-93	92.56	25.80	23.74	0.80
94-95	94.56	25.35	23.36	1.13
96-97	96.54	24.88	22.96	1.63
98-99	98.58	24.55	22.64	2.68
100-101	100.56	24.24	22.38	3.95
102-103	102.50	23.88	22.04	5.53
104-105	104.50	23.54	21.74	5.93
106-107	106.53	23.12	21.35	6.18
108-109	108.46	22.64	20.94	5.85
110-113	111.32	22.10	20.40	9.08
114-136	127.10	20.10	18.60	17.09
137-140	138.52	18.71	17.30	11.05
141-143	141.90	18.04	16.68	8.68
144-146	144.93	17.47	16.18	7.75
147-149	147.84	16.95	15.68	5.50
150-152	150.94	16.30	15.03	3.25
153-156	154.20	15.55	14.39	2.05
157-163	159.19	14.40	13.30	1.03

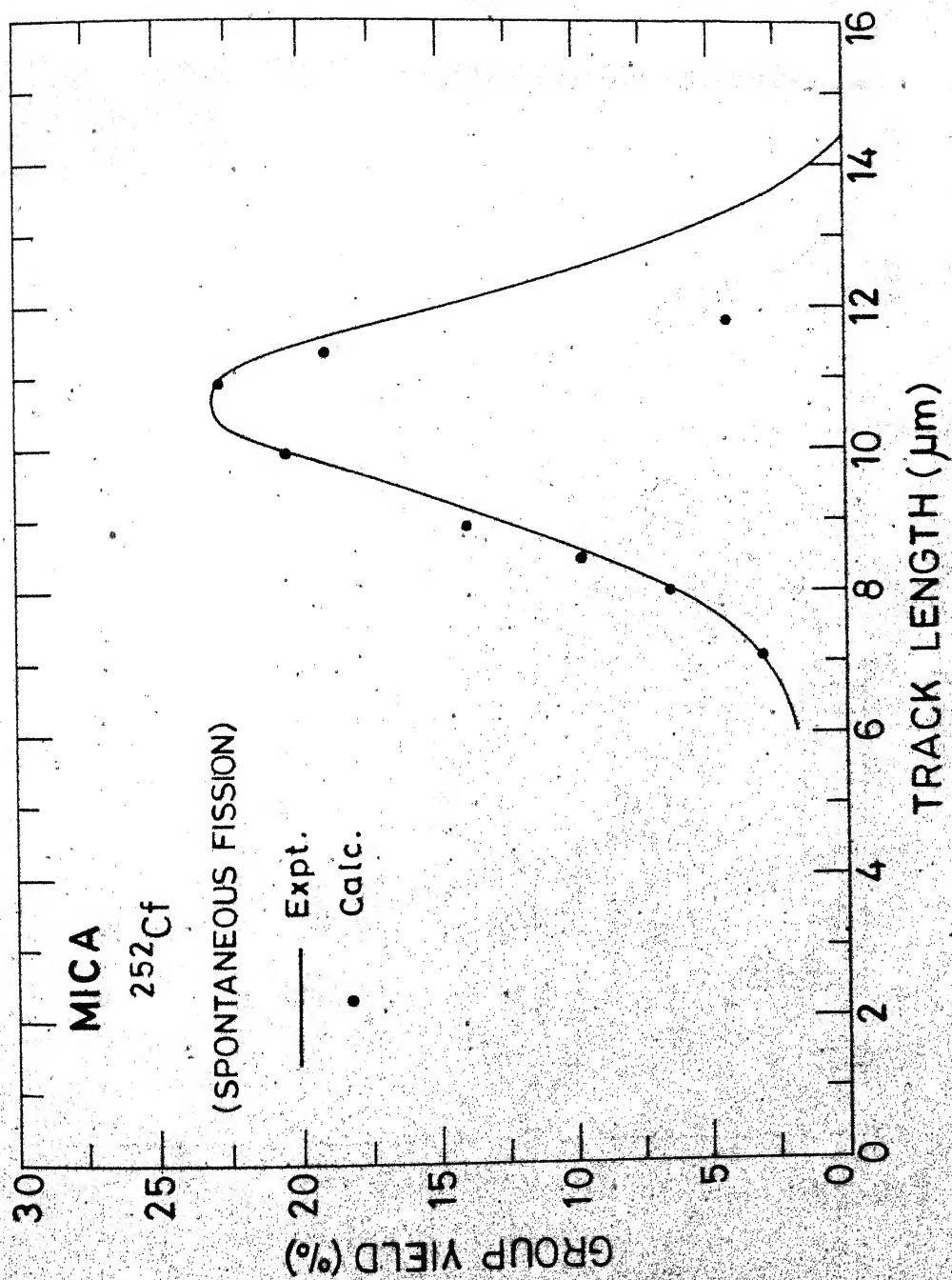


Fig. 25. Constructed distribution curve for the track lengths of the fission products from ^{252}Cf in mica.

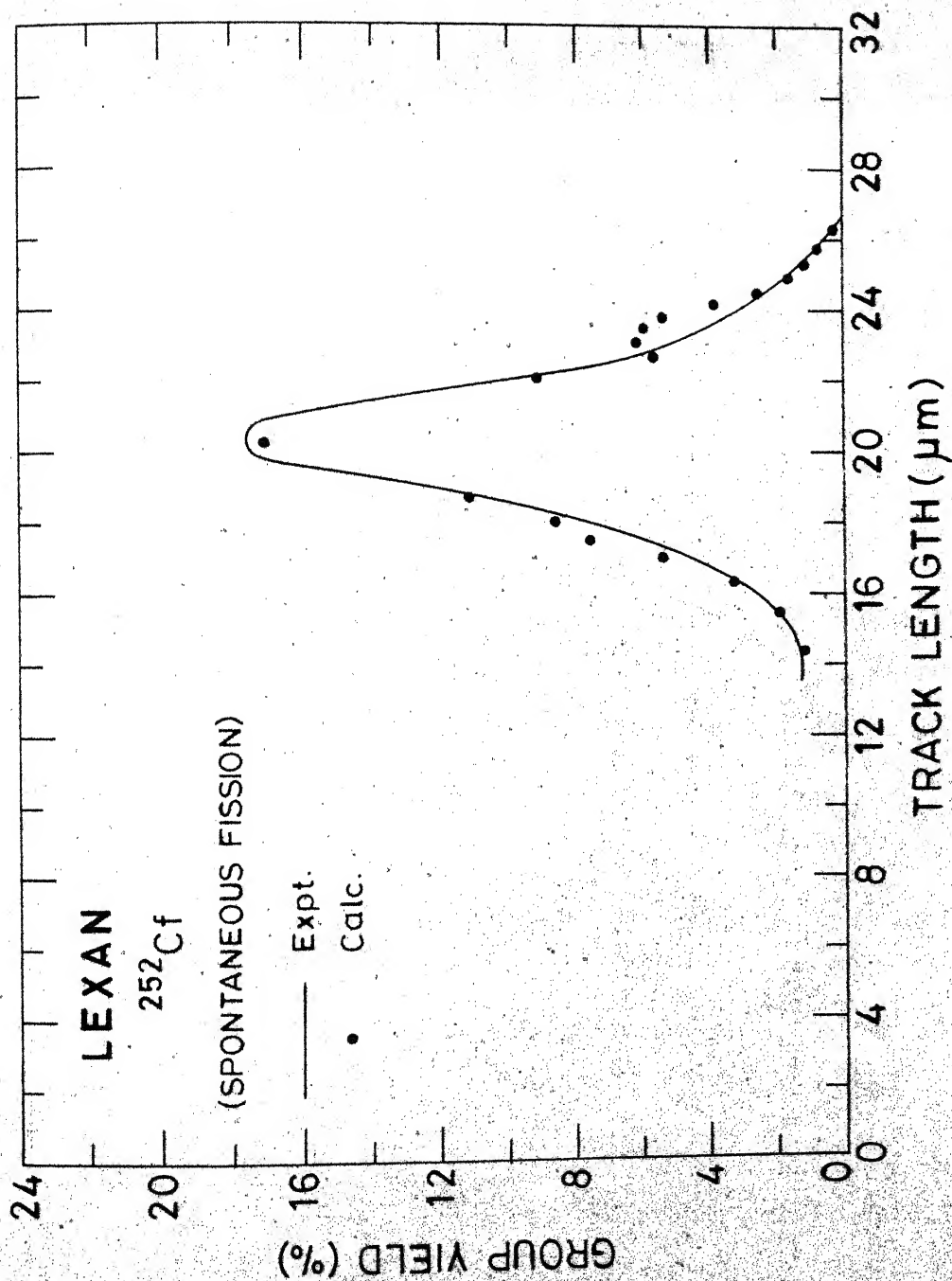


Fig. 26. Constructed distribution curve for the track lengths of the fission products from ^{252}Cf in Lexan.

smaller and the relative uncertainties in the track lengths are much larger. Several trials at various types of grouping might lead to better agreement but since the constructed curve is not of any serious theoretical significance, it was decided to leave it at this stage.

IV.2 RELATION BETWEEN THE TRACK-ETCH RATE V_T AND THE ENERGY-DEPOSITION RATE dE/dX

In Chap. III, Sec. III.4, the experimental method for determining the track-etch rate V_T has been described. Experimentally, the quantity that has been determined is the track-etch rate V_T at different points on the track. In Chapter V, the method of computing the range of a heavy ion in a complex medium is described in detail. The computer output lists the velocity of the ion after it penetrates a certain thickness of the medium and the dE/dX at that point and ultimately gives the thickness required to reduce the velocity to V_0 , which is considered as the range of the ion. The total track length of a fission product, however, is usually less than the range, since no track are visible as soon as the dE/dX of the ion falls below $(dE/dX)_c$.³⁸ In Chap. III, Sec. III.4, the experimental values of the track-etch rate V_T at different etched track lengths have been obtained as shown in Figs. 17-21. The maximum etchable track length L for each of these tracks corresponding to etching time t_c are also known (Tables III.8 -

III.12). From Figures 42 and 43 one can obtain the calculated values of the track lengths L of the various fission products of known mass. Hence, from the experimental maximum etchable track length L and Figs. 42 and 43 one can identify which fission product is involved in a particular track one is studying. Further, from the computer output, the dE/dX values corresponding to different etched track lengths (i.e., penetration depths) have been obtained as shown in Figs. 28-30 for the appropriate fission product in Lexan, cellulose acetate and mica. Thus from Figs. 17-21 and Figs. 28-30 the plot of V_T versus dE/dX has been obtained as shown in Figs. 31-35. In spite of the large uncertainties in V_T , it seems possible that a linear relationship exists between the track-etch rate and the energy-deposition rate. The straight lines representing the weighted least-square fit to the data cut the line representing V_G at dE/dX which equals $(dE/dX)_C$ of the different media. Values of $(dE/dX)_C$, thus obtained, are listed in Table IV.8 along with the corresponding experimental values available in literature.⁴⁰⁻⁴²

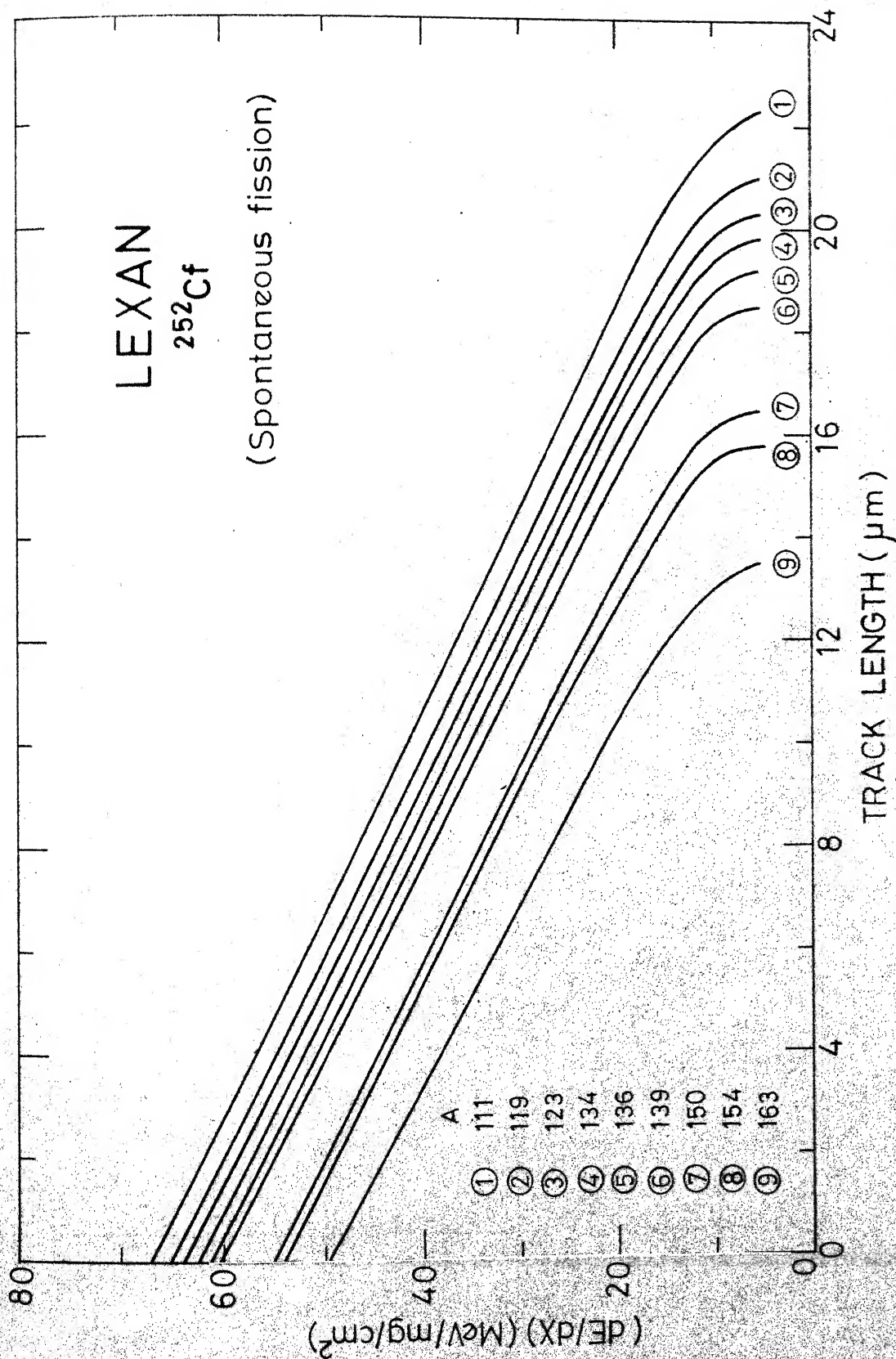


Fig. 28. Computed values of the energy-deposition rate (dE/dX) of a few individual fission products in Lexan plotted as a function of track length.

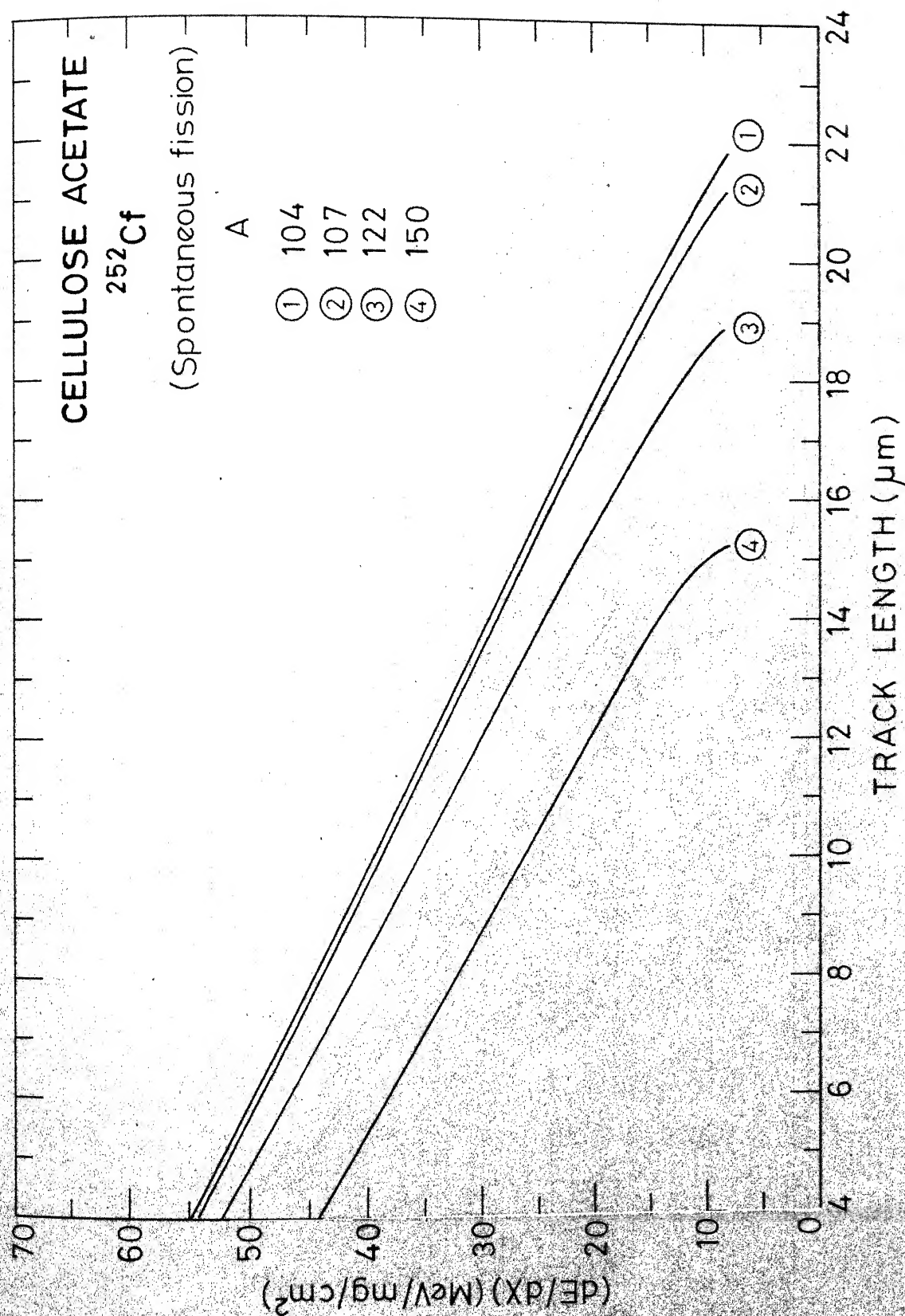


Fig. 29. Computed values of the energy-deposition rate (dE/dX) of a few individual fission products in cellulose acetate plotted as a function of track length.

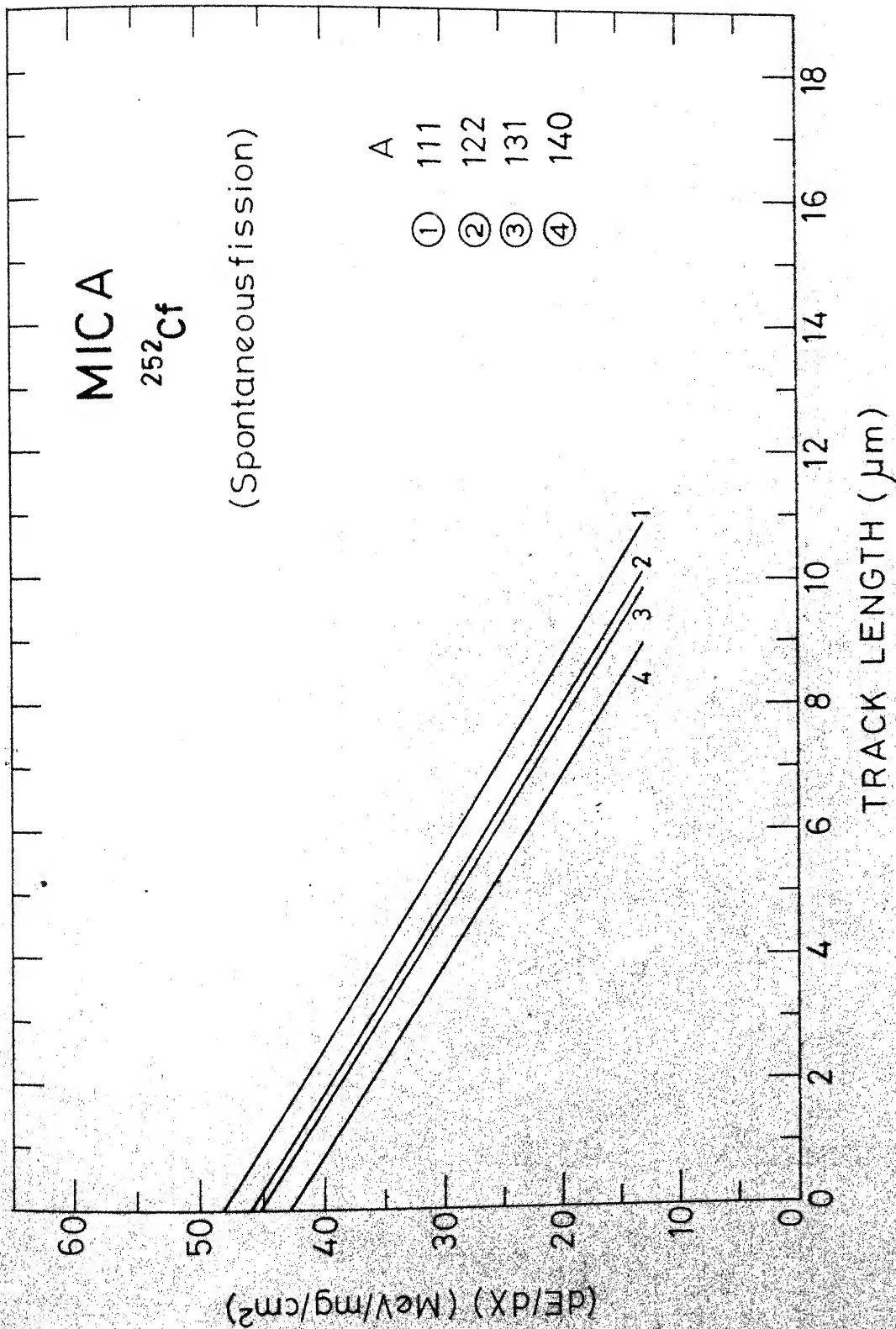


Fig. 30. Computed values of the energy-deposition rate (dE/dX) of a few individual fission products in mica plotted as a function of track length.

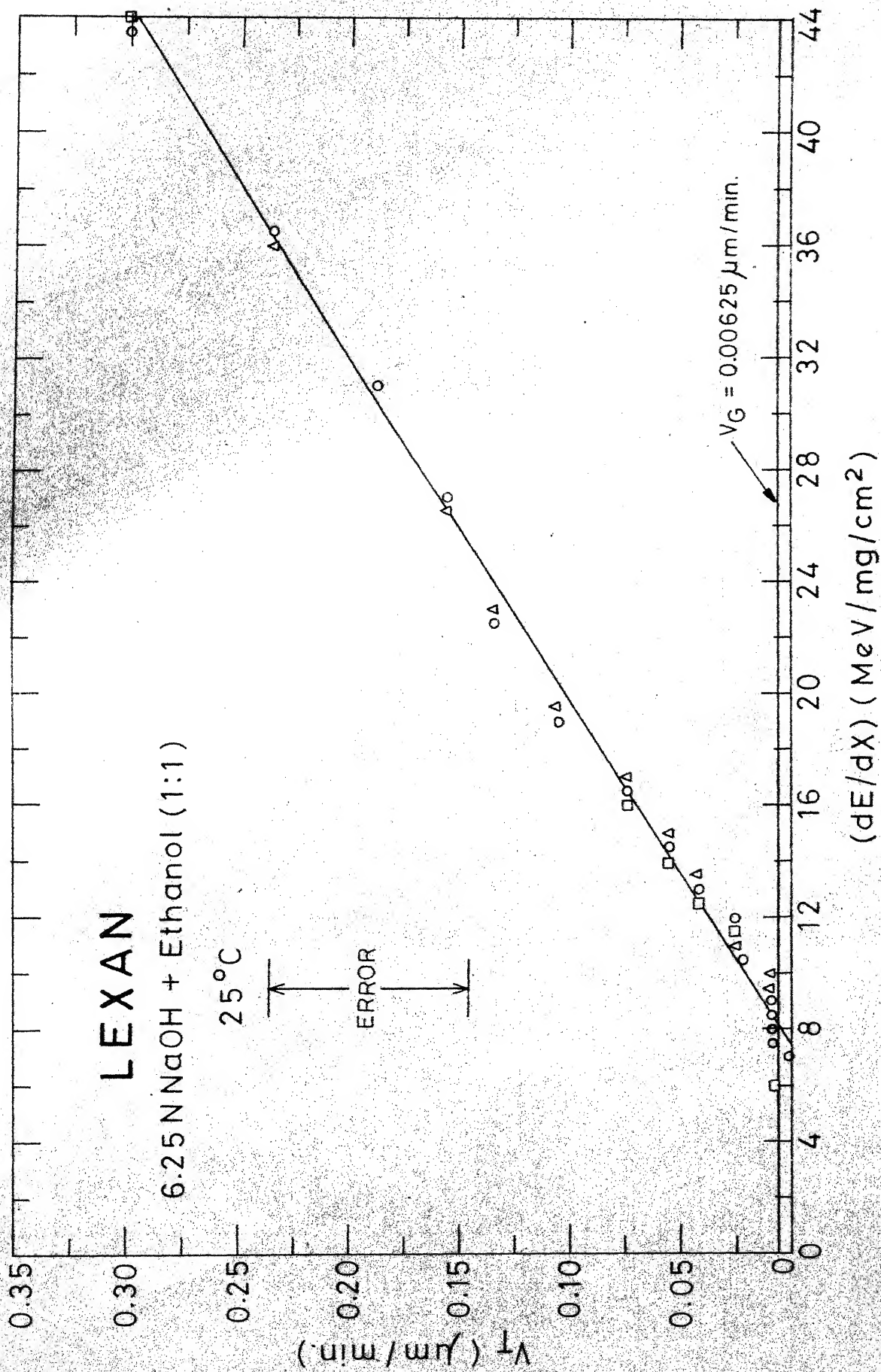


Fig. 31. Dependence of track-etch rate V_T on the energy-deposition rate (dE/dX) in Lexan.

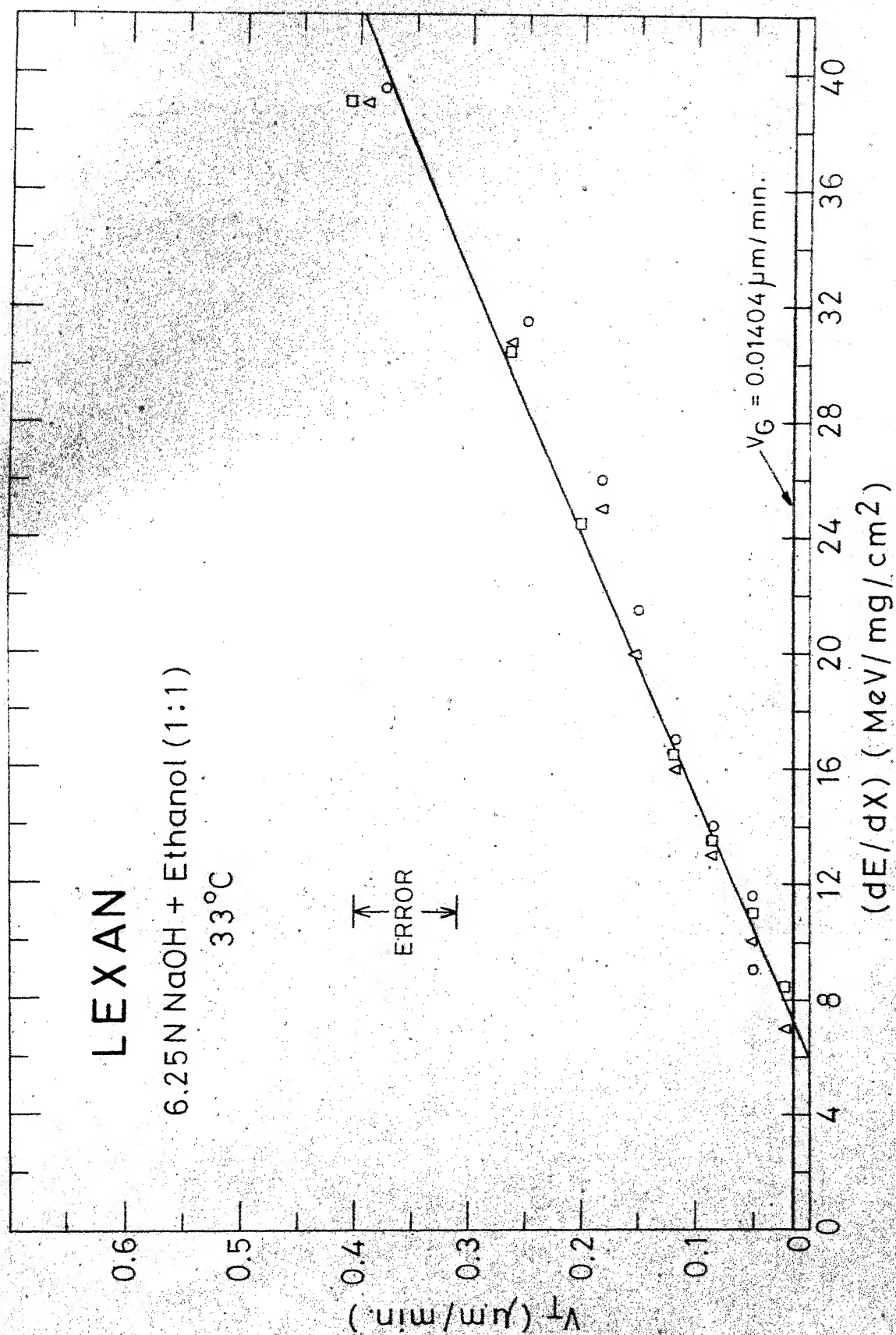


Fig. 32. Dependence of track-etch rate V_T on the energy-deposition rate (dE/dX) in Lexan.

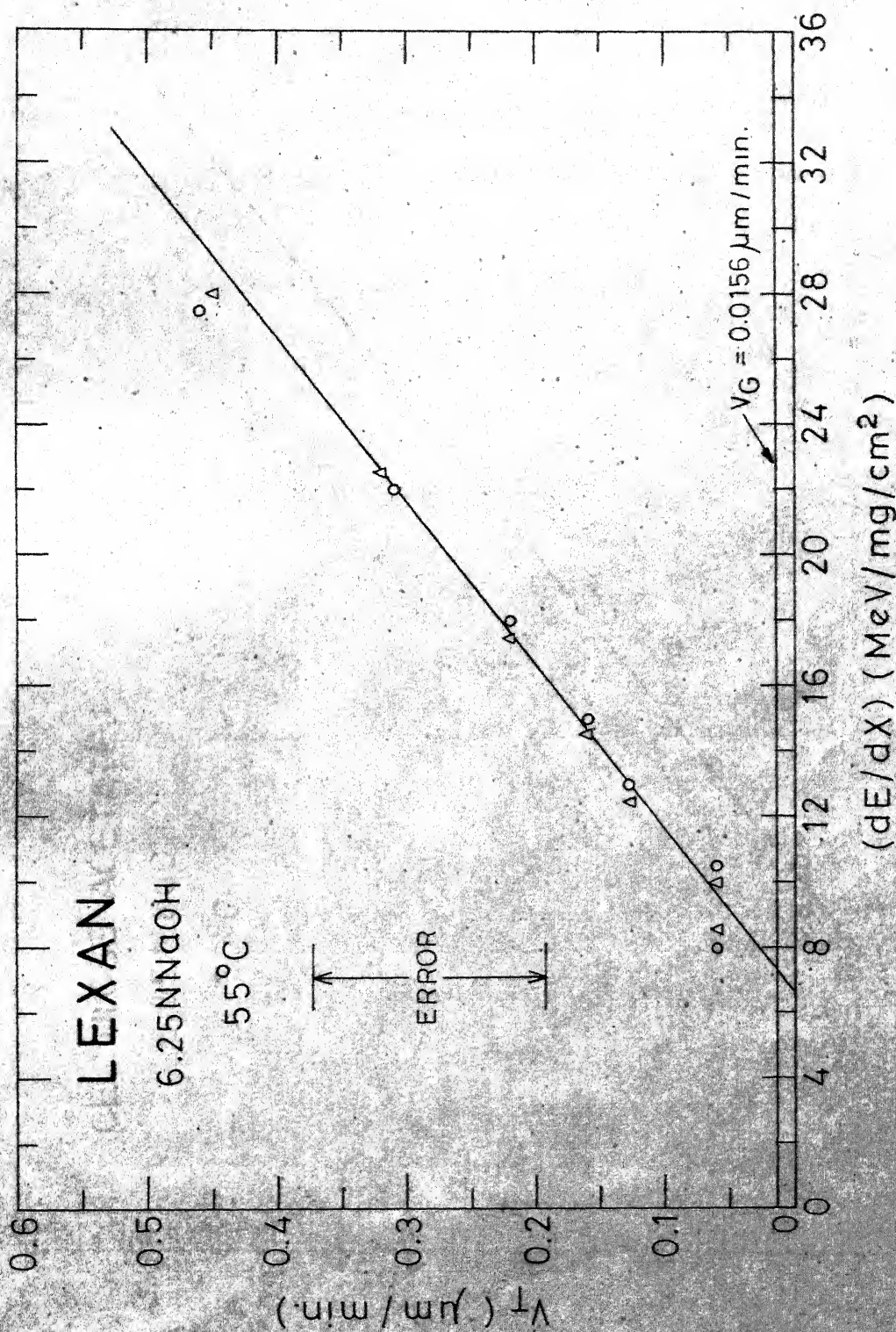


Fig. 33. Dependence of track-etch rate V_T on the energy-deposition rate (dE/dX) in Lexan.

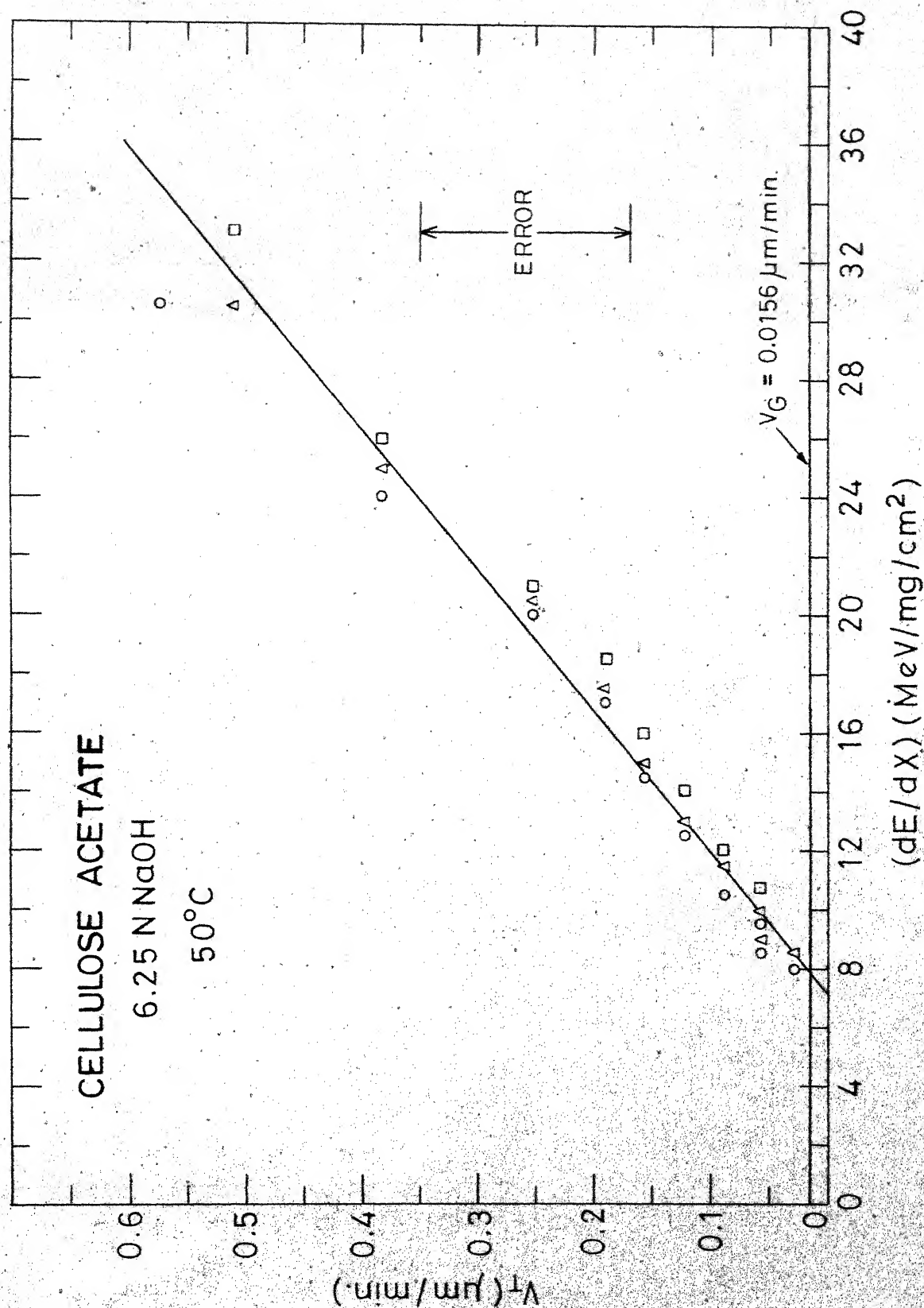


Fig. 34. Dependence of track-etch rate V_T on the energy-deposition rate (dE/dX) in cellulose acetate.

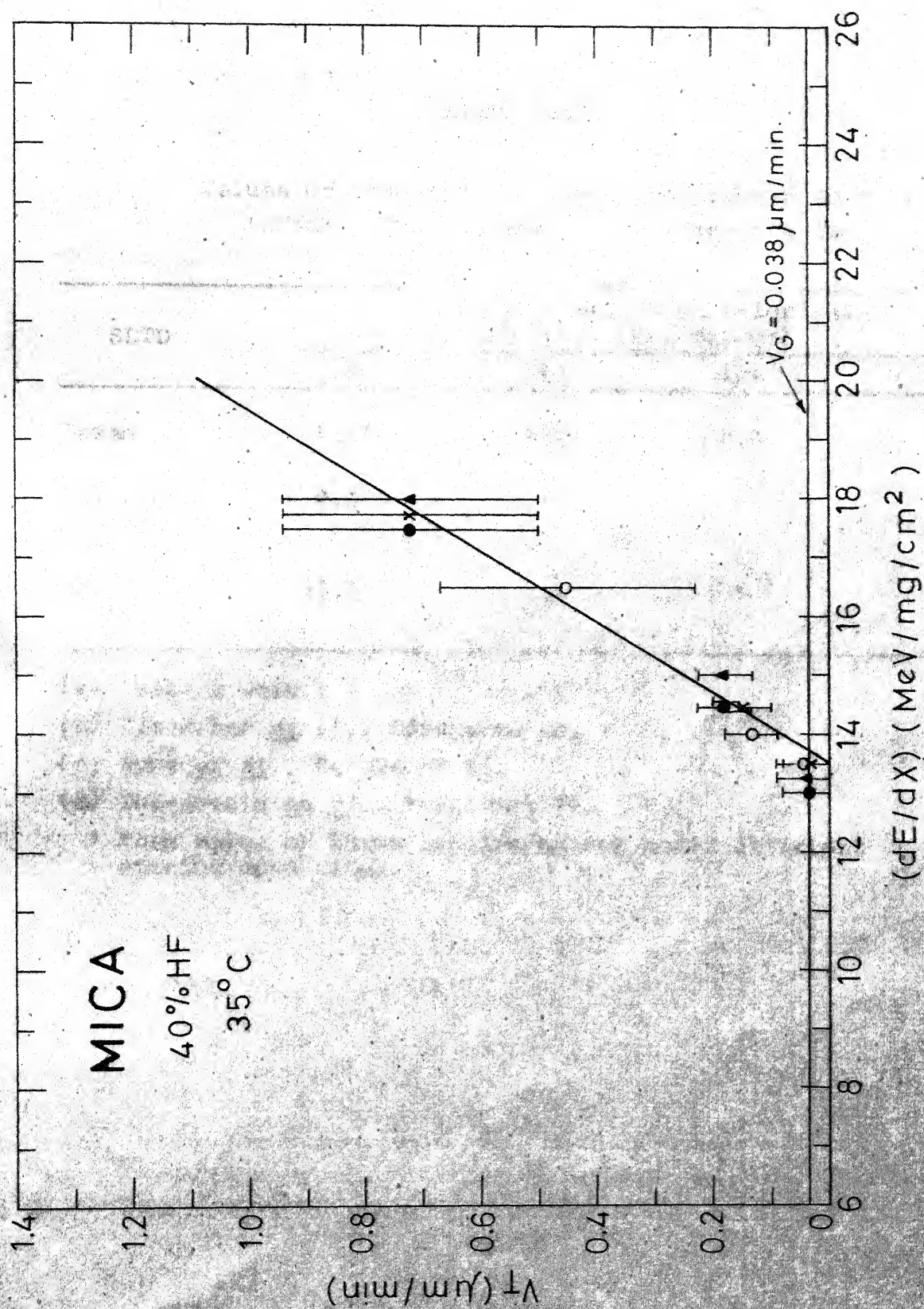


Fig. 35. Dependence of track-etch rate V_T on the energy-deposition rate (dE/dX) in mica.

TABLE IV.8

Values of the critical energy-deposition rate
 $(dE/dx)_c$ for different solid dielectrics

SDTD	Critical energy-deposition rate, $(dE/dx)_c$, (MeV/mg/cm ²)			
	(a)	(b)	(c)	(d)
Lexan	7.6*	4.0	8.0	5.5
Cellulose acetate	8.0	-	-	-
Mica	13.7	13.0	-	15.0

(a) Present work.

(b) Fleischer et al., Reference 40.

(c) Remy et al., Reference 41.

(d) Debeauvais et al., Reference 42.

* Mean value of three determinations under different etching conditions.

CHAPTER V

CHAPTER V

THEORETICAL CALCULATION OF THE TRACK LENGTHS OF HEAVY IONS AND FISSION PRODUCTS IN SOLID DIELECTRICS

V.1 INTRODUCTION

The theoretical calculation of the track lengths of energetic heavy ions in solid dielectrics poses two difficult problems. The first problem is that one has to find reliable stopping-power equations which do not contain any arbitrary parameter and which predict satisfactorily the available experimental stopping-powers and ranges of heavy ions in elemental media. Once such equations are found, stopping-powers in complex media of known molecular formula can be calculated on the basis of Bragg's additivity rule which states that the stopping-power of a complex medium is the sum of the stopping-

powers of the atoms of the constituent atomic species. The second problem is due to the observed fact that in a solid dielectric the track length of a heavy ion is not always equal to the penetration depth or range of the ion. It has been reported by some workers^{12,38} that no visible tracks are formed by a heavy ion even when it has a considerable amount of kinetic energy left in it. Thus, even if the range is calculated with the help of suitable stopping-power equations, one does not know how to calculate the track length with any degree of precision. The first problem has been solved by Mukherji and Srivastava,^{13a} Srivastava and Mukherji^{13b} and Mukherji and Nayak.¹⁵ A brief description of their work would be given first before proceeding to the solution of the second problem in the second half of this chapter.

V.2 STOPPING-POWER EQUATIONS FOR COMPLEX MEDIA

Niday⁴³ was the first to show that a stopping-power equation due to Bohr¹⁴ could be used, with a minor modification, to calculate the ranges of fission products in metallic uranium as the medium. Mukherji and Srivastava^{13a} then developed a method for using the same equation to calculate the ranges of fission products in both heavy as well as light media. The basis for this generalization came from the observation that the velocity distribution among the orbital electrons of an element of atomic number Z is given by^{13a}

$$n(U_s) = f(Z) \frac{U_s}{V_0} \quad (5.1)$$

where $n(U_s)$ is the number of orbital electrons with orbital velocity less than U_s , $V_0 (= e^2/\hbar)$ is the velocity of the electron in the hydrogen atom in its ground state and $f(Z)$ is given by

$$f(Z) = 0.28 Z^{2/3} \quad \text{for } Z \leq 45.5 \quad (5.2)$$

$$f(Z) = Z^{1/3} \quad \text{for } Z > 45.5 \quad (5.3)$$

Further, the ionic charge of the ion, in units of the electronic charge, was found to be given by the quantity Z^{eff}

$$Z^{\text{eff}} = f(Z) \frac{V}{V_0}, \quad (5.4)$$

where V is the ion velocity. Using these ideas, the range R in units of mg/cm^2 , was found to be given by

$$R = \frac{A_1 A_2 (V_i - V_0)}{127.3 f(Z_2) [4.7622 \{f(Z_1)\}^{5/3} + f(Z_1)]}, \quad (5.5)$$

where A_1 , A_2 and Z_1 , Z_2 represent, respectively, the mass numbers and atomic numbers of the ion and the medium, V_i is the initial velocity of the ion and V_0 is the velocity of the

electron in the hydrogen atom in its ground state. Both V_i and V_o in Eq. (5.5) are to be expressed in units of 10^8 cm/sec. The expressions for both $f(Z_1)$ and $f(Z_2)$ are given by Eqs. (5.2) and (5.3). Eq. (5.5), however, is applicable only for partially stripped heavy ions like fission products with velocities not high enough to excite or ionize the innermost electrons of the media in which they are slowing down. Mukherji and Srivastava^{13a} later obtained a set of general stopping-power equations from the same basic stopping-power equation of Bohr.¹⁴ These stopping-power equations are applicable in the case of all heavy ions at any energy and in any elemental medium. From these equations the range of any heavy ion were computed by these authors^{13b} as

$$\int_{E_i}^{E_o} \frac{\delta E}{\left(\frac{dE}{dX}\right)_E} ,$$

where $(dE/dX)_E$ indicates the stopping-power at ion-energy E , E_i is the initial ion-energy, E_o is the energy at which the velocity of the ion is V_o and δE is a small energy-interval (~ 0.01 MeV) over which $(dE/dX)_E$ remains practically constant. The final velocity V_o indicates that below this velocity the ion undergoes screened-coulomb-field interactions to a predominant extent and, because of severe large angle scatterings, the distance travelled by it in its original direction at $V < V_o$

is negligible.^{13a} Recently, Mukherji and Nayak¹⁵ have made corrections to these equations and have shown that the new set of stopping-power equations are in excellent agreement with all available experimental data, without any exception, in the case of elemental media. Since these equations have been used in the present work, they are listed below along with the conditions of their validity.

$$(i) \chi > 1, v \geq \frac{zv_o \chi}{2} :$$

$$\frac{dE}{dX} = \frac{63.65 z^2 Z}{AV^2} \log_{10} \left(\frac{11.39 v^2}{\bar{I} \chi} \right) \quad (5.6)$$

$$(ii) \chi > 1, \frac{zv_o \chi^{1/3}}{2} > \frac{(z-2)v_o \chi}{2f(Z)}, \frac{zv_o \chi}{2} > v > \frac{zv_o \chi^{1/3}}{2} :$$

$$\frac{dE}{dX} = \frac{63.65 z^2}{AV^2} \left[(z-2) \log_{10} \left(\frac{11.39 v^2}{\bar{I}_1 \chi} \right) + 3 \log_{10} \left(\frac{2v}{zv_o \chi^{1/3}} \right) \right] \quad (5.7)$$

$$(iii) \chi > 1, \frac{zv_o \chi^{1/3}}{2} > \frac{(z-2)v_o \chi}{2f(Z)}, \frac{zv_o \chi^{1/3}}{2} > v > \frac{(z-2)v_o \chi}{2f(Z)} :$$

$$\frac{dE}{dX} = \frac{63.65 z^2}{AV^2} (z-2) \log_{10} \left(\frac{11.39 v^2}{\bar{I}_1 \chi} \right) \quad (5.8)$$

$$(iv) \chi > 1, \frac{zv_o \chi^{1/3}}{2} < \frac{(z-2)v_o \chi}{2f(Z)}, \frac{zv_o \chi}{2} > v > \frac{(z-2)v_o \chi}{2f(Z)} :$$

Eq. (5.8) would be also applicable in this region.

$$(v) \quad \chi > 1, \quad \frac{z v_o \chi^{1/3}}{2} < \frac{(z-2)v_o \chi}{2f(z)}, \quad \frac{(z-2)v_o \chi}{2f(z)} > v > \frac{z v_o \chi^{1/3}}{2};$$

$$\frac{dE}{dX} = \frac{13.79}{AV^2} z^2 \left[3(z-2) + 3(z-2) \ln \left\{ \frac{2f(z)v}{(z-2)v_o} \right\} + 6 \ln \frac{2v}{z v_o} + \frac{2f(zv)}{v_o \chi} - z \ln \chi \right] \quad (5.9)$$

$$(vi) \quad \chi > 1, \quad \frac{z v_o \chi^{1/3}}{2} < \frac{(z-2)v_o \chi}{2f(z)}, \quad \frac{z v_o \chi^{1/3}}{2} > v > \frac{(z-2)v_o \chi^{1/3}}{2f(z)};$$

$$\frac{dE}{dX} = \frac{13.79}{AV^2} z^2 \left[3(z-2) + \frac{2f(z)v}{v_o \chi} - 3(z-2) \ln \left\{ \frac{(z-2)v_o \chi}{2vf(z)} \right\} \right] \quad (5.10)$$

$$(vii) \quad \chi > 1, \quad \frac{z v_o \chi^{1/3}}{2} > \frac{(z-2)v_o \chi}{2f(z)}, \quad \frac{(z-2)v_o \chi}{2f(z)} > v > \frac{(z-2)v_o \chi^{1/3}}{2f(z)};$$

Eqn. (5.10) would be also applicable in this region.

$$(viii) \quad \chi > 1, \quad v < \frac{(z-2)v_o \chi^{1/3}}{2f(z)};$$

$$\frac{dE}{dX} = \frac{12.68}{AV} f(z) z^2 \left(3 \chi^{-1/3} + \chi^{-1} \right) \quad (5.11)$$

$$(ix) \quad \chi < 1, \quad v \geq \frac{z v_o}{2} :$$

$$\frac{dE}{dX} = \frac{63.65}{AV^2} z^2 z \log_{10} \left(\frac{11.39}{I} \frac{v^2}{I} \right) \quad (5.12)$$

At relativistic energies of the ion^{13b}

$$\frac{dE}{dX} = \frac{63.65 z^2 Z}{AV^2} \left\{ \log_{10} \left(\frac{11.39 v^2}{I(1-\beta^2)} \right) - \frac{\beta^2}{2.303} \right\} \quad (5.13)$$

$$(x) \quad \chi < 1, \quad \frac{ZV_o}{2} > v > \frac{(Z-2)V_o}{2f(Z)} :$$

$$\frac{dE}{dX} = \frac{63.65 z^2 (Z-2)}{AV^2} \log_{10} \left(\frac{11.39 v^2}{I_1} \right) \quad (5.14)$$

$$(xi) \quad \chi < 1, \quad v < \frac{(Z-2)V_o}{2f(Z)} :$$

$$\frac{dE}{dX} = \frac{50.6 f(Z) z^2}{AV} \quad (5.15)$$

The following three equations hold in the case of hydrogen as the medium.

$$(xii) \quad \chi > 1, \quad v > \frac{V_o \chi}{2} :$$

$$\frac{dE}{dX} = \frac{63.65 z^2}{V^2} \log_{10} \left(\frac{11.39 v^2}{I \chi} \right) \quad (5.16)$$

$$(xiii) \quad \chi > 1, \quad \frac{V_o \chi}{2} > v > \frac{V_o \chi^{1/3}}{2} :$$

$$\frac{dE}{dX} = \frac{47.74 z^2}{V^2} \log_{10} \left(\frac{11.39 v^2}{I \chi^{2/3}} \right) \quad (5.17)$$

(xiv) $\chi < 1, v > \frac{v_0}{2}$:

$$\frac{dE}{dx} = \frac{63.65 z^2}{v^2} \log_{10} \left(\frac{11.39 v^2}{I} \right) \quad (5.18)$$

where $I = 13.6$ eV.

All the stopping-powers, given by the equations above, are in units of MeV/mg/cm², v and v_0 are in units of 10^8 cm/sec., z is the ionic charge of the heavy ion in units of the electronic charge, and $\chi = 2Z \frac{v_0}{v}$; \bar{I} , and \bar{I}_1 are the mean ionization potentials of the medium, in electron volts, considering all the orbital electrons in the first case and leaving out the two K-shell electrons in the second case. Z is the atomic number of the medium and A , its mass number. The values of $f(Z)$ were originally given by Eqs. (5.2) and (5.3), but recently, Mukherji and Nayak¹⁵ have shown that a better expression for $f(Z)$ is given by

$$f(Z) = 0.3634 Z^{0.555}, \quad (5.19)$$

for $Z > 4$. The mean ionization potential \bar{I} (eV) can be calculated from the equation of Mukherji⁴⁴

$$Z \ln \bar{I} = (Z-2) \ln \left[13.6 \left\{ \frac{Z-2}{2.717 f(Z)} \right\}^2 \right] + 2 \ln (13.6 Z^2) \quad (5.20)$$

where the first term on the right hand side gives the contribution of the outer $(Z-2)$ electrons of the medium, while the

second term is that of the two K-shell electrons. If the two K-shell electrons do not participate in the energy-loss process then the new mean ionization potential \bar{I}_1 would not include the contribution of the two K-shell electrons and would be given by

$$(Z-2) \ln \bar{I}_1 = (Z-2) \ln \left[13.6 \left\{ \frac{Z-2}{2.717 f(Z)} \right\}^2 \right]$$

or
$$\bar{I}_1 = 13.6 \left\{ \frac{Z-2}{2.717 f(Z)} \right\}^2 . \quad (5.21)$$

The values of $f(Z)$ in Eqs. (5.20) and (5.21) have to be taken from Eq. (5.19). The values of z at any velocity V is given by two different expressions, depending upon the value of V

$$z = f(Z_1) \frac{V}{V_0} \quad \text{for } V < \frac{Z_1 V_0}{2f(Z_1)} \quad (5.22)$$

$$\text{and } z = Z_1 \left[1 - 2.03 \exp \left\{ - \frac{2V f(Z_1)}{Z_1 V_0} \right\} \right]^{1/2}$$

for $V > \frac{Z_1 V_0}{2f(Z_1)} , \quad (5.23)$

where Z_1 is the atomic number of the ion and $f(Z_1)$ is given by Eq. (5.19) with $Z = Z_1$. Mukherji and Nayak¹⁵ have shown that the ranges and energy-losses calculated by means of Eqs. (5.6) - (5.15) and Eqs. (5.19) - (5.23) in the case of various heavy ions in several elemental media are in excellent agreement with the corresponding experimental values. Assuming the

validity of Bragg's additivity rule, the expression for the stopping-power of a complex medium in terms of those of the constituent atomic species is given by

$$\left[\left(\frac{dE}{dX} \right)_E \right]_c = \frac{1}{A_c} \sum_i \left\{ Y_i A_i \left[\left(\frac{dE}{dX} \right)_E \right]_i \right\} \quad (5.24)$$

where $\left[(dE/dX)_E \right]_c$ is the stopping-power of the complex medium at the ion-energy E (MeV), $\left[(dE/dX)_E \right]_i$ is the stopping-power of the i th atomic species at the same ion-energy; Y_i and A_i are the number of atoms per molecule and the atomic number respectively of the i th atomic species. If both $\left[(dE/dX)_E \right]_c$ and $\left[(dE/dX)_E \right]_i$ are expressed in units of MeV/cm²/mg, then $\left[(dE/dX)_E \right]_i$ can be obtained directly from Eqs. (5.6) - (5.18) with the help of eqs. (5.19) - (5.23). The total penetration depth or range R is then given by

$$R(\text{mg/cm}^2) = \sum_{E_i}^{E_0} \frac{\delta E}{\left[\left(\frac{dE}{dX} \right)_E \right]_c}, \quad (5.25)$$

where δE is a small but finite energy interval (~ 0.01 MeV) over which the stopping-power remains virtually constant, E_i is the initial ion-energy, and E_0 is the final energy corresponding to the ion-velocity V_0 . Using this procedure, Mukherji and Nayak¹⁵ have recently, with the help of a computer (IBM 7044), obtained the range-energy and energy-loss curves for several

heavy ions (^{10}B , ^{11}B , ^{12}C , ^{14}N , ^{16}O , ^{19}F and ^{20}Ne) in some complex media (Mylar, polyethylene, human tissue material and nuclear emulsion) and found them to be in very good agreement with the corresponding experimental data. The same procedure has been used in the present work to obtain the track lengths in solid dielectrics as discussed in the next section.

V.3 DISTINCTION BETWEEN TRACK LENGTH AND RANGE OF A HEAVY ION IN SOLID DIELECTRICS

It has been mentioned earlier that heavy ions fail to register any track in a high density solid dielectric even when they have considerable amount of kinetic energy. Fleischer et al.⁴⁰ derived the important conclusion, on the basis of the available data, that, for each solid dielectric, there exists a critical or threshold stopping-power $(dE/dX)_c$ which is independent of the penetrating ion; if an ion has an energy such that its stopping-power is less than $(dE/dX)_c$ then it would not register a track in that medium. Since for every heavy ion the curve obtained by plotting the stopping-power dE/dX against the ion-energy E has a typical shape as shown in Figs. 36-38, the total track length would be given by the thickness of the dielectric required to reduce the energy of the ion from E_2 to E_1 , where E_2 and E_1 are the higher and lower energies of the ion at which $(dE/dX)_c$ is reached (Fig.36), if $E_i > E_2$, where E_i is the initial ion-energy. On the other

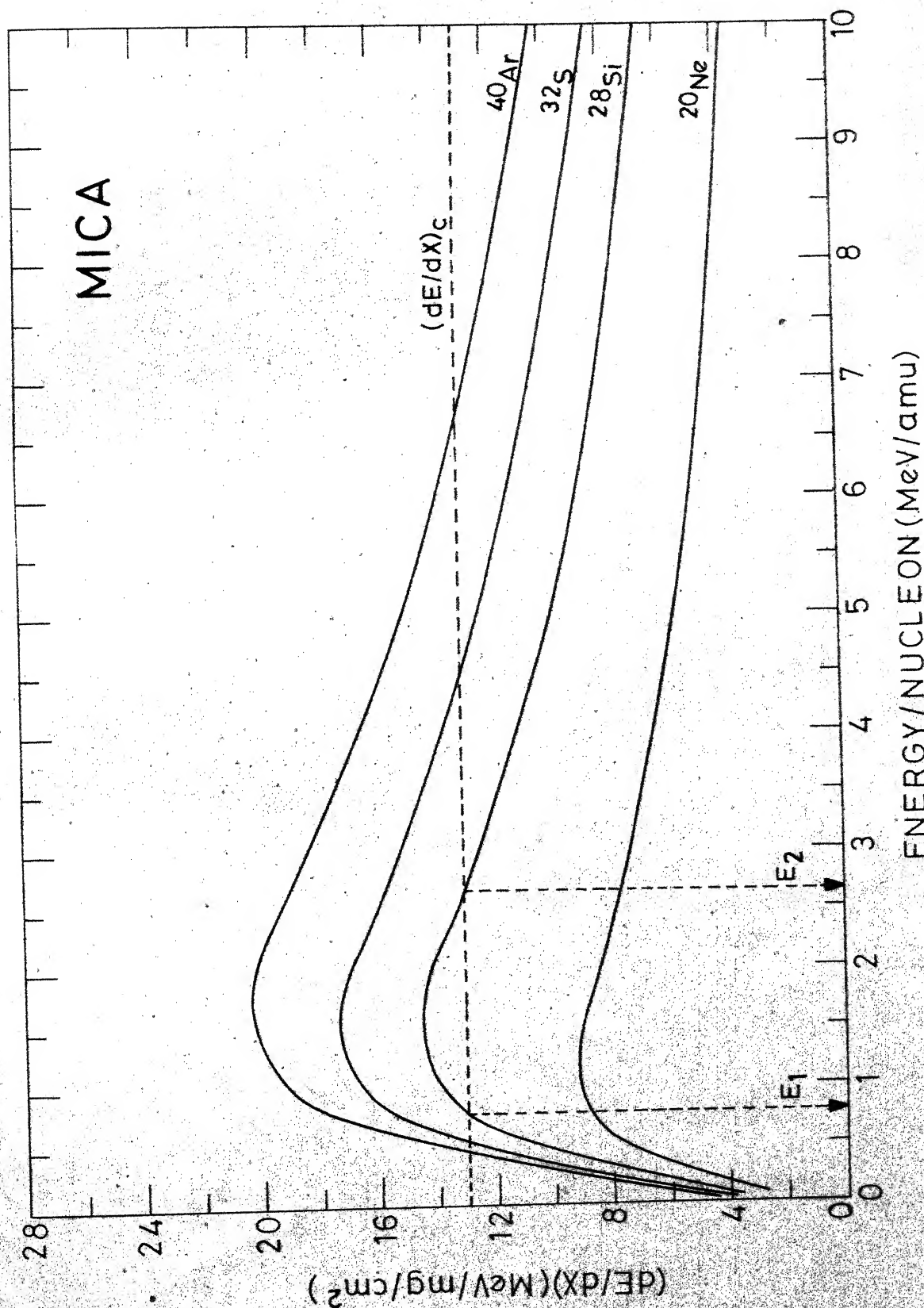


Fig. 36. Plot of the calculated stopping-power versus ion energy for mica. Energies E_1 and E_2 correspond to the lower and the higher energies of ^{28}Si ion at which the critical stopping-power is reached.

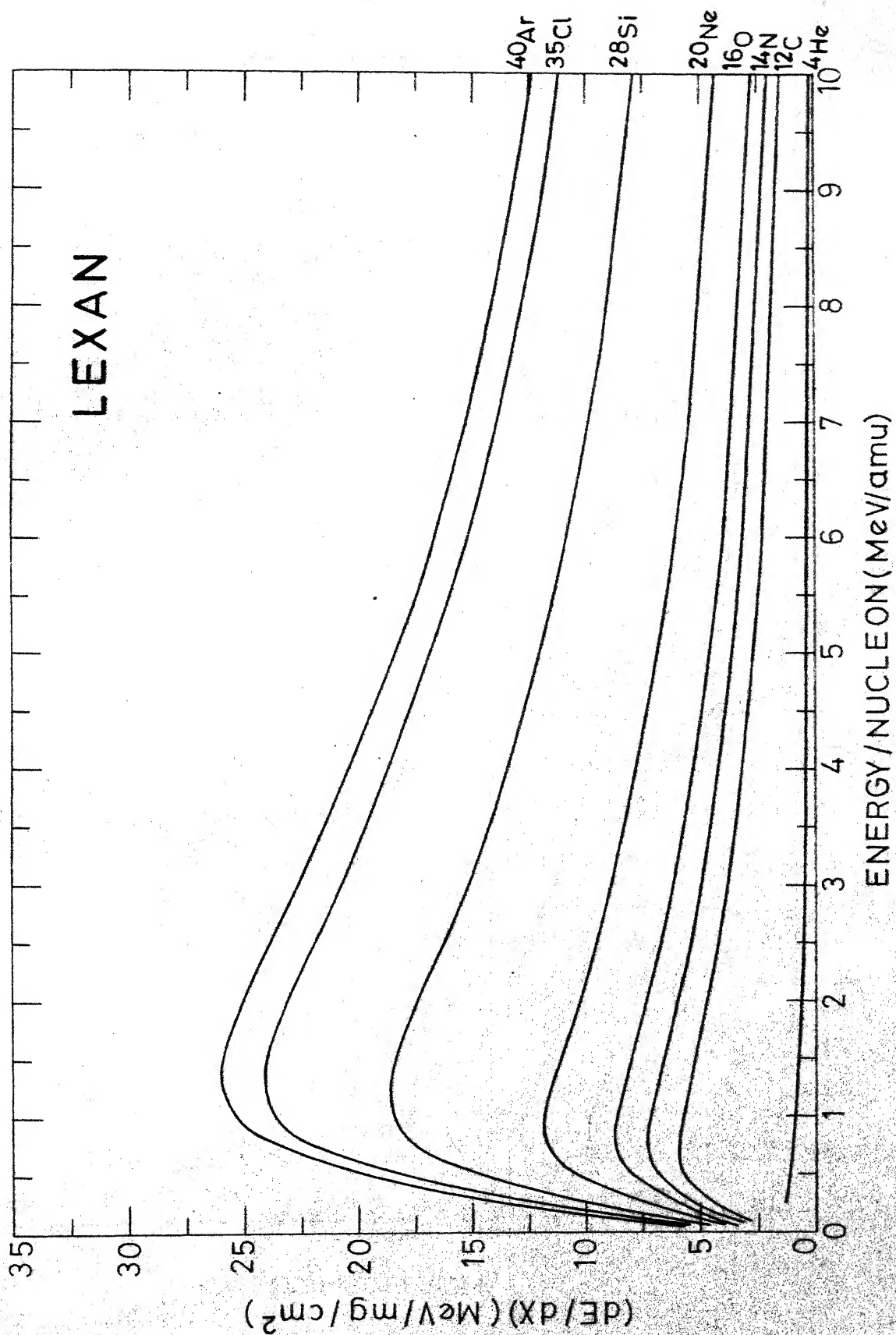


Fig. 37. Plot of the calculated stopping-power versus ion energy for Lexan.

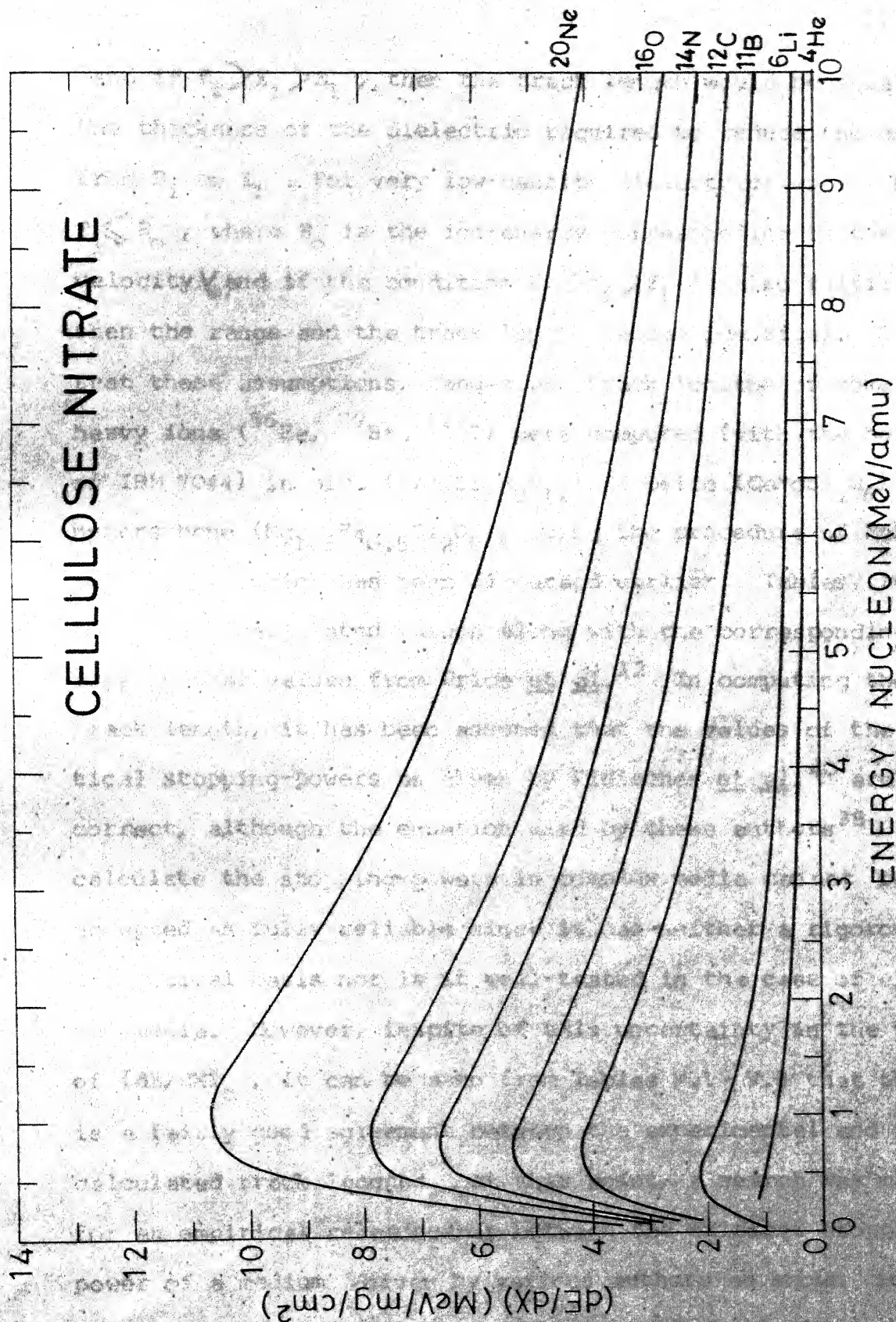


Fig. 38. Plot of the calculated stopping-power versus ion energy for cellulose nitrate.

hand if $E_2 > E_i > E_1$, then the track length would be equal to the thickness of the dielectric required to reduce the energy from E_i to E_1 . For very low-density dielectrics we may have $E_1 \ll E_0$, where E_0 is the ion-energy corresponding to the ion-velocity V_0 , and if the condition $E_2 > E_i > E_1$ is also fulfilled, then the range and the track length become identical. To test these assumptions, ranges and track lengths of some heavy ions (^{56}Fe , ^{79}Br , ^{127}I) were computed (with the help of IBM 7044) in mica ($\text{KAl}_3\text{Si}_3\text{H}_2\text{O}_{12}$), diopside ($\text{CaMgSi}_2\text{O}_6$) and hypersthene ($\text{Mg}_{1.5}\text{Fe}_{0.5}\text{Si}_2\text{O}_6$), using the procedure of Mukherji and Nayak¹⁵ which has been discussed earlier. Tables V.1-V.3 show these calculated values along with the corresponding experimental values from Price *et al.*¹² In computing the track length, it has been assumed that the values of the critical stopping-powers as given by Fleischer *et al.*⁴⁰ are correct, although the equation used by these authors³⁸ to calculate the stopping-powers in complex media cannot be accepted as fully reliable since it has neither a rigorous theoretical basis nor is it well-tested in the case of elemental media. However, inspite of this uncertainty in the values of $(dE/dX)_c$, it can be seen from Tables V.1 - V.3 that there is a fairly good agreement between the experimental and the calculated track lengths. At this point, a search was made for an empirical relationship between the critical stopping-power of a medium given by various authors as shown in Table V.4 (along with their densities and chemical

TABLE V.1

Ranges and track lengths of some heavy ions in mica.
 The calculated track lengths are based on
 $(dE/dX)_c = 13.0 \text{ MeV/mg/cm}^2$

Heavy ions	Initial energy E_i (MeV)	Range R (μm)	Track length (μm)	
			Experimental*	Theoretical
^{127}I	60.0	8.28	7.20	7.03
	29.4	5.10	4.00	3.85
	21.6	4.00	2.80	2.75
	15.0	2.95	2.20	1.70
^{79}Br	60.0	9.98	7.10	7.48
	29.4	6.35	3.50	3.85
	21.6	5.10	2.70	2.60
	15.0	3.90	1.50	1.40
^{56}Fe	69.0	12.80	8.50	8.70
	62.5	12.10	7.50	8.00
	54.0	11.10	7.30	7.00
	41.3	9.55	5.70	5.45
	30.4	7.90	4.20	3.80

*Price et al. (Reference 12). The experimental uncertainty is $\pm 0.5 \mu\text{m}$.

TABLE V.2

Ranges and track lengths of some heavy ions in diopside.
The calculated track lengths are based on

$$(dE/dX)_C = 19.0 \text{ MeV/mg/cm}^2$$

Heavy ions	Initial Energy E_i (MeV)	Range R (μm)	Track length (μm)		
			Experimental*		Theoretical
			Set I	Set II	
^{127}I	60.0	7.62	4.00	-	4.82
	29.4	4.65	1.60	-	1.85
	21.6	3.68	1.00	-	0.88
	15.0	2.70	0	< 0.50	-
^{79}Br	60.0	9.20	4.20	4.20	4.80
	29.4	5.85	1.00	1.50	1.45
	21.6	4.77	0.70	0.70	0.37
	15.0	3.58	-	< 0.50	-
^{56}Fe	69.0	11.80	-	5.80	5.10
	62.5	11.14	-	4.50	4.44
	54.0	10.25	-	3.20	3.55
	41.3	8.81	-	3.00	2.11
	30.4	7.30	1.40	2.10	0.60

*Price et al. (Reference 12). The experimental uncertainty is $\pm 0.5\mu\text{m}$.

TABLE V.3

Ranges and track lengths of some heavy ions in hypersthene.
 The calculated track lengths are based on
 $(dE/dX)_c = 20.0 \text{ MeV/mg/cm}^2$

Heavy ions	Initial Energy E_i (MeV)	Range R (μm)	Track length (μm)		
			Experimental* Set I Set II		Theoretical
^{127}I	60.0	7.20	3.50	-	4.10
	29.4	4.48	1.50	-	1.38
	21.6	3.45	-	-	0.35
	15.0	2.55	-	-	-
^{79}Br	60.0	8.80	3.40	3.40	4.00
	29.4	5.60	<1.00	-	0.80
	21.6	4.45	0	0	-
	15.0	3.42	0	0	-
^{56}Fe	69.0	11.35	5.00	5.60	4.55
	62.5	10.70	4.20	4.80	3.90
	54.0	9.80	-	2.80	3.00
	41.3	8.40	2.20	2.20	1.60
	30.4	6.95	-	1.00	0.15

*Price et al. (Reference 12). The experimental uncertainty is $\pm 0.5 \mu\text{m}$.

TABLE V.4

Values of the critical energy-loss rate $(dE/dX)_c$
and the density for various solid dielectrics^c

SDTD	Density ρ (g/cm ³)	$(dE/dX)_c$ (MeV/mg/cm ²)	$(dE/dX)_c$ (10 ³ MeV/cm)	Ref.
Cellulose nitrate (C ₆ H ₈ O ₉ N ₂)	1.33-1.49	0.86 2.0 \pm 1.0	2.82 \pm 1.60	45,40
Cellulose acetate (C ₁₀ H ₁₄ O ₇)	1.27-1.34	8.0 \pm 2.0	10.40 \pm 2.64	Present work
Cellulose acetate butyrate (C ₂₀ H ₃₂ O ₅)	1.15-1.22	3.0 \pm 1.0	3.66 \pm 1.22	40
HBPAlT Polyester (C ₁₇ H ₉ O ₂)	1.40	3.0 \pm 1.0	4.20 \pm 1.40	40
Lexan polycarbonate (C ₁₆ H ₁₄ O ₃)	1.20	4.0 5.5 8.0	7.20 \pm 2.40	40,42, 41
Mylar (C ₁₀ H ₈ O ₄)	1.20-1.35	4.0 \pm 2.0	5.10 \pm 2.55	40
Tektite glass (74SiO ₂ .12Al ₂ O ₃ .4FeO)	2.43	15.0 \pm 2.0	36.45 \pm 4.86	40
Sodalime glass (67SiO ₂ .14Na ₂ O.14CaO. 5Al ₂ O ₃)	2.49	15.0 \pm 2.0	37.35 \pm 4.98	40
Phosphate glass (63P ₂ O ₅ .11UO ₂ .8Al ₂ O ₃ . 9Ag ₂ O.9K ₂ O)	3.10	15.0 \pm 2.0	46.5 \pm 6.20	40
Mica (KAl ₃ Si ₃ H ₂ O ₁₂)	2.93	13.0 \pm 2.0	38.09 \pm 5.86	40
Quartz (SiO ₂)	2.65	15.0 \pm 2.0	39.75 \pm 5.30	40
Zircon (ZrSiO ₄)	4.68	19.0 \pm 2.0	88.92 \pm 9.36	40
Diopside (CaMgSi ₂ O ₆) ₂	3.27	19.0 \pm 2.0	62.13 \pm 6.54	12
Hypersthene (Mg _{1.5} Fe _{0.5} Si ₂ O ₆) ₂	3.45-3.65	20.0 \pm 2.0	71.00 \pm 7.10	40
Olivine (MgFeSiO ₄)	3.32-3.35	20.0 \pm 2.0	66.70 \pm 6.67	40

composition) and some of its physical properties. It was found that a plot of $(dE/dX)_c$ in MeV/cm (obtained by multiplying the stopping-power in MeV/mg/cm² by the density of the medium) against the density ρ of the medium yields a straight line. Fig. 39 shows the straight line representing the least-square fit to the experimental data on $(dE/dX)_c$ and from this one gets

$$\left(\frac{dE}{dX}\right)_c = 25.5 (\rho - 1) \quad (5.26)$$

where $(dE/dX)_c$ is in units of 10^3 MeV/cm and ρ is the density in g/cm³. Eq. (5.26) permits the calculation of the track length of any heavy ion of known initial energy in any solid dielectric of known molecular formula and density. Further calculation on the track lengths were carried out for several heavy ions (¹¹B, ¹²C, ¹⁴N, ¹⁶O, ²⁰Ne, ²²Ne, ³²S, ⁴⁰Ar and ¹²⁷I) in Lexan and cellulose nitrate. The calculated track lengths are shown in Figs. 40 and 41 along with the corresponding experimental values from Tripier *et al.*⁴⁶ The values of $(dE/dX)_c$ for Lexan and cellulose nitrate have been taken as 5.0 and 3.5 in units of MeV/mg/cm², respectively. While the agreement seems to be excellent in the case of Lexan for all the ions, it is not so good in the case of cellulose nitrate, particularly for the ions lighter than ¹⁶O. The density of cellulose nitrate as well as its exact composition are somewhat uncertain and the present calculations have been made on

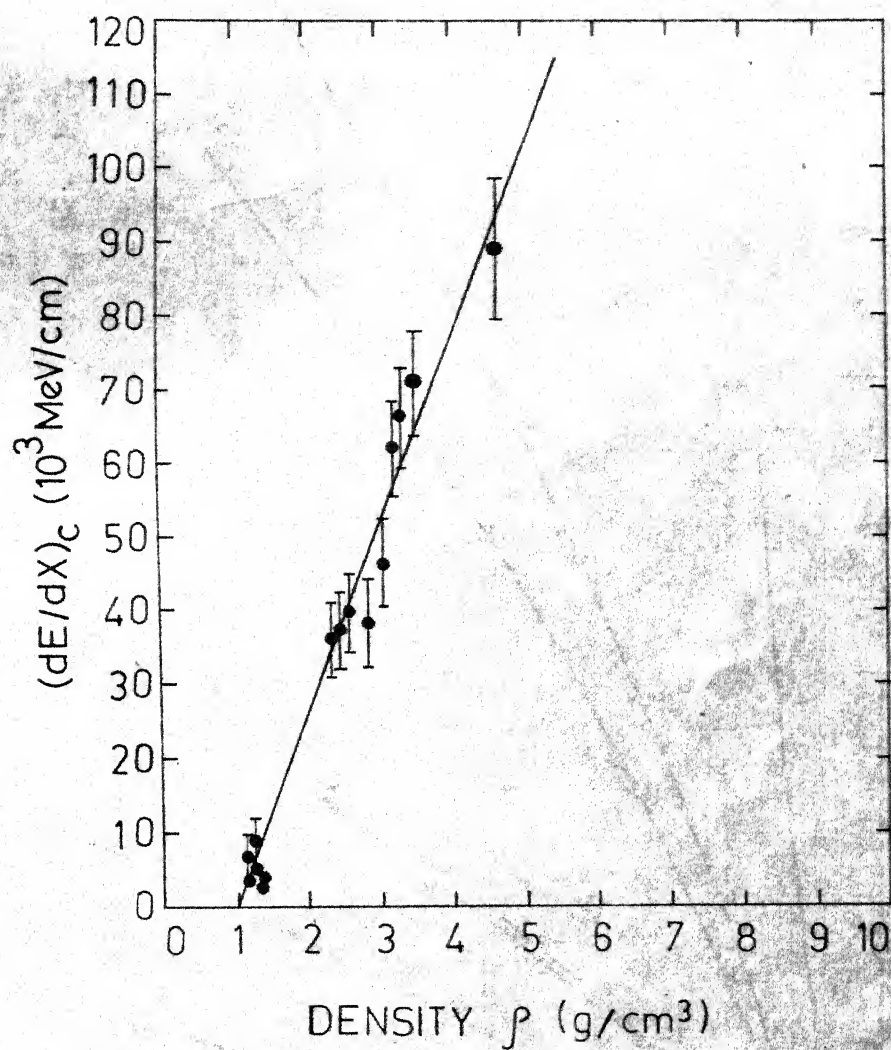


Fig. 39. Plot of the critical stopping-power versus the density for various solid dielectrics.

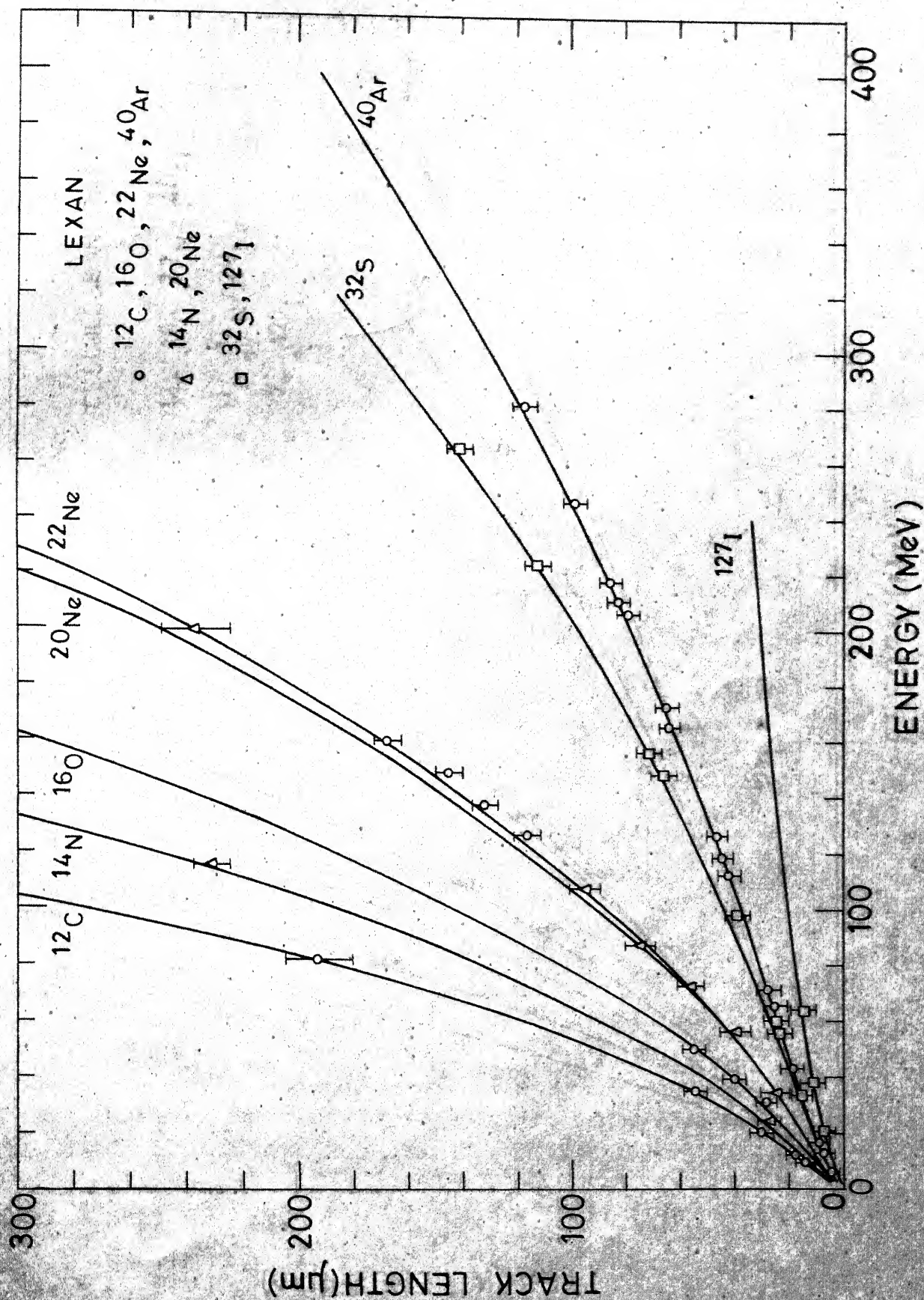


Fig. 40. Track length versus energy curves for various ions in Lexan. The experimental points are from Tripler et al.⁴⁶

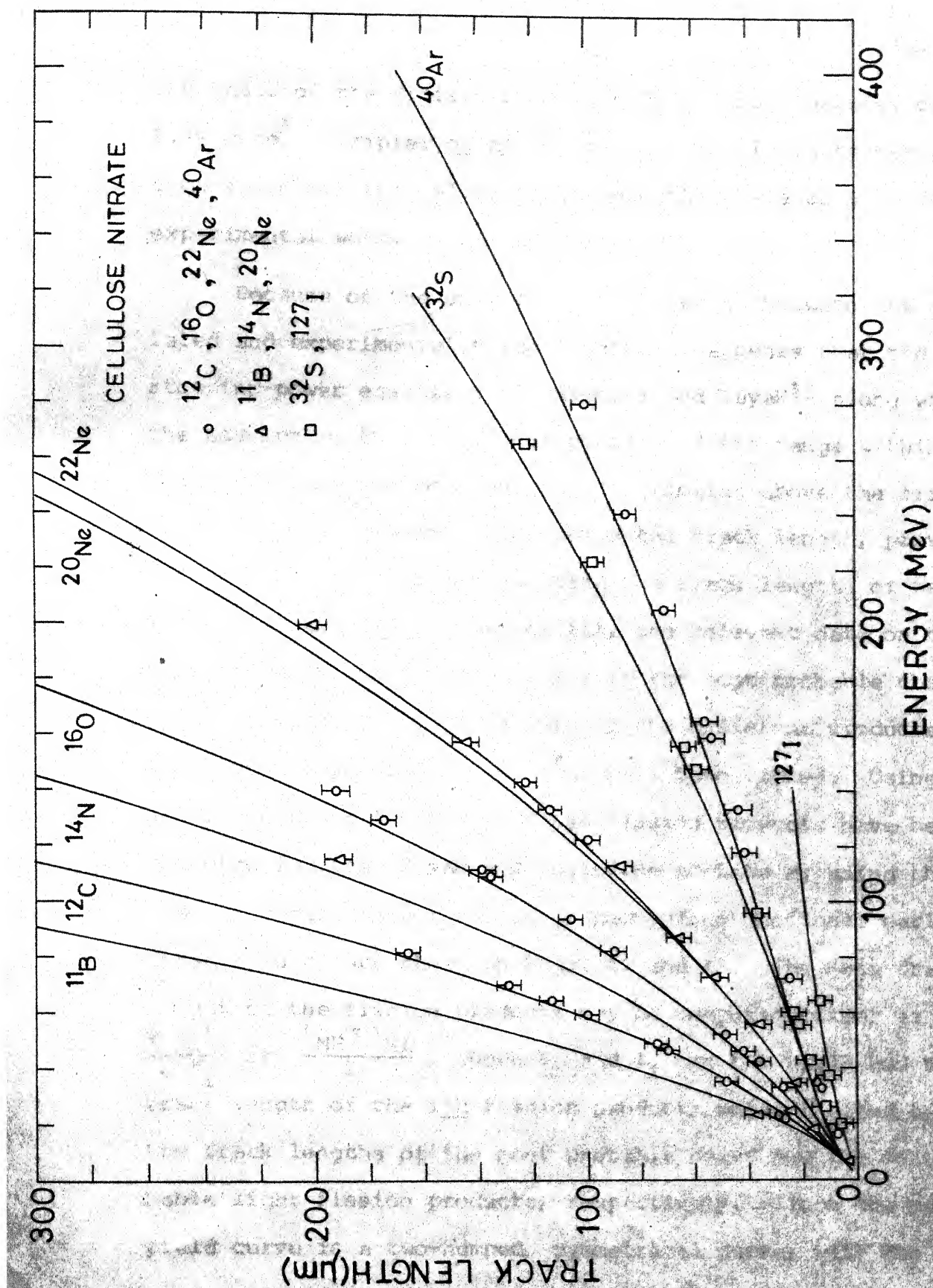


Fig. 41. Track length versus energy curves for various ions in cellulose nitrate. The experimental points are from Tripier *et al.*⁴⁶

the basis of the dinitro form ($C_6H_8O_9N_2$) and a density of 1.49 g/cm^3 . Tripier et al.⁴⁶ have not mentioned the exact composition of the cellulose nitrate they have used in their experimental work.

Because of the overall good agreement between the calculated and experimental track lengths it appears that the stopping-power equations of Mukherji and Nayak¹⁵ along with the assumption that only that portion of the range within which the stopping-power of the ion remains above the critical stopping-power $(dE/dX)_c$ represents the track length, provide a reliable method for calculating the track lengths of heavy ions. In Table II.1 (Chapter II), the relevant data on the mass number A , the atomic number or the most probable charge $Z_p(A)$, and the initial energies of the different products from the spontaneous fission of ^{252}Cf have been listed. Using these data, the track lengths of these fission products have been computed in mica, Lexan and cellulose acetate by using the same procedure as for the other heavy ions mentioned earlier. These results are shown in Figs. 42 and 43. The mean track length of the fission products may be computed either as $\frac{\sum Y_i L_i}{\sum Y_i}$ or $\frac{L_{MH} + L_{ML}}{2}$, where Y_i and L_i are the yield and the track length of the i th fission product, while L_{MH} and L_{ML} are the track lengths of the most probable heavy and the most probable light fission products, respectively. Since the mass yield curve is a two-humped, symmetrical curve, with the two

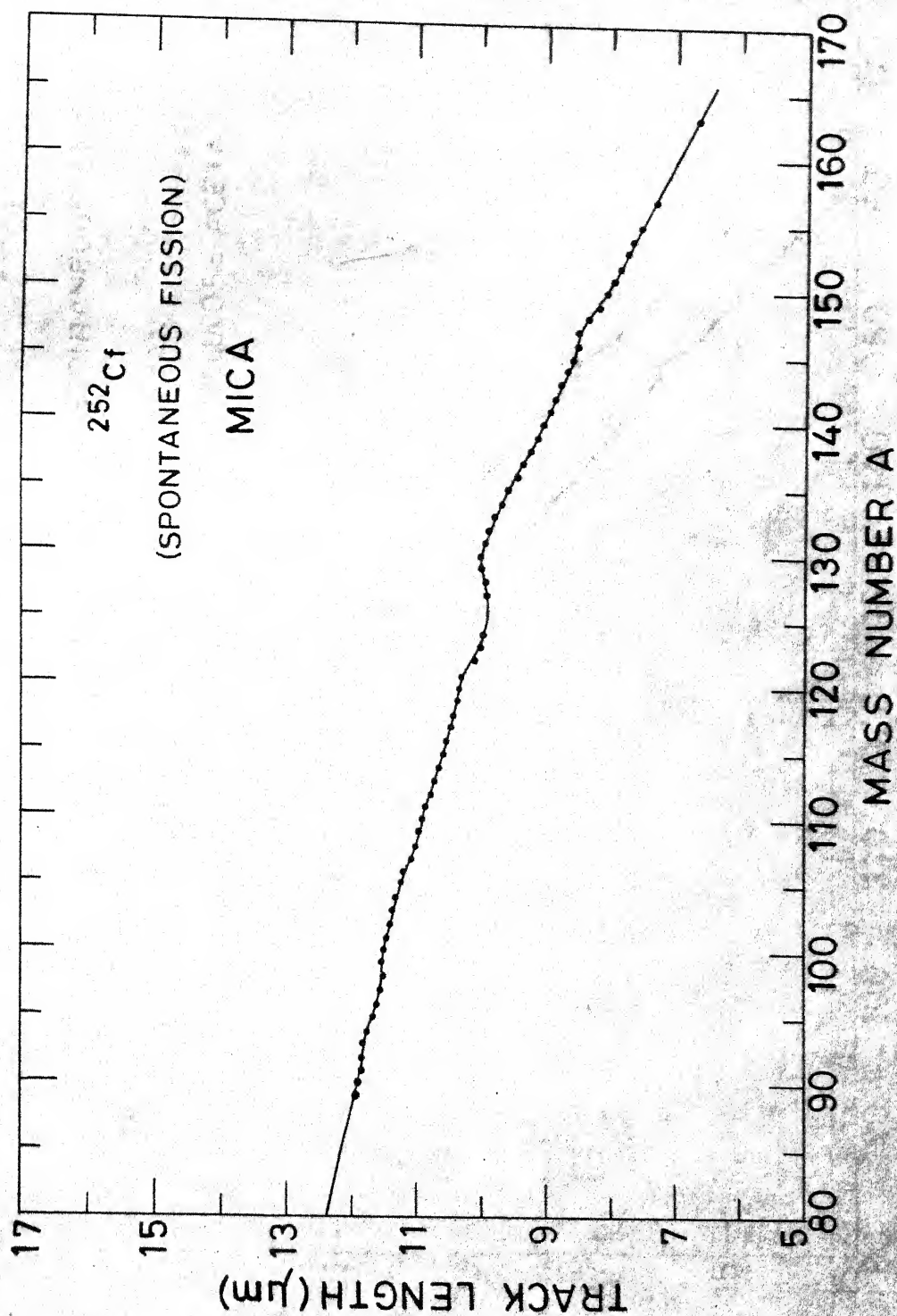


Fig. 42. Plot of the computed track length versus mass number for the fission products from ^{252}Cf in mica.

peaks corresponding to the yields of the most probable light and heavy fission products, both the procedures yield the same value for the mean track length. Table IV.5 shows that the agreement between the calculated and the experimental values of the mean track length of the fission products in all the three solid dielectrics mica, Lexan and cellulose acetate, is excellent. Further, the earlier experimental values reported by Fleischer et al.³⁸ are also in good agreement with the present experimental and calculated values, considering the fact that those authors³⁸ possibly have not made any systematic surface-etching and over-etching corrections to their observed track lengths.

During the computation of the track length, the computer keeps account of the energy-loss rate at every new energy E of the ion, as also the distance it penetrates while the energy gets reduced from its initial energy E_i to the energy E . Thus, the computer output provides automatically the stopping-powers of the medium corresponding to different penetration depths. Since, for all fission products, the stopping-power corresponding to the initial energy E_i is always greater than $(dE/dX)_c$, the penetration depths are identical with the different etched-track lengths in the experiments done on track-etch rates as a function of the etched-track length. Thus, the theoretical stopping-power or energy-loss rates have been read out from

the computer output by:

(a) First identifying the fission product responsible for the track from the maximum etched track length after correcting for surface-etching and over-etching from Figs. 42 and 43, and (b) Taking the computer output for the identified fission product and noting down the stopping powers corresponding to the etched-track lengths at different etching times. The relation between the stopping-power and the track-etch rate has been obtained by noting the track-etch rate determined experimentally at a given experimental etched-track length and reading out the theoretical stopping-power corresponding to the etched-track length or the penetration depth. The plots of the track-etch rate against the stopping-powers of the identified tracks have been shown in Figs. 31-35.

CHAPTER VI

CHAPTER VI

SUMMARY AND CONTRIBUTION TO KNOWLEDGE

The present work represents a detailed experimental study on the etching conditions required for a precise knowledge of the experimental track length of a heavy ion of a given initial energy in a given solid dielectric. This study has shown the need of knowing the complete etching time and bulk-etch rate for obtaining the true track length from the observed track length. Further, an empirical observation has shown that when a track is fully etched it has a definite diameter d_c in a particular medium. From the activation energy for bulk-etch rate, determined in the present work, it is possible to theoretically calculate the complete etching time for a given medium at a given temperature, using

the etchants for which the bulk-etch rates are known experimentally.

Theoretically, a new idea has been introduced that the track length is, in general, not equal to the range. The track length represents only that portion of the range over which the actual stopping-power of the ion is greater than the critical or threshold stopping-power for a given medium. Further, a linear relationship has been deduced empirically between the critical stopping-power of a medium and the density of the medium. This is of considerable practical importance, since it would make possible the theoretical computation of the track lengths of any heavy ion in any solid dielectric of known molecular formula and density and thus widens the scope of heavy particle identification from the track length. Lastly, within the limits of experimental error, the track-etch rate has been found to be linearly dependent on the stopping-power at any point on the track. This points towards the correctness of the widely held idea that the rate of attack by the etchant at any point on the track should obviously depend on the rate at which energy is deposited by the moving ion at that point.

...

APPENDIX A

DETERMINATION OF THE CRITICAL ANGLE OF INCIDENCE ϕ_c

In Fig. 13, the track geometry is given for plastics. As the angle of incidence ϕ approaches the track cone angle θ , the major axis of the ellipse '2a' approaches infinity, and thus for $\phi < \theta$, a track can not be revealed by etching.^{7,20} Hence, the critical angle of incidence ϕ_c may be taken as equal to the cone angle θ_c of the fission product tracks at the time of complete etching.

The maximum etchable or true track lengths of fission products have been measured in the case of mica, Lexan and cellulose acetate and their distributions are shown in Figs. 22, 23 and 24. The average true track lengths L are found to be $10.06 \mu\text{m}$, $19.25 \mu\text{m}$ and $18.67 \mu\text{m}$ for mica, Lexan and cellulose acetate respectively. In a particular solid dielectric, all the tracks were found to have equal diameters d_c (minor axes) at the time of complete etching. Different solids have different values for the track-diameter when the tracks are etched to their full lengths L . The values of these in the case of mica, Lexan and cellulose acetate are found to be

1.5 μm , 2.5 μm and 2.0 μm respectively.

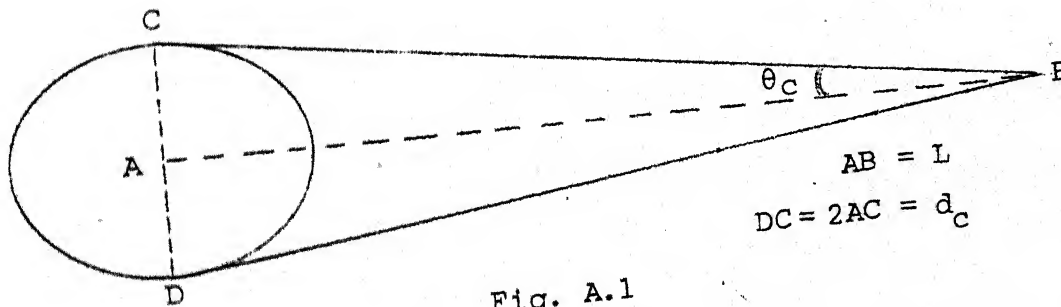


Fig. A.1

From the above Fig. A.1, the cone angle θ_c is given by

$$\theta_c = \tan^{-1} \left(\frac{AC}{AB} \right) = \tan^{-1} \left(\frac{d_c}{2L} \right) \quad (\text{A.1})$$

The values of the critical angle of incidence θ_c ($=\theta_c$) are given in Table II.2.

For mica, the value of the critical angle of incidence agrees fairly well with the value of $4^{\circ}30'$ quoted by Khan and Durrani⁴⁷ whereas in the case of Lexan it is slightly higher than the reported value of $2^{\circ}30'$ by the same authors. Further, the present values of θ_c are within the ranges of the cone angle θ (0° - 5°) for most of the plastics as reported by Fleischer *et al.*⁴⁸

APPENDIX B

ESTIMATION OF THE RELATIVE ERRORS INVOLVED IN TWO DIFFERENT METHODS OF TRACK LENGTH MEASUREMENT

As shown in Fig. 13, a conical track with an incident angle \emptyset forms an ellipse at the surface on etching and the centre of the track does not pass through the centre of the ellipse but undergoes a slight displacement towards the right. In the present measurements, the track lengths have been estimated on the assumption that the centre of the track passes through the centre of the ellipse. The percentage error involved in this is as follows. The centre of the track divides the major axis into two unequal portions of lengths X_1 and X_2 . From Price and Fleischer,⁹ we have

$$X_1 = V_G t (1 - \sin \theta / \sin \emptyset) / \sin (\emptyset - \theta) \quad (B.1)$$

$$X_2 = V_G t (1 - \sin \theta / \sin \emptyset) / \sin (\emptyset + \theta) \quad (B.2)$$

$V_G t$ is known as also θ , so X_1 and X_2 are calculable for different values of \emptyset . The error 'r' in the measurement of track length is $[(X_1 + X_2) / 2 - X_2] / \cos \emptyset$ and the percentage error is $100 [(X_1 + X_2) / 2 - X_2] / L \cos \emptyset$. For each angle of incidence the percentage error associated with the above mentioned

method has been calculated and is given in Table B.1.

Table B.1

Percentage error involved in measuring
the track length from centre to tip

Angle of incidence ϕ	X_1 (μm)	X_2 (μm)	Error 'r' (μm)	Percentage error
15°	4.79	3.01	0.92	4.60
30°	2.46	1.99	0.28	1.40
45°	1.72	1.53	0.14	0.70

The second method involves measurement of the depth Z

$$L = (V_G t + Z) / \sin \phi \quad (\text{B.3})$$

From the value $L = 20 \mu\text{m}$ for the average fission product track length in Lexan and $\phi = 15^\circ$, 30° and 45° , the theoretical values of Z are given in Table B.2. If Z were measured directly (by our microscope) then the error introduced would have been $\pm 0.7 \mu\text{m}$, since one can read down to half a vernier displacement in the vertical direction (one vernier division corresponds to $2.82 \mu\text{m}$) with accuracy. Thus the percentage error would be as shown in Table B.2.

It is apparent that the percentage error in track length estimation through depth measurement (Table B.2) is much larger

than that associated with the approximation that the centre of the track passes through the centre of the ellipse (Table B.1).

Table B.2

Percentage error involved in the depth measurement for a track of length = 20 μm . $V_G^t = 1.25 \mu\text{m}$.

Angle of incidence θ	Depth 'Z' (μm)	Track length (μm)	Percentage error
15°	3.93 \pm 0.70	20.00 \pm 2.72	13.6
30°	8.75 \pm 0.70	20.00 \pm 1.40	7.0
45°	12.89 \pm 0.70	20.00 \pm 1.00	5.0

REFERENCES

1. D.A. Young, Nature, 182, 375 (1958).
2. E.C.H. Silk and R.S. Barnes, Phil. Mag., 4, 970 (1959).
3. A.N. Goland, in 'Radiation Damage Studies', 1 (G.T. Dienes, Ed., Gordon and Breach Publ., New York).
4. P.B. Price and R.M. Walker, Phys. Rev. Letters, 8, 217 (1962).
5. P.B. Price and R.M. Walker, J. Appl. Phys., 33, 3407 (1962).
6. R.L. Fleischer and P.B. Price, J. Appl. Phys., 34, 2903 (1963).
7. R.L. Fleischer and P.B. Price, Science, 140, 1221 (1963).
8. R.L. Fleischer and P.B. Price, Geochim. Cosmochim. Acta, 28, 1705 (1964).
9. P.B. Price and R.L. Fleischer, Ann. Rev. Nucl. Sci., 21, 295 (1971).
10. W.H. Barkas, "Nuclear Research Emulsions", (Academic Press, New York and London), Vol. 1 (1963).
11. H.H. Heckman, B.L. Perkins, W.G. Simon, F.M. Smith, and W.H. Barkas, Phys. Rev., 117, 544 (1960).
12. P.B. Price, R.L. Fleischer, and C.D. Moak, Phys. Rev., 167, 277 (1968).
- 13a. S. Mukherji and B.K. Srivastava, Phys. Rev., B9, 3708 (1974).
- 13b. B.K. Srivastava and S. Mukherji, Phys. Rev., A14, 718 (1976).
14. N. Bohr, Kgl. Danske Videnskab. Selskab, Mat.-Fys. Medd., 18, 8 (1948).
15. S. Mukherji and A.K. Nayak, Private communication, (submitted to Phys. Rev.)
16. H.W. Schmitt, J.H. Neiler, and F.J. Walter, Phys. Rev., 141, 1146 (1966).

17. S. Mukherji, Nucl. Phys., A129, 297 (1969).
18. H.W. Schmitt, R.W. Lide, and F. Pleasonton, Nucl. Instr. and Meth., 63, 237 (1968).
19. R.L. Fleischer, P.B. Price and R.M. Walker, J. Geophys. Res., 69, 4885 (1964).
20. R.L. Fleischer and P.B. Price, J. Geophys. Res., 69, 331 (1964).
21. R.L. Fleischer and H.R. Hart (Jr.), Fission Track Dating: Techniques and Problems, "Calibration of Hominoid Evolution", Recent advances in isotopic and other dating methods applicable to the origin of man, (Ed. W.W. Bishop and J.A. Miller), p. 135-170 (1972).
22. K. Endo and T. Doke, Nucl. Instr. and Meth., 111, 29 (1973).
23. P.B. Price, R.L. Fleischer, D.D. Peterson, C. O'Ceallaigh, D. O'Sullivan, and A. Thompson, Phys. Rev., 164, 1618 (1967).
24. H. Block, F.M. Kiely and B.D. Pate, Nucl. Instr. and Meth., 100, 403 (1972).
25. P.B. Price and R.M. Walker, J. Appl. Phys., 33, 3407 (1962).
26. G.E. Blanford, Jr., R.M. Walker and J.P. Wefel, Radiation Effect, 3, 267 (1970).
27. W. Enge, K. Grabisch, R. Beaujean and K.-P. Bartholmă, Nucl. Instr. and Meth., 115, 263 (1974).
28. W. Enge, K. Grabisch, L. Dallmeyer, K.-P. Bartholomă and R. Beaujean, Nucl. Instr. and Meth., 127, 125 (1975).
29. G. Somogyi, Nucl. Instr. and Meth., 42, 312 (1966).
30. S. Somogyi, ATOMKI Köz1, 8, 218 (1966).
31. G. Somogyi, B. Schlenk, M. Várnagy, L. Meskó and A. Valek, Nucl. Instr. and Meth., 63, 189 (1968).
32. U. Höppner, E. Konecny and G. Fiedler, Nucl. Instr. and Meth., 74, 285 (1969).
33. J. Tripier, M. Debeauvais, R. Stern, and J. Ralarosy, J. Microscopic, 7, 811 (1968).

34. D. Hasegan, *Rev. Roum. Phys.*, 17, 1023 (1972).
35. G.E. Blanford, Jr., R.M. Walker, and J.P. Wefel, *Radiation Effect*, 5, 41 (1970).
36. G. Somogyi and S.A. Szalay, *Nucl. Instr. and Meth.*, 109, 211 (1973).
37. W.T. Crawford, W. Desorbo, and J.S. Humphrey, *Nature*, 220, 1313 (1968).
38. R.L. Fleischer, P.B. Price, R.M. Walker, and E.L. Hubbard, *Phys. Rev.*, 133, A1443 (1964).
39. W.H. Bragg, "Studies in Radioactivity", Macmillan & Co., Ltd., London, 1912 (Chap. 22, Sec. 5; Chap. 25, Sec. 2).
40. R.L. Fleischer, P.B. Price and R.M. Walker, *Ann. Rev. Nucl. Sci.*, 15, 1 (1965).
41. G. Remy, J. Ralarosy, R. Stein, M. Debeauvais, and J. Tripier, *J. de Physique*, 31, 27 (1970).
42. M. Debeauvais, R. Stein, J. Ralarosy, and P. Cüer, *Nucl. Phys.*, A90, 186 (1967).
43. J.B. Niday, *Phys. Rev.*, 121, 1471 (1961).
44. S. Mukherji, *Phys. Rev.*, B12, 3530 (1975).
45. M. Debeauvais and M. Monnin, *Comp. Rend.*, 260, 4728 (1965).
46. J. Tripier, G. Remy, J. Ralarosy, M. Debeauvais, R. Stein, and D. Huss, *Nucl. Instr. and Meth.*, 115, 29 (1974).
47. H.A. Khan and S.A. Durrani, *Nucl. Instr. and Meth.*, 98, 229 (1972).
48. R.L. Fleischer, P.B. Price, and R.M. Walker, "Nuclear Tracks in Solids", University of California Press, Berkeley, 1975 (Chap. 2, Sec. 2.3).